PERFORMANCE OF VARIOUS PHOTOVOLTAIC MODULE TECHNOLOGIES IN TROPICAL CLIMATE CONDITIONS

YE Jiaying

B.Sc. (Microelectronics), Sun Yat-Sen University

NATIONAL UNIVERSITY OF SINGAPORE

2014

PERFORMANCE OF VARIOUS PHOTOVOLTAIC MODULE TECHNOLOGIES IN TROPICAL CLIMATE CONDITIONS

YE Jiaying

A THESIS SUBMITTED

FOR THE DEGREE OF DOCTOR OF PHILSOPHY

NUS GRADUATE SCHOOL FOR INTEGRATIVE SCIENCES AND ENGINEERING

NATIONAL UNIVERSITY OF SINGAPORE

2014

DECLARATION

I hereby declare that the thesis is my original work and it has been written by me in its entirety. I have duly acknowledged all the sources of information which have been used in the thesis.

This thesis has also not been submitted for any degree in any university previously.

_____

YE Jiaying

12 December 2014

ACKNOWLEDGEMENTS

I would like to take this opportunity to express my deep gratitude to all the people who have been supporting me during my PhD study.

I would like to firstly thank my supervisors - Prof. Armin Aberle, Dr. Thomas Reindl and Dr. Timothy Walsh - for their continuous support and guidance during my PhD study at the Solar Energy Research Institute of Singapore (SERIS). I would also like to thank Prof. Joachim Luther for his supervision during the first two years of my study. I thank Prof. Aberle and Dr. Reindl for the invaluable feedback on my research progress and journal publications. I personally thank Dr. Tim Walsh for his daily supervision and continuous encouragement. Tim is recognized as a great mentor and friend. He cares about the progress and needs of students and helped me overcome my doubts and keep going. I thank my Thesis Advisory Committee chairperson Prof. Charanjit Singh Bhatia and member Prof. Andrew A.O. Tay for their invaluable time and feedback during our meetings.

I would like to thank the PVMD group mates: Khoo Yong Sheng, Jai Prakash Singh, Chai Jing for the scientific discussions, and fun activities on weekends; the PVMT group colleagues for the module testing; the SES group mates for the help with experiments. I would also like to thank Dr. Rolf Stangl and Miss. Guo Siyu for the very helpful discussions and cooperation, resulting in a well-received journal publication.

The PhD marathon would be joyless without my friends in SERIS: Wang Juan, Qiu Zixuan, Lu Fei, Ge Jia, and other office mates. Thank you for the pleasant study atmosphere and all the joyful memories.

I am truly grateful for the scholarship from the NUS Graduate School for Integrative Sciences and Engineering.

Finally, the nonstop love and support of my parents have kept me positive and strong. Thank you for being with me when I was happy or frustrated. I would also like to thank my boyfriend, Mr. Manuel Danner and my best friends in Singapore, Miss Huang Wenwen and Miss Zhang Mei, for their warm company.

Table of Contents

Summary

While tropical climate zones are gaining momentum in the global photovoltaic (PV) market, very little scientific work has been carried out on the performance of PV modules under such climatic conditions. This PhD thesis compares and analyses the performance of various PV modules (several thin-film technologies as well as several crystalline silicon wafer based technologies) in the tropics by conducting comprehensive indoor measurements and outdoor monitoring tests. A thorough study of the modules' spectral responses is performed, revealing that the blue-shifted spectrum in the tropics causes significant differences in the module performance. Based on outdoor testing data, a model is derived to extract the temperature coefficients of the modules' maximum power points and to understand their dependence on irradiance and module temperature. Module degradation rates are found to be relatively high compared to temperate climates. Finally, 'Tropical Test Conditions' are defined, which enable a standardised performance comparison across different PV module technologies in tropical regions.

Table of figures

Nomenclature

Pmpp	Maximum power output (W)
P_0	Nameplate maximum power output (W)
Vmpp	Voltage at maximum power point (V)
Impp	Current at maximum power point (A)
R_S	Series resistance (Ohm)
R_{Shunt}	Shunt resistance (Ohm)
P^*	Power output at standard test conditions (W)
V_{OC}^*	Open-circuit voltage at standard test conditions (V)
I_{SC}^*	Short-circuit current at standard test conditions (A)
I_{SC}	Short-circuit current (A)
V_{OC}	Open-circuit voltage (V)
α	Relative temperature coefficient of the short-circuit current (%/°C)
β	Relative temperature coefficient of the open-circuit voltage (%/°C)
γ	Relative temperature coefficient of the maximum power (%/°C)
T_{mod}	Temperature of a PV module, measured at the backsheet (°C)
G	In-plane irradiance (W/m^2)
G^*	Irradiance at standard test conditions (1000 W/m^2)
G'	Effective irradiance after spectral correction (W/m^2)
θ_Z	Solar zenith angle (degree)
θ	Solar incident angle of a tilted surface (degree)
E	Energy produced by a PV module in a given time period (Wh)
E_i	In-plane solar radiation in a given time period (Wh)
STC	Standard test conditions

Chapter 1 Introduction

1.1 Motivation

As the demand of electric energy consumption keeps rising with the world's ever-growing population, one of the key challenges facing humanity in the long run will be to generate electricity in a carbon-neutral and sustainable way. Among the different renewable energies, solar energy is by far the most abundant and available virtually everywhere [1]. The effect of generation of voltage or electric current in a material upon exposure to light is called photovoltaics (PV) [2]. The application of PV modules has seen a massive growth since the 2000s, thanks to the introduction of feed-in tariffs, predominantly in Europe. This development is expected to continue at a smaller growth rate, however now from a higher level (see Figure 1.1).

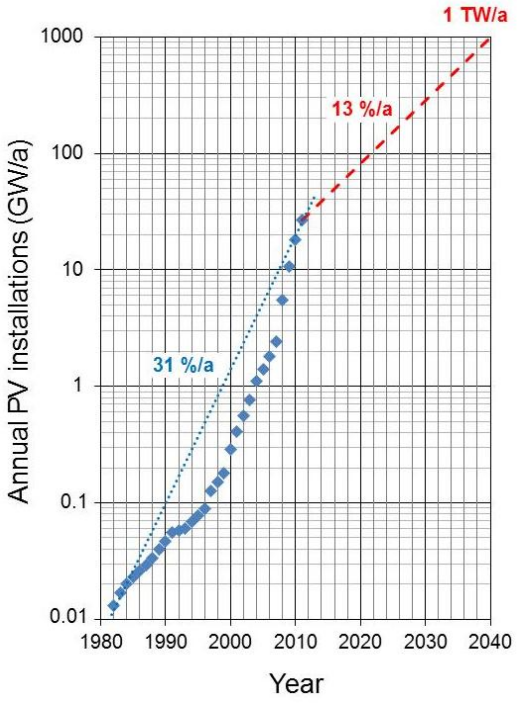

Figure 1.1: Historic and expected development of the global solar PV market [3].

Based on a fast and continuous economic development, the Asia Pacific region is predicted to account for more than half of the planet's energy consumption by 2035, according to a study by the Asian Development Bank [4]. The high demand of energy has raised social, political, and economic challenges, which call for sustainable solutions. Renewable energy has thus been given more attention and grown continuously in this region.

The Asian tropical sunbelt, with about 50 per cent more annual solar radiation than temperate regions like Japan or Germany [4], makes it more appropriate for solar applications. The market size for PV in south-east Asia is expected to reach 20 GW by 2017 [5]. Presently, Thailand, Malaysia and Indonesia are driving the south-east Asian PV market. Thailand has accounted for the majority of installations in the region and became the fifth largest market in Asia in 2012 (after China, Japan, India and Australia). Malaysia has aimed for 55 MW of PV system installations by the end of 2015 [6], and Indonesia also plans to install solar systems for thousands of more households in rural eastern Indonesia [7]. The Singapore government has invested large efforts into PV development and realization. Given the rapid decreases in the cost of solar panels in the past several years, solar electricity has become cost-competitive with traditional energy from the grid in Singapore, reaching the so-called "grid parity" in 2012 for larger roof-top systems [8]. The Singapore government has an ambitious target of 80% green buildings by 2030, and is pioneering various solar projects on the island [9]. It is expected that the PV system market in South-East Asia will grow continuously and substantially in the coming years. However, the environmental conditions in the tropics (constantly high ambient temperature, high humidity, and fast-changing

irradiance) are very different from those in temperate climates, under which PV module performance is widely reported. The performance and reliability of PV modules depends on the operating conditions. It is therefore important to fill the knowledge gap on PV module performance in the tropics. This information can provide constructive advice to manufacturers to produce PV modules optimized for the tropical climates and is also desirable for system integrators and investors to easily determine which type of PV module technology gives the best performance at the given conditions in the tropics.

1.2 Background and review

1.2.1 Current status of PV module technologies

Solar PV module production is set to reach 49 gigawatts (GW) in 2014 [10]. Among all the technologies in the PV market, wafer-based crystalline silicon ("c-Si") is so far the most developed material for PV cells and modules, and huge achievements have been reached in improving its costs and conversion efficiencies [11]. The market share of monocrystalline silicon (mono c-Si) and multicrystalline silicon (multi c-Si) together was over 90% at the end of 2013 [12]. The multicrystalline Si technology itself accounts for 62% of all modules produced. Although thin-film modules comprise less than 10% of the global PV market, the production keeps growing due to the overall growth of the industry. The major materials for thin-film PV modules are (1) amorphous silicon ("a-Si"), (2) microcrystalline silicon ("μc-Si"), (3) Cadmium telluride ("CdTe"), and (4) Copper indium gallium diselenide ("CIGS") [13]. Figure 1.2 shows the expected production capacities of thin-film materials until 2015 [14].

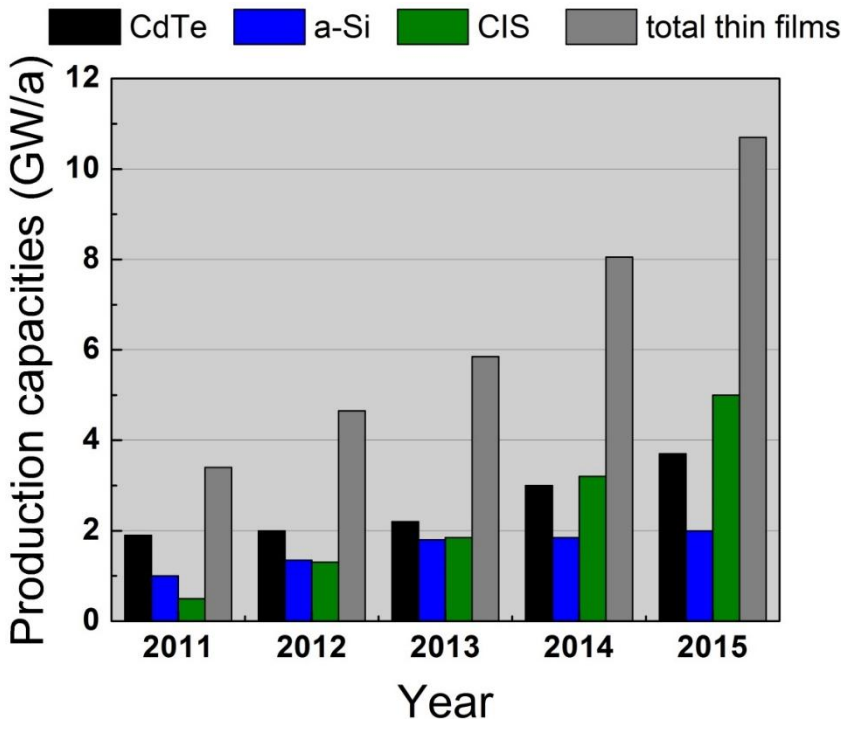

Figure 1.2: Production capacities of thin-film PV module for CdTe, a-Si/μc-Si and CIGS [14].

The much lower share of thin-film modules is mainly due to their lower efficiencies compared to c-Si modules at comparable prices [15]. While c-Si modules have an average efficiency between 13% to 20%, thin-film modules are only between 7% to 16% [16]. It was believed that thin-film technologies generically have the potential of lower manufacturing cost due to less material usage and standardised, high-throughput machines [17]. However, due to a current over-capacity in the c-Si PV industry and the availability of low-cost silicon feedstock, prices for c-Si modules have fallen constantly over the past few years to below 0.7 EURO/W_p today, which is comparable to that of thin-film modules (0.6 EURO/W_p) [18]. Thin-film technologies have the advantage to be deposited at low temperatures, which enables the photo-active layers to be deposited onto a number of materials including glass, plastic, metal as well as flexible substrates [1, 19]. In addition, the room for efficiency improvement is large and the world records for CIGS and CdTe modules are being broken

every few months [20, 21]. Since the aim of this study is to provide advice on how different PV module technologies perform under tropical climates, this work will thus focus on the module technologies available on the market, including crystalline Si, amorphous Si, micromorph Si, CdTe, and CIGS modules. Based on the findings, suggestions to industrial production are also proposed for optimized module performance in the tropics. The characteristics of each technology and the influence of environmental factors to the module performance are reviewed in the following part of this chapter.

1.2.2 Characteristics of various PV module technologies

1.2.2.1 Crystalline Si

Crystalline Si refers to both monocrystalline Si (mono c-Si) and multi-crystalline Si (multi c-Si), depending on the presence of grain boundaries in the Si. Monocrystalline Si is also often called “single-crystal” Si. It is mainly produced using the Czochralski process, which requires high temperatures (~1500°C) and long process times to grow single-crystal ingots [22]. Multi c-Si is produced in a simpler and faster way, including the melting and cooling of silicon [23]. The grain sizes of the resulting multi c-Si can range from millimetres to centimetres, depending on the temperature control of the process [24]. Since mono c-Si solar cells do not have grain boundaries which introduce discontinuities in the silicon and deteriorate the local electronic properties, their conversion efficiency is higher than multi c-Si solar cells if the same cell structure is used. The present average prices for a 156-mm mono c-Si solar cell and a 156-mm multi c-Si solar cell are around $2.7 and $2.2, respectively [25]. The efficiency gap of about 1-2 % (absolute) between mono c-Si solar cells and multi c-Si solar cells has remained stable over the years

[26]. The rated module efficiencies of conventional crystalline Si modules are about 13% to 16% [27-29]. The warranty for crystalline Si modules usually covers 25 years. The performance of c-Si modules is generally stable and the performance degradation rate is relatively low, usually less than -1%/year [30].

1.2.2.2 High-efficiency crystalline Si

Various approaches have been devised to enhance the conversion efficiency of c-Si solar cells. To improve the c-Si cell efficiency, high-carrier-lifetime substrates are usually required, in combination with extra processing and sophisticated structures, such as laser grooved buried contacts (LGBC), emitter wrap through (EWT), all back contact (ABC), and heterojunction with intrinsic thin layer (HIT) cells [31-35]. The first three technologies enhance the cell efficiency through the reduction of shading losses caused by the front metal contacts. HIT is a technology using the excellent surface passivation properties of a-Si on c-Si to improve the cell conversion efficiency. Module efficiencies beyond 20% have been commercialized with these novel solar cell technologies [36]. But these high-efficiency modules usually have a higher manufacturing cost due to the numerous and complicated fabrication processes.

1.2.2.3 Amorphous Si

Amorphous Si (a-Si) PV modules have been in commercial production since 1980 [37]. The production of a-Si requires only about 1% of the silicon that would have been used to produce a c-Si based solar cell, so in theory they should be much cheaper than c-Si based solar cells [38]. However, the conversion efficiency of a-Si modules is about 6 to 8 % (absolute) lower than that of c-Si modules, and thus one would have to cover a larger surface with

a-Si solar panels compared to crystalline-based solar panels for an equal output of electrical power. The low space-efficiency also means that the costs of space and support structures will increase.

The amorphous structure results in high defect density and low doping efficiency. Hydrogen is thus used to passivize the defects and enhance doping efficiency for a-Si module production [39]. Some weak Si-H bonds are broken due to light soaking and dangling bonds are generated, which causes significant reduction in efficiency during the initial implementation [40, 41]. The number of dangling bonds reaches equilibrium after prolonged illumination so that further photodegradation is limited. The efficiency reduction can be up to 30% in the first several months [42], and the wide-range variation in power and voltage causes additional difficulty in sizing the inverter because inverters can work with high efficiency only in certain voltage ranges [43]. Even after this initial degradation, a combination of the light-induced degradation (also called Staebler-Wronski effect) [44] and annealing effect, which reverses the photodegradation effects [45], continue to cause seasonal variations in the efficiency of a-Si PV modules. These changes in efficiency are driven by the module's operating temperature, but also by its history of exposure to light and the temperature of operation [46]. The density of these so-called "light-induced defects" can be decreased by annealing at temperatures above a hundred degrees Celsius [47], while in real-life operation, the annealing effect causes a-Si modules to perform relatively better in summer than in winter in temperate regions [48]. The nameplate power of a-Si modules are usually stated as the stabilized power, which is under-rated to accommodate for the degradation effects.

1.2.2.4 Multi-junction Si

Since the efficiency of solar cells based on single-junction a-Si is too low to be competitive for power applications, tandem-cell technologies were developed to better utilize the solar spectrum and thereby boost the PV efficiency [49]. Adding germanium (Ge) to the silicon can reduce the bandgap of the amorphous material, thus enabling the double- ('tandem') or triple-junction (e.g., a-Si/a-Si/a-SiGe) solar cells. One company, United Solar Ovonic, was commercially making such triple-junction modules [50], but it went bankrupt in 2012. Amorphous Si cells can also be combined with another silicon based material such as nano- or microcrystalline silicon (nc-Si or μc-Si) to form a tandem solar cell [51]. Such technology is usually referred to as "micromorph" Si. Sharp and Kaneka are presently the two main companies producing multi-junction Si modules. Multi-junction cells are interconnected in series, and the current of the two stacked cells is usually optimized for the standard Air Mass 1.5 global (AM1.5G) spectrum.

1.2.2.5 Cadmium telluride (CdTe)

The world-record efficiency for CdTe solar cells and modules to date are 19.6% and 16.1%, respectively [15], held by First Solar, the most successful company producing commercial CdTe modules. CdTe is, in principle, one of the best-suited materials for photovoltaics with its direct bandgap of 1.44 eV, close to the optimum for solar conversion [14]. There are, however, environmental issues with products that rely on cadmium – a heavy metal and potential carcinogen that can accumulate in plant and animal tissues [52]. While the threat is minimal so long as the compound is contained within the solar panel [53], the safety is still an issue in case of fire accidents. In addition,

the disposal and recycling remains a concern [54]. Compared to a-Si, CdTe exhibits relatively better stability, but it is also reported to show light-induced metastabilities after extended light soaking (more than 5000 hours) [55, 56].

1.2.2.6 Copper indium gallium diselenide (CIGS)

In 2013, a CIGS solar cell with a new record efficiency of 20.4% was achieved on flexible polymer foils [20]. This makes CIGS-based solar panels the highest performing thin-film solar panels to date. The commercial CIGS modules sold today usually have efficiencies in the range of 10 to 14 % [57-59]. Although CdS is used as an n-type window layer (as in CdTe modules), much less of the toxic material cadmium is present in CIGS solar cells compared to CdTe solar cells. There are now also Cd-free CIGS modules commercially available [60]. CIGS solar cells are reported to exhibit pronounced metastabilities and performance variation with light exposure [61, 62]. If the devices are stored for a long time in in the dark, the fill factor and V_{OC} are considerably smaller (especially at elevated cell temperatures) than would otherwise be the case [63]. The quasi-stable properties of CIS or CIGS modules are still not clearly identified, and the light soaking effects vary greatly depending on the device structure and especially the buffer layer composition [64, 65]. Some module types were reported to be very sensitive to illumination and even an exposure to light for less than a second can vary the material states, whereas others show better stability [66, 67]. Despite the high sensitivity, it has been verified that the flash test (with a sweep time of less than1 second) itself does not cause significant light-induced effects to CIGS modules [68].

1.2.3 PV module power rating and outdoor performance indicator

1.2.3.1 Standard test conditions (STC)

The current internationally accepted standard test conditions (STC) specify 25°C module temperature, Air Mass 1.5 Global (AM1.5G) solar spectrum, and a solar irradiance intensity of 1000 W/m^2 for power measurements of terrestrial non-concentrating ('flat-plate') PV devices. The conditions represent a compromise between the measurements that can be performed indoors with accurate research equipment and the actual operating conditions. Manufacturers usually assign a nameplate power to a module type based on the power output measured at STC. Because this number is a typical value for a given model, the difference between a particular PV module's nameplate power and its actual output power under STC is accounted for by the power tolerance (typically ±3% for c-Si modules and -5%/+10% for thin-film modules).

The accuracy of the STC power measurement is mainly affected by three factors: spectral mismatch correction, pre-measurement conditions, and possible capacitance effects [68-76]. Spectral mismatch occurs when the spectral response (SR) of the PV module is different from that of the reference sensor for irradiance calibration. To apply a correction, it is necessary to measure the spectral response on module level, which will be discussed in detail in Chapter 2. The effect of the pre-measurement conditions and the capacitance effects are outside of the scope of this thesis, while proper procedures were applied to minimise their influences.

1.2.3.2 Performance Ratio (PR)

As the outdoor conditions in real-life operations are different from the indoor test conditions, the outdoor module efficiency can deviate significantly from the indoor measurements [75, 77]. The "Performance Ratio" (PR), relating the outdoor performance with the STC measured efficiency, is widely applied as a gauge to evaluate the relative merits of PV installations of different sizes, locations, technologies, and climates [78]. The Performance Ratio has been established by the International Energy Agency (IEA) Photovoltaic Power Systems Programme and defined in IEC standard 61724 [79], given by

$$\mathrm{PR} = \frac{Y_\mathrm{f}}{Y_\mathrm{r}} \tag{1.1}$$

where the final PV system yield Y_f is the net energy output E_{AC} divided by the nameplate DC power P_0 of the installed PV array. It represents the number of hours that the PV array would need to operate at its rated power to provide the same energy. The reference yield Y_r is the total in-plane solar radiation E_i divided by the reference irradiance G^*. It represents an equivalent number of hours at the reference irradiance to provide the equivalent solar energy.

The Performance Ratio calculated as described indicates the various losses due to the operating conditions (e.g., temperature, irradiance intensity and spectrum), system component inefficiencies (e.g., cabling and inverter), and incomplete utilization of the radiation (e.g., shading, soiling, reflection). Typical values of the performance ratio of PV systems are reported to be in the 70 - 90 % range [80].

The term "Performance Ratio" was actually set up for systems, but can be applied to modules as well. For module analysis, the practical calculation of PR is as follows:

$$PR = \frac{E_{DC} \times G^*}{E_i \times P_0} \tag{1.2}$$

where E_{DC} is the cumulative DC energy output of the module, G^* is the irradiance under STC condition (1000 W/m^2), E_i is the in-plane radiation (measured with an irradiance sensor), and P_0 is the nameplate power output of the module.

PR calculations are based on the irradiance incident on the plane-of-array (POA) and the module power rating under STC. Error in field measurements of the solar irradiance can contribute directly to the uncertainty in calculation of module Performance Ratio [81, 82]. For a-Si modules, the actual module power during the first few months of deployment can be significantly higher (up to 30%) than the nameplate power to accommodate for initial degradation effects. Thus the PR results might be significantly higher in the initial months of implementation.

1.2.4 Environmental factors affecting the module performance

1.2.4.1 Irradiance

The irradiance intensity incident on a PV module in the field is not constant, and may only reach 1000 W/m^2 around solar noon. Ideally, the power output of a solar panel is proportional to the incident irradiance since the photo-current is proportional to the irradiance [83]. However, the irradiance intensity will affect the conversion efficiency of a PV module due to the parasitic resistances and the diode quality of the solar cells [84-87].

The power loss due to series resistance (Rs) increases with irradiance intensity because the loss goes with the square of the electric current ($I^2 \cdot R_S$). When the light intensity decreases, the current through the solar cell decreases as well. The equivalent resistance of the solar cell may thus approach the shunt resistance [2]. When these two resistances are similar, the fraction of the total current flowing through the shunt resistance increases, thereby increasing the fractional power loss due to the shunt resistance [88]. Thus, at low light levels (below 400 W/m^2), the effect of the shunt resistance (R_{Shunt}) becomes increasingly important.

The loss due to non-standard irradiance intensity depends on the low-light performance of individual modules [86, 89]. Crystalline Si and CIGS modules show similar efficiency variation with irradiance, while the efficiencies of CdTe and a-Si modules remain more or less constant under low-light conditions [90].

1.2.4.2 Module temperature

The module temperature is one of the most important parameters affecting the power output of PV modules. The efficiency of c-Si modules decreases with increasing temperature, while thin-film modules show a less predictable trend, with additional dependence on the operating histories [91]. The effect of temperature originates from the semiconductor properties, whereby the bandgap decreases with increasing temperature. With decreasing bandgap the short-circuit current increases slightly, since lower-energy photons may excite an electron across the bandgap. However, with the decrease in bandgap, the quasi-Fermi-level splitting also decreases, hence the V_{OC} of the device decreases [2]. The decrease in voltage is inversely proportional to the increase

in temperature, while the increase in current is only logarithmically proportional to the increase in temperature [1]. Thus, the V_{OC} effect dominates and the net effect is a reduction in PV efficiency.

The temperature sensitivity of a solar cell depends on its open-circuit voltage [92]. Solar cells with a higher V_{OC} are less affected by temperature. As an example, HIT modules show a lower temperature dependence with a correspondingly higher open-circuit voltage [93].

Temperature coefficients are widely applied to yield and performance ratio predictions for PV systems. Conventional PV performance analysis software (for example PVsyst [94] and PV*SOL [95]) use fixed temperature coefficients over all irradiance and temperature ranges. However, the dependence of the temperature coefficient on irradiance and module temperature is not well studied and remains a controversial topic [96-99]. Power temperature coefficients γ measured indoors at 1000 W/m^2 (as given on product datasheets) are always negative, meaning an increase in temperature leads to a reduced power output. Interestingly, the magnitude of the γ is not always confirmed outdoors, with significant differences between technologies, and even positive coefficients reported in some cases (e.g., a-Si) [100]. Thus, further investigation on this topic is required.

1.2.4.3 Spectrum

For most solar cell measurements, the spectrum is standardised to the AM1.5G spectrum (as defined and tabulated in IEC standard 60904-3 [101]) to allow comparison of photovoltaic devices from different manufacturers and measured with different solar simulators. Hence most solar cells are optimised

according to the AM1.5G spectrum. However, the outdoor spectrum is also a variable and location-dependent parameter.

The Air Mass (AM) in the "AM1.5G" is the path length that light goes through the atmosphere normalized to the shortest possible path length when the sun is directly overhead (see Eq. (1.3)) [2].

$$AM = \frac{1}{\cos\theta} \tag{1.3}$$

where θ is the zenith angle. When the sun is directly overhead, the Air Mass is 1.0.

The Air Mass relates the reduction in the power of sunlight to the absorption and scattering by air and dust as it passes through the atmosphere [102]. AM1.5 was chosen because it represents the average air mass (AM) at solar noon for optimally tilted PV arrays at latitudes in the continental USA. For a specific location, a higher air mass corresponds to a red-shifting of the solar spectrum and vice versa [103-105]. Besides air mass, the spectral distribution is also influenced by other meteorological factors such as the relative humidity and the aerosol content of the air [106].

The influence of spectral irradiance distributions has been studied widely in mid-latitude regions [78, 107-109], e.g., the performances of a-Si and multi c-Si modules on the basis of two-year accumulated outdoor data in Japan [110]. The results show that the efficiency difference of the a-Si module between summer and winter was about 15%. Studies from the same group calculated the average photon energy (APE) and compared the influence of spectrum and temperature on the performance of a-Si and multi c-Si [111]. The results indicate that the output energy of a-Si modules depends more on the spectral distribution and is less sensitive to the module temperature than for multi c-Si

modules. Another study showed that a micromorph silicon module was highly spectrally sensitive compared to multi c-Si modules installed under the same conditions [112]. A linear relation between the average photon energy and the energy yield of a-Si modules was found in Thailand, and the authors suggested that a-Si PV modules might be better suited for tropical climates considering the blue-rich spectrum [113].

1.2.4.4 Incident angle

PV modules are rated under standard test conditions (STC) with normally incident light, while under outdoor conditions photons arrive on a PV module surface at various angles. Irradiance coming at high angles of incidence can be reflected significantly from the module's front surface and depends, to some extent, on the surface type and soiling [114, 115]. On the other hand, for thin-film modules with very thin absorber layer, large incidence angles caused by diffuse light can lead to longer optical path length in the solar cells and therefore better light absorption [116]. The effect of the incident angle on the PV performance in Singapore was studied and a theoretical annual angular loss of 3.3% was calculated [117]. Since in the measurement setups of this work a c-Si irradiance sensor is used to measure the in-plane irradiance, it is reasonable to assume that the irradiance sensor and the test modules experience similar angular loss. Thus, angular loss is not considered further in this work.

1.3 Considerations for PV modules operating in the tropics

Although PV has been widely applied and studied in temperate climates, very little scientific work has been carried out on how the modules perform in

tropical regions. Literature studies indicate that the performance of PV modules is very location dependent [118], and specifically is a function of the operating conditions and environmental factors such as irradiance intensity and spectrum, ambient temperature, and humidity. Due to its geographical location near the equator, Singapore's climate is characterized by constantly high ambient temperatures (daily variation between 25 and 33 °C), high humidity (mean annual relative humidity 84.2%) and abundant rainfall (annual average 2156 mm) [119]. Unlike in temperate climates, the module temperature in Singapore will never go below 25°C (STC temperature). The lowest module temperature observed at noon time is around 30°C, which incurs under fast-changing irradiance. The highest module temperatures can be up to 70°C [120]. The irradiance intensity varies substantially during the day because of differences in cloud coverage. In addition, the solar spectrum deviates from the standard spectrum (AM1.5G). Thus the operating conditions of PV modules in tropical Singapore are highly variable during the day. Located close to equator (1° north), the irradiance and ambient temperature at solar noon are not varying significantly throughout the year.

The long-term reliability of PV modules is another consideration for PV applications in tropical regions. Most markets require that c-Si module manufacturers qualify their modules according to international standards, such as IEC 61215 [121] for c-Si modules or IEC 61646 for thin-film modules [122]. These standards prescribe stress tests to accelerate failure mechanisms identified during historical outdoor exposure. The standard tests specify, for example, 1000 hours of damp heat exposure at 85°C and 85% relative humidity. The stress tests in the standard are designed to identify and detect

early failure mechanisms [123]. Some studies claim that c-Si modules would last for 15 to 20 years in a fairly moderate climate, if they had initially passed IEC 61215 [124]. However, according to field aging tests, passing the standard tests does not necessarily indicate good long-term reliability under outdoor operation [125]. Sometimes, a product that has passed the test can degrade faster (compared to those not passing the test) under outdoor monitoring [126]. In addition, the assumption that the tests are valid to identify previously identified failure mechanisms for the various module technologies may not always be the case. For thin-film modules (a-Si, CIGS and CdTe) that generally use a transparent conductive oxide (TCO) at the front surface of the cells, the reliability of the TCO might play an important role in the field [127, 128]. Many studies reported on the corrosion of TCO under accelerated damp heat tests [126, 129-131]. It was found that the electro-migration of sodium atoms from the glass is the root cause for the degradation of the TCO layer. The degradation is accelerated if the modules are under negative voltage bias. BP Solar successfully identified the potential TCO delamination problem of a newly developed product by applying a bias voltage during the standard damp heat tests [125]. Field studies are necessary to identify the different failure mechanisms of different PV technologies, followed by an amendment of the testing procedures for truly reflecting the module degradation modes [132].

As mentioned earlier in this section, the ambient temperature and the relative humidity in Singapore are constantly high. When a module is operating under high stable irradiance, the module temperature can reach 70°C. High temperatures are the root-cause of several failure (or degradation) modes of PV modules [133, 134]. Elevated temperatures increase stresses associated

with thermal expansion and trigger temperature-related chemical degradation processes [126]. High relative humidity also accelerates the degradation of power output of PV modules [135, 136]. It is thus reasonable to consider that PV modules operating in the tropics might show a higher degradation rate compared to modules deployed in temperate climates. For its CdTe modules, First Solar recommended degradation modelling with -0.5%/year for temperate climates and -0.7%/year for hot climates, considering that heat increases the impurity diffusion and leads to faster degradation [137, 138].

1.4 Thesis aims and objectives

This PhD work aims to study the performance of PV modules of various technologies in a tropical climate. A main objective is to understand the impact of tropical operating conditions (e.g., constantly high ambient temperature and humidity, fast-changing irradiance conditions, blue-shifted spectrum) on the performance of different module technologies. Another key task is to define the proper conditions to standardize PV module performance measurements across different PV technologies for benchmark comparisons in tropical regions.

To achieve these goals, outdoor monitoring tests were conducted, together with rigorous indoor measurements. For outdoor monitoring, the methodology was to continuously record the module current-voltage characteristics (I-V curves) at regular intervals. At the same time the in-plane solar irradiance and the temperature of the module's rear surface was logged. The monitored data are analysed systematically and statistically for each individual environmental factor. For indoor measurements, special attention was paid to the accurate measurement of the spectral response of different PV module technologies.

Some of the results in this thesis were presented at international conferences and published in peer-reviewed journals. A list of the publications arising from this thesis is given in Appendix A.

1.5 Thesis outline

The remainder of this thesis is organized as follows:

Chapter 2 focuses on the spectral response of full-sized PV modules. The spectrum in the tropics is usually blue-shifted compared to the AM1.5G spectrum. In order to determine how this non-standard spectrum affects the performance of different PV module technologies, the spectral response (SR) of the various module technologies was analysed, using both simulation and experimental methods. Circuit simulations illustrate the impact of the series interconnection of the individual cells within the module to the module SR. Measurements of module spectral response using the full-sized illumination method are given, including a detailed uncertainty analysis. Spectral mismatch correction factors are calculated based on the measured module SR. Spectral correction to indoor characteristic measurement is discussed.

Chapter 3 starts with a review of studies on the effects of the solar spectrum on the module performance. The solar spectrum in Singapore is measured and analysed. Thereafter the effects of the non-standard spectrum on the module performance are investigated on an annual basis, a monthly basis, and for an averaged day. The results obtained from the present study are compared to those of prior studies, and special attention is paid to the severe haze events occasionally observed in Singapore during the forest burning season in neighbouring countries.

Chapter 4 focuses on the fast-changing irradiance in the tropics and its effect on PV module performance. The distribution of fast-changing irradiance is studied statistically based on the duration of stable irradiance. The influence of the fast-changing irradiances on the short-circuit current (I_{SC}), module temperature, and efficiency of different technologies are analysed.

Chapter 5 focuses on the effects of module temperature on the module power output. The dependence of the temperature coefficient on irradiance and module temperature remains a controversial topic. This chapter thus starts with a discussion of the temperature coefficient. A mathematical method based on the one-diode model is proposed to extract the temperature coefficient of power from measured outdoor data. The dependence of the temperature coefficients on irradiance and temperature is studied. Then, the module operating temperature in the tropics is presented. The chapter ends with calculations of the annual power loss due to the high operating temperature.

Chapter 6 presents the performance assessment of PV modules operating in the tropics over a three-year continuous monitoring period. The in-field degradation rate of various PV module technologies is investigated. First, a statistical method to decompose the trend and the seasonal components of a data set is introduced. Then the degradation trend of the performance ratios of the monitored modules operating in tropical Singapore is extracted using the statistical decomposition method. The degradation of individual I-V curve parameters is also analysed. Seasonal performance variations are found to be minimal for modules operating in Singapore.

Chapter 7 discusses the typical operating conditions of PV modules in tropical Singapore, including irradiance level, irradiance spectrum, and module temperature. Based on the experimental and theoretical analysis of this work, “Tropical Test Conditions” (TTC) are defined, which enable a standardised performance comparison across different PV module technologies in tropical regions.

Finally, the conclusion chapter summarizes the main scientific contributions of this work.

Chapter 2 Study of the spectral response of full-sized PV modules*

Spectral response (SR) measurements at the solar cell level are well established and understood [76, 114, 139-143]. However, at a PV module level they are not yet fully understood and the standard measurement procedure is still under development. This is because the SR measurement of PV modules has a higher complexity, owing to the fact that they consist of series-connected cells, which may have different SRs and often are additionally connected to bypass diodes. Complications arise because (1) the series interconnection itself will influence the measurement, and (2) there is to date no steady-state high-intensity monochromatic light source available for full-area module illumination. The existing IEC standard 60904-8 [144] describes different experimental setups (i.e., monochromator, filter wheel and pulsed flash-light) to measure the SR of a PV module, but the impact of series interconnection to the module SR is not discussed. Additional standards for an adequate measurement procedure to determine the SR of a PV module are still under discussion [145-148]. In this chapter, the spectral response of full-sized PV modules is studied thoroughly by both simulations and experiments.

2.1 Simulation

2.1.1 Methodology

* The work described in this chapter is based on the publication "On the spectral response of PV modules," *Meas. Sci. Technol.* **25** 095007 DOI:10.1088/0957-0233/25/9/095007. The circuit simulation work is mainly done by Siyu Guo.

To study the influence of the series interconnection of cells in a PV module on the module SR, numerical computer simulation was conducted on how shunt resistances and bypass diodes affect the resulting module SR.

A typical silicon wafer-based PV module usually consists of 60 solar cells connected in series with 3 bypass diodes, see Figure 2.1. A typical thin-film PV module, such as a single-junction a-Si module, usually consists of more than 100 solar cells connected in series without bypass diodes. The shunt resistances R_{Shunt} within a thin-film module are usually much smaller (half or less) compared to those of wafer-based modules [149, 150].

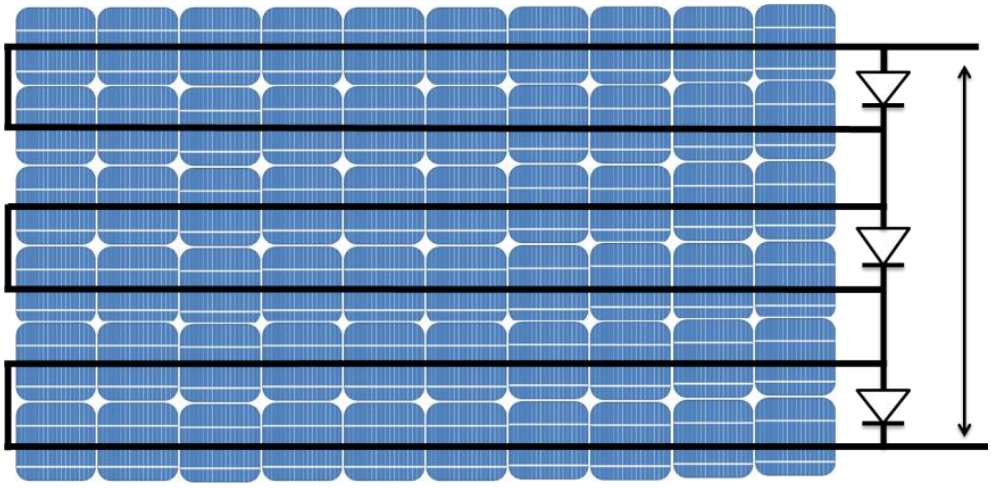

Figure 2.1: Sketch of a typical silicon wafer-based c-Si module as used in the simulation.

If all solar cells within the module are identical, the SR of the PV module would be the same as the SR of the individual cells. However, under realistic conditions, the solar cells within a PV module will have different properties and thus there is a spread in the cell SRs. This will influence the spectral response of the PV module.

The R_{Shunt} of the cells and the bypass diodes of the module can affect the operation point of the cells within the module and thus might also influence the spectral response of the PV module. As described below, individual cells

with high R_{Shunt} values will have a pronounced influence on the resulting module SR. Thus in the simulation study, a silicon wafer-based module (exhibiting higher R_{Shunt} values than thin-film modules) was chosen.

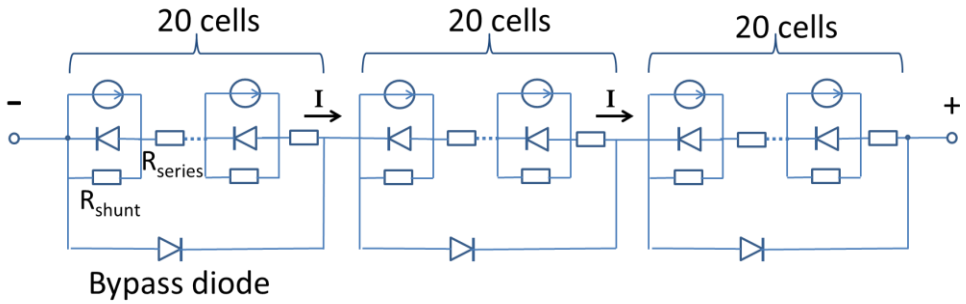

Figure 2.2: Sketch of the circuit simulation model of a silicon wafer-based PV module based on the one-diode model.

In order to test how the individual cell spectral responses, their shunt resistances and the bypass diodes influence the spectral response of a PV module, circuit modelling using the LTSPICE simulation software was conducted [151]. The corresponding circuit model of a wafer-based PV module is shown in Figure 2.2. The circuit model is based on the one-diode model (see Equation (2.1)) describing the individual cells within the module, including a current source, a shunt resistance and a series resistance. The reverse saturation current I_0 for all cells is set to 1×10^{-10} A and the cell area is assumed to be 156 mm × 156 mm. As cells are connected in series, variation of the series resistance of individual cells can be accumulated as a lumped series resistance of the whole module and will not affect the module SR. Thus the series resistances of all cells are specified by the same value of 0.24 $\Omega\cdot cm^2$, and only the shunt resistances (and the SRs) of the cells are varied statistically. The light-generated current I_L is assumed to be equal to the short-circuit current I_{SC} (see Equation (2.2)), and the I_{SC} of individual cells within the

module under monochromatic illumination is specified by the given spectral response of this cell as described in the IEC standard 60904-7 [152].

$$I = I_L - I_0\, exp\left[\frac{q(V + IR_{series})}{n\, kT}\right] - \frac{V + IR_{series}}{R_{shunt}} \tag{2.1}$$

$$I_L = I_{sc} = A \cdot \int SR(\lambda) \cdot E_{mono}^{ideal}(\lambda) \cdot d\lambda \tag{2.2}$$

where I_0, n, k, T, A are the reverse saturation current, the ideality factor, the Boltzmann constant, the cell temperature and the cell area and $E_{mono}^{ideal}(\lambda)$ is the ideal monochromatic spectral irradiance according to the standardized global solar spectrum (AM1.5G).

First, PC1D (a standard computer programme for semiconductor solar cell simulation [153]) is used to simulate 60 slightly different cell SRs by varying individual solar cell parameters (thickness of front AR coating (68 to 73 nm) and front texture angle (56 to 58 nm)) with uniform distribution. The short-circuit currents (I_{SC} in Equation (2.2)) for the individual cells under the same monochromatic illumination intensity (corresponding to the AM1.5G solar spectrum) are simulated using PC1D. In a second step, the individual cell I_{SC} are used as input parameters within the circuit model in LTSPICE to calculate the resulting module current $I_{sc}^{Test}(\lambda)$ under zero external bias. The spectral response of the module can then be calculated according to

$$SR(\lambda)^{Test} = \frac{I_{sc}^{Test}(\lambda)}{A \cdot G_{mono}^{ideal}(\lambda)} \tag{2.3}$$

where $G_{mono}^{ideal}(\lambda)$ is the ideal monochromatic radiation of the AM1.5G solar spectrum at wavelength λ.

Four scenarios of shunt resistances R_{Shunt} are assigned to the network in order to study how shunt resistances affect the resulting module SR: (1) idealized case: all cells have an infinite shunt resistance; (2) all cells have a high realistic shunt resistance of 250 kΩ·cm^2; (3) all cells have a low realistic shunt resistance of 1.7 kΩ·cm^2; (4) 59 cells have a low shunt resistance of 1.7 kΩ·cm^2 but one cell has a high shunt resistance of 250 kΩ·cm^2. Typical values for area-normalized shunt resistances are in the magnitude of MΩ·cm^2 for laboratory-type solar cells and kΩ·cm^2 for commercial solar cells [154, 155]. Thus 1.7 kΩ·cm^2 is a reasonable value for low shunt resistances, as well as 250 kΩ·cm^2 for high R_{Shunt}. The reason to show these four cases is that they have covered, and can explain, all realistic conditions, as we will discuss in the later section. For each condition, the SR of the module with and without bypass diodes was calculated.

2.1.2 Results

2.1.2.1 Idealized case: module with infinite shunt resistances

A spectral response is usually measured at zero voltage bias across the module. If no bypass diodes are used, the current passing through each cell must be the same due to the series connection. Current mismatch causes some cells to work under voltage bias other than short-circuit conditions. Cells with lower I_{SC} operate under negative voltage bias (i.e., reverse bias). This can be as high as -25 V for a module consisting of 60 cells in serial connection (shown later in Figure 2.6(a), where current matching is sketched for two cells for illustration). Assuming infinite R_{Shunt} values, the I-V curve of the cell with minimum I_{SC} is "flat" even under high negative bias, so the short-circuit current of the module is equal to that cell's I_{SC}. Thus for every wavelength of

light applied, the module current must be the minimum I_{SC} of all the individual cells. Correspondingly, for each wavelength, the SR of the module is the minimum of all cell SRs, see Figure 2.3. An increase of the response for wavelengths above 500 nm and below 1000 nm is obtained using bypass diodes, while below 500 nm and above 1000 nm the SR remains the same as the one without bypass diodes. The effect of the shunt resistance is much more pronounced under low illumination (as explained in Figure 2.4). Thus, under the low irradiance level, the reverse bias of the string with lower current is not high enough to activate the bypass diode. As the current increases, the bypass diodes are activated and thus transport additional current. The effect of bypass diodes on module SR is discussed in later section in more detail.

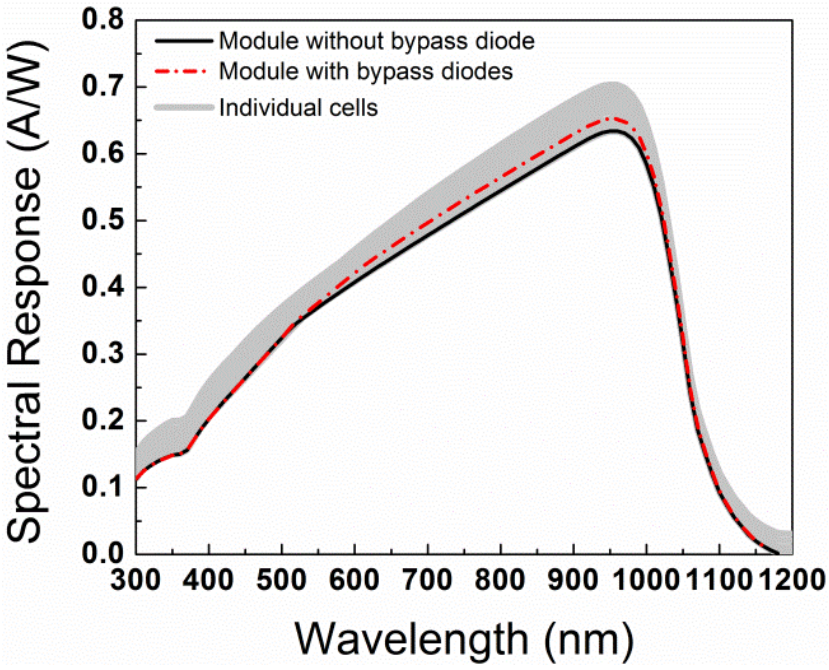

Figure 2.3: Simulated SR of a 60-cell PV module with (red dashed line) and without (black solid line) bypass diodes. Each cell has an infinite shunt resistance, but a slightly different SR. The SR curves of all individual cells fall into the grey band.

2.1.2.2 Influence of shunt resistances

Figure 2.4 shows the current-voltage curves of an individual solar cell, exhibiting either a high R_{Shunt} of 250 kΩ·cm^2 or a low R_{Shunt} of 1.7 kΩ·cm^2,

comparing 1-sun radiation (AM1.5G spectrum) to monochromatic radiation (400 nm light with an intensity of 50 W/m^2). Obviously, the effect of a low shunt resistance is much more pronounced under low radiation, which is the case during the spectral response measurement.

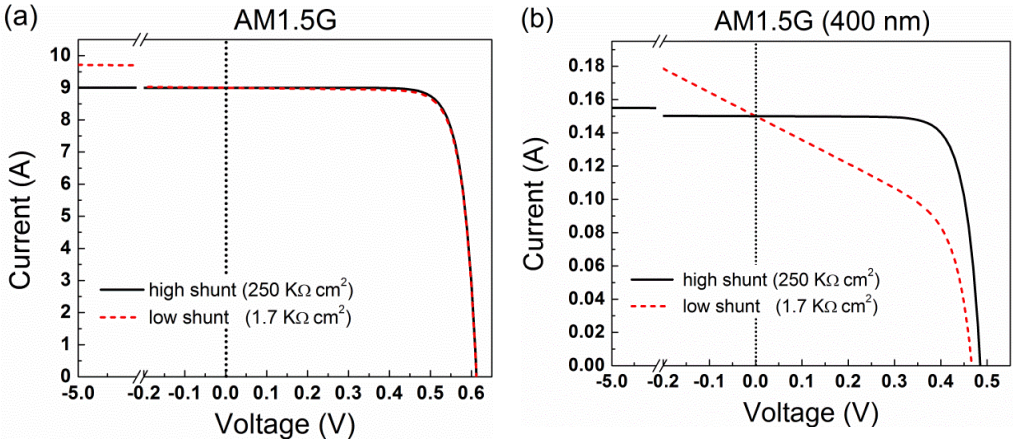

Figure 2.4: I-V curves of cells with high shunt resistance of 250 kΩ·cm^2 (black solid) and low shunt resistance of 1.7 kΩ·cm^2 (red dashed) under (a) 1 sun condition (AM1.5G solar irradiance) and (b) monochromatic illumination (400 nm light with an intensity of 50 W/ m^2).

When the shunt resistances are not infinite, the module SR is no longer the minimum of the cell SRs, see Figure 2.5. As discussed before, current mis-match causes some cells to operate under positive bias and some other cells to operate under negative bias (refer also to Figure 2.6). As can be seen in Figure 2.4, even a high realistic shunt value (R_{Shunt} = 250 kΩ·cm^2) still leads to significantly higher current at negative bias (i.e., at -5 V). When the module is illuminated with monochromatic light, the operating current of the current-limiting cell can be higher than its short-circuit current because of the negative bias applied to this cell, see Figure 2.4(b). Therefore, the resulting module current is no longer the minimum of the short-circuit currents of individual cells in the module.

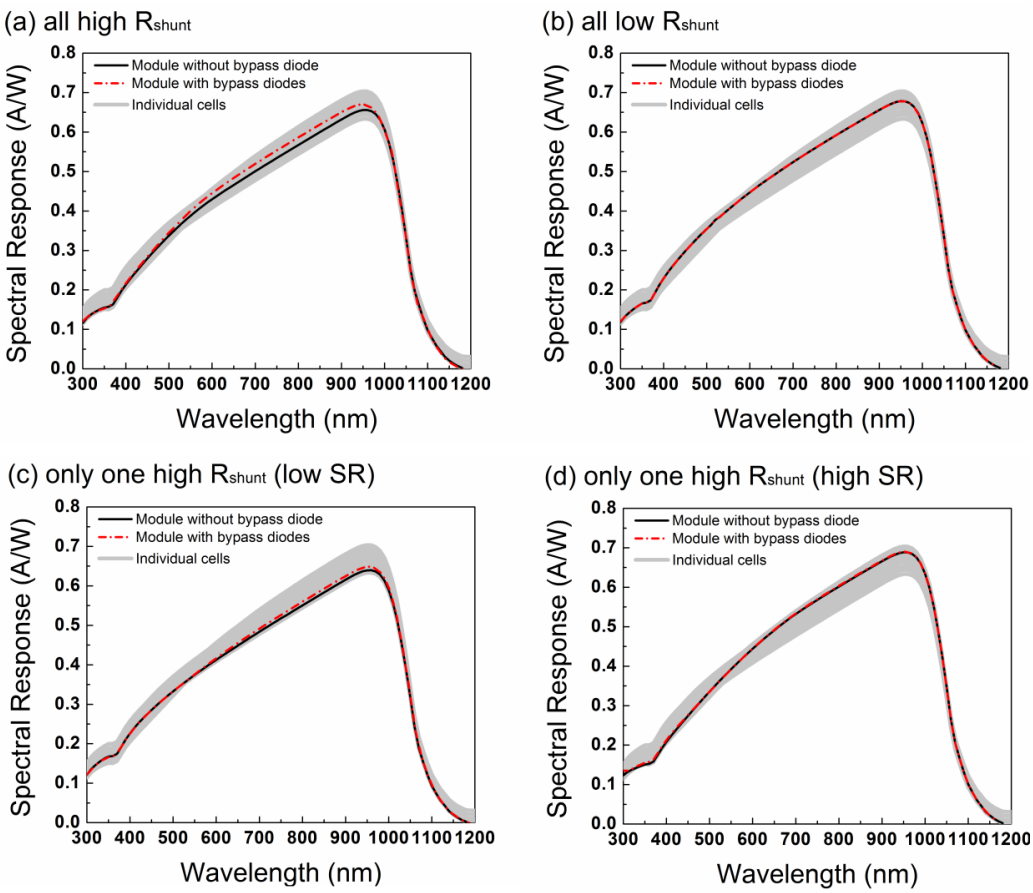

Figure 2.5: Simulated module SR of a silicon wafer-based module with (red dashed line) and without (black solid line) bypass diodes, consisting of 60 cells as sketched in Figure 2.1, exhibiting a slightly different SR. (a) Each cell has a high shunt resistance of 250 kΩ·cm^2; (b) each cell has a low shunt resistance of 1.7 kΩ·cm^2; (c) 59 cells have a low shunt resistance of 1.7 kΩ·cm^2, and 1 cell has a high shunt resistance of 250 kΩ·cm^2 and this one cell having a low SR in the wavelengths of 500 nm to 1000 nm; and (d) this one cell having a high SR in the wavelengths of 500 nm to 1000 nm. The SR curves of all individual cells are shown in grey.

If realistic low shunt resistances of R_{Shunt} = 1.7 kΩ·cm^2 are assumed for all cells, the module SR is now higher compared to the high shunt resistance case (see Figure 2.5(b)). The negative-biased cells allow transporting a higher current compared to the high shunt resistance case (compare Figure 2.6(a) to Figure 2.6(b)). Thus a higher module current can be transported, and the resulting SR is higher.

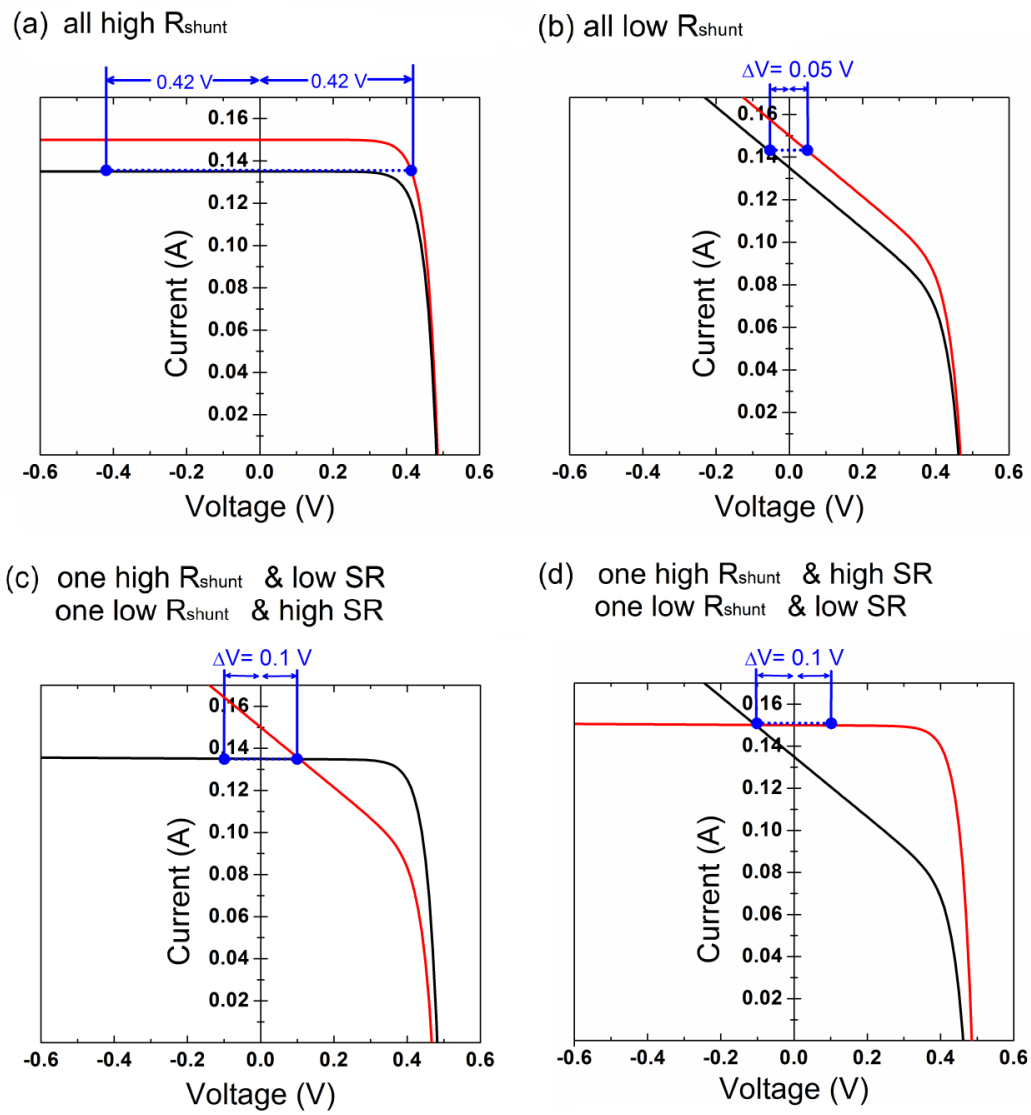

Figure 2.6: Current-voltage curves of two crystalline Si solar cells with different short-circuit currents due to different SR and (a) the same high shunt resistances; (b) the same low shunt resistances; (c) the cell with the low SR having a high shunt resistance and the cell with the high SR having a low shunt resistance; and (d) the cell with the low SR having a low shunt resistance and the cell with the high SR having a high shunt resistance. The corresponding operating points when the two cells are connected in series are indicated as blue points.

Cells with a high shunt resistance will dominate the resulting SR of the PV module. This is illustrated in Figure 2.5 (c-d), where we assume only one cell having a high R_{Shunt} in the module (all other cells are assumed to have low shunt resistance values). This cell is then always determining the SR of the module, irrespective of exhibiting a low SR (Figure 2.5(c)) or a high SR (Figure 2.5(d)). When the high shunt resistance cell has a low SR, it is

negative biased (see Figure 2.6(c)). When the high shunt resistance cell has a high SR, it is positive biased (see Figure 2.6(d)). In both cases, the operating points under series connection are determined by the "flat" region of the high shunt resistance cell (compare Figure 2.6(c) to Figure 2.6(d)). Thus the module current is determined by this cell.

The distribution of R_{Shunt} might also affect the module SR. The cases discussed in Figure 2.6(c) and Figure 2.6(d) are for two cells connected in series to explain the series-interconnection effect. If there are more cells connected in one string (such as 20 cells in this simulation study), more different cases should be considered. For Figure 2.6 (c), if more than half of the cells with low SR and high R_{Shunt}, the negative bias is shared so there is less negative bias for each cell. The operating point of the string tends to move towards the short-circuit conditions, and thus lower SR is expected. For Figure 2.6(d), if the proportion of the cells with higher Isc and R_{Shunt}, increases, the negative bias increases, and thus the operating point of the string moves towards higher current, resulting in a higher SR.

2.1.2.3 Influence of bypass diodes

Figure 2.7 shows the simulated I-V curves and operating points of two series-connected strings when they are illuminated with low intensity. Each of the strings comprises 20 cells with high R_{Shunt} (250 $k\Omega \cdot cm^2$). Assuming the two strings generate different photocurrents, if the strings are not connected with bypass diodes, the voltage bias resulting from the different photocurrents is very high (9.8 V); if bypass diodes are applied, the current difference is

compensated by the bypass diode connected to the string with lower current, and the voltage bias decreases to 0.42 V. Thus bypass diodes help to keep the voltage bias of the string within a small range.

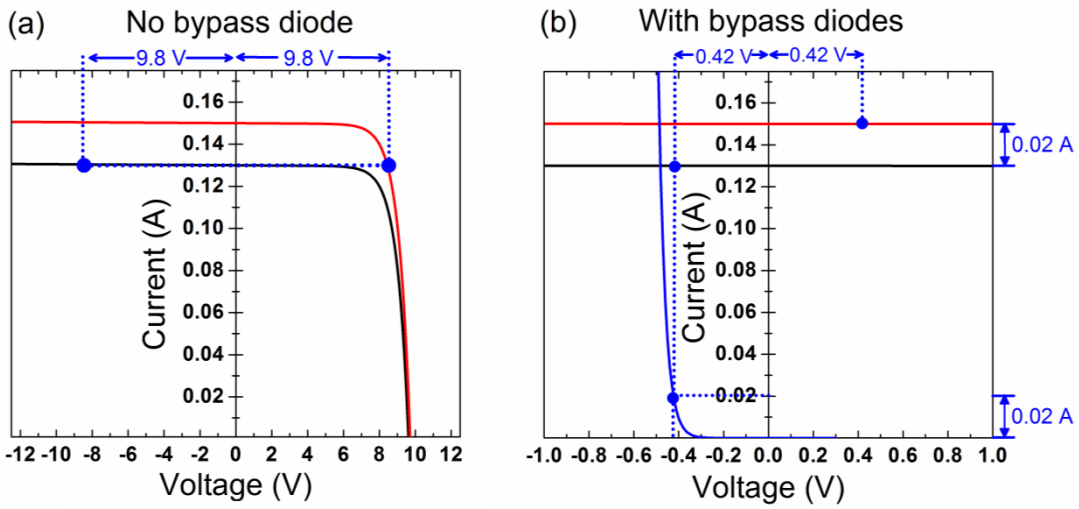

Figure 2.7: I-V curves of two strings, each with 20 silicon wafer-based cells connected in series, having different photocurrents. The red curve is the I-V curve of the string with the higher photocurrent, and the black curve is the one with the lower photocurrent. Blue points are the operating points when the two strings are connected in series (a) without bypass diodes and (b) with bypass diode (the I-V curve of the bypass diode is sketched as blue solid line).

As shown in Figure 2.5(b), if all cells have low R_{Shunt} values, there is no difference in the module SR with and without bypass diodes. This is because the negative voltage bias of the string with the lower current is not high enough to activate the bypass diode. However, if the current-limiting cells have high R_{Shunt} values (see Figure 2.3 and Figure 2.5(c)), the bypass diode of the string with the current limiting cell will be activated due to the highly negative voltage bias and thereafter transport additional current. Thus the module current is no longer limited by the string with the lowest current, and the module with bypass diodes shows a higher SR (compare Figure 2.5 (a) and (c)).

2.1.3 Summary of the simulation results

The spectral response of a PV module depends on: (1) the SRs of the individual cells, (2) the shunt resistances of the individual cells, and (3) the bypass diodes. Only when R_{Shunt} is infinite and no bypass diodes are used, the module SR is the minimum SR of all cells (for each wavelength). Realistic shunt values (in the order of 20 $k\Omega \cdot cm^2$) lead to a module SR which is somewhere between the minimum and maximum of all cell SRs. Without bypass diodes, cells with high R_{Shunt} will dominate the module SR. Bypass diodes only have an influence on the module SR if the shunt resistances of all cells are large. Modules using bypass diodes generally show higher (or equal) SR compared to the case of using no bypass diodes.

2.2 Experimental measurement

Ideally, the SR of a whole module should be measured by irradiating the module uniformly with a narrow-bandwidth light source at a series of different wavelengths covering its response range [144] with an irradiance (in W/m^2) similar to that of the standard AM1.5G reference solar spectrum, and measuring the module's short-circuit current at each of these wavelengths. The module SR (in Amperes per Watt) is then obtained by dividing the current densities by the irradiances at each wavelength measured [144]. However, currently such a high-intensity large-area uniform monochromatic light source is not readily available.

In reality, in order to measure the SR of a PV module, currently either (1) SR measurements of some individual cells within the module are performed (applying a monochromatic partial illumination on a small area of the module)

[140, 152, 156], or (2) an SR measurement of the whole module is performed (applying a pulsed full-area illumination, with band-pass filters to generate quasi-monochromatic radiation) [147, 157, 158]. As the partial illumination method measures the SR of some chosen cells within the module, an averaging procedure is needed to estimate the SR of the whole PV module. On the other hand, it is also of interest to measure the uniformity of SR among the component cells in a module and within a cell in a module. The full-area illumination method measures the SR of the whole module in a direct way. However, since it applies wide-bandwidth filters to generate high-intensity quasi-monochromatic radiation, uncertainty related to the wide bandwidth as well as to the spatial inhomogeneity of the quasi-monochromatic radiation will occur. At the Solar Energy Research Institute of Singapore (SERIS), the full-area illumination method is used to measure the SR of full-sized modules. The measurement uncertainty is studied for five modules with different technologies. The overview of this method is described in the following.

2.2.1 Full-area illumination method to determine the spectral response of PV modules

For full-area module measurements, usually a pulsed solar simulator is used to provide enough illumination intensity for a large area. Using a set of band-pass filters, high-intensity quasi-monochromatic radiation can be obtained to measure the SR of a PV module directly [147, 159]. However, the bandwidths of the band-pass filters have to be sufficiently wide to ensure a high enough intensity of the quasi-monochromatic radiation. This wide bandwidth can introduce large errors to the SR measurement [140]. Thus the conventional full-area illumination method has been improved by using a reference solar

cell (i.e., a calibrated crystalline silicon solar cell for which the SR is known), and the short-circuit current for the PV module as well as for the calibrated reference solar cell are measured under quasi-monochromatic radiation [160]. Doing so, the above stated errors can be considerably reduced as only the difference in the slope of the module SR and the calibrated cell SR contributes to the error, which is discussed in detail later.

Using a calibrated reference solar cell, the SR of the PV module is calculated as:

$$SR^{Test}(\lambda) = \frac{I_{sc}^{Test}(\lambda)/A^{Test}}{I_{sc}^{Ref}(\lambda)/A^{Ref}} \times SR^{Ref}(\lambda) \tag{2.4}$$

where $SR^{Test}(\lambda)$ is the SR of the module under test, $I_{sc}^{Test}(\lambda)$ and $I_{sc}^{Ref}(\lambda)$ are the measured short-circuit currents of the test module and the reference cell under quasi-monochromatic illumination. A^{Test} and A^{Ref} are the cell area of the test module and the reference cell, and $SR^{Ref}(\lambda)$ is the calibrated SR of the reference cell. A further advantage of this improved full-area measurement procedure is that the SR of the PV module is directly measured as absolute SR, by using a calibrated reference cell. Although the relative SR is enough for the calculation of the spectral mismatch factor [152], the absolute SR is helpful for the cell-to-module loss analysis and also for the improvement of module structure.

2.2.2 Test modules

Since the present setup in SERIS is not equipped with coloured bias light, it is not readily applicable to multi-junction modules. Thus, only single-junction modules are studied here. In this work, a wafer-based multicrystalline Si

module, a heterojunction crystalline Si module, a single-junction amorphous silicon (a-Si) module, a CIGS module, and a CdTe module were measured. The specifications of the five modules are listed in Table 2.1.

Table 2.1. Specifications of the five modules under test

Module technology	**Nominal power (W)**	**Module area (m^2)**	**Number of cells**	**Number of bypass diodes**
Multicrystalline Si	230	1.64	60	3
Heterojunction c-Si	210	1.26	72	3
Single-junction a-Si	60	0.95	108	0
CIGS	70	0.76	118	1
CdTe	75	0.72	116	0

2.2.3 Experimental setup

A pulsed solar simulator (PASAN IIIB) with a constant illumination intensity plateau of about 12 ms is used at SERIS to measure the I-V characteristics of full-size PV modules. Besides a lamp unit with its control unit, the setup also includes a thermostatic chamber for the measurement of temperature coefficients, and a set of filters for testing I-V curves at different irradiance levels [161]. The schematic is shown in Figure 2.8.

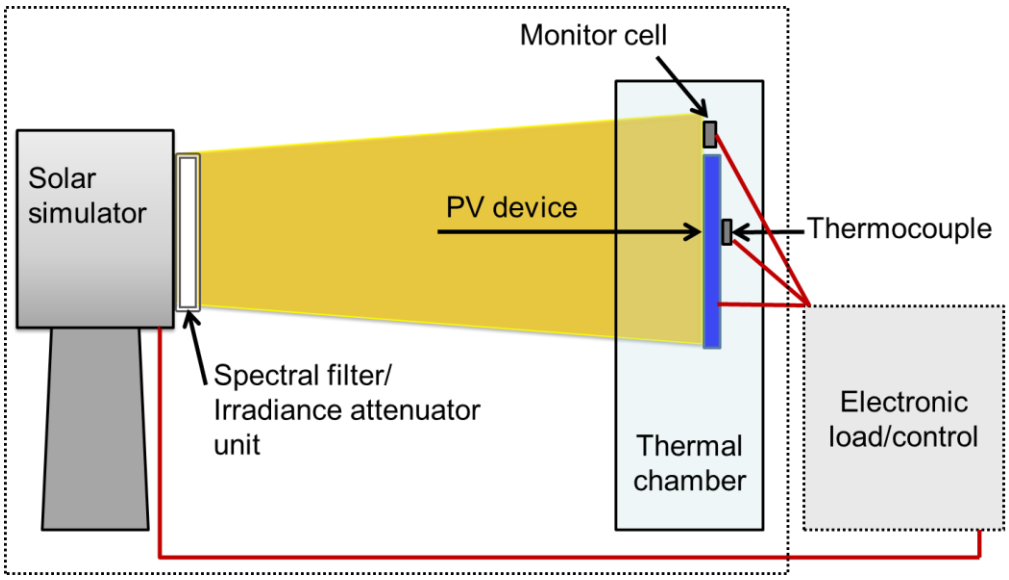

Figure 2.8: Setup for I-V curve and SR measurement.

The 15 quasi-monochromatic filters cover the 400 - 1100 nm range with approximately one filter per 50-nm wavelength interval, providing a quasi-monochromatic beam with a comparatively high light intensity over a large area. The width of the transmission band of the filters is about 100 nm (see later in Figure 2.11). Due to the large band-width of the filters, the quasi-monochromatic irradiance passing through the filters is comparable with the corresponding AM1.5G illumination filtered with ideal rectangular on/off filters of 50 nm bandwidth. Since spectral response is defined as the quotient of short-circuit current over the incident monochromatic light intensity using a narrow-bandwidth high-intensity light source [144], in principle no bias light is needed for this method. If the non-linear effect of the module SR is not negligible at this intensity, then either the intensity of the monochromatic light source used has to be increased to a level with the same order as the AM1.5G monochromatic illumination, or an additional bias light should be applied as described in [162]. The exact illumination intensity to be used depends on the non-linearity of the device itself [142]. The light source used in our setup

already provides quasi-monochromatic high-intensity radiation close to the AM1.5G solar spectrum (however with a lower spectral resolution, which will cause errors, see Figure 2.11, and the detailed uncertainty analysis as described later in this section). So the spectral response can be measured directly for linear modules (instead of measuring the differential spectral response via the bias light method). The linearity of the studied modules was confirmed by measuring the short-circuit current under different illumination levels as shown in Figure 2.9.

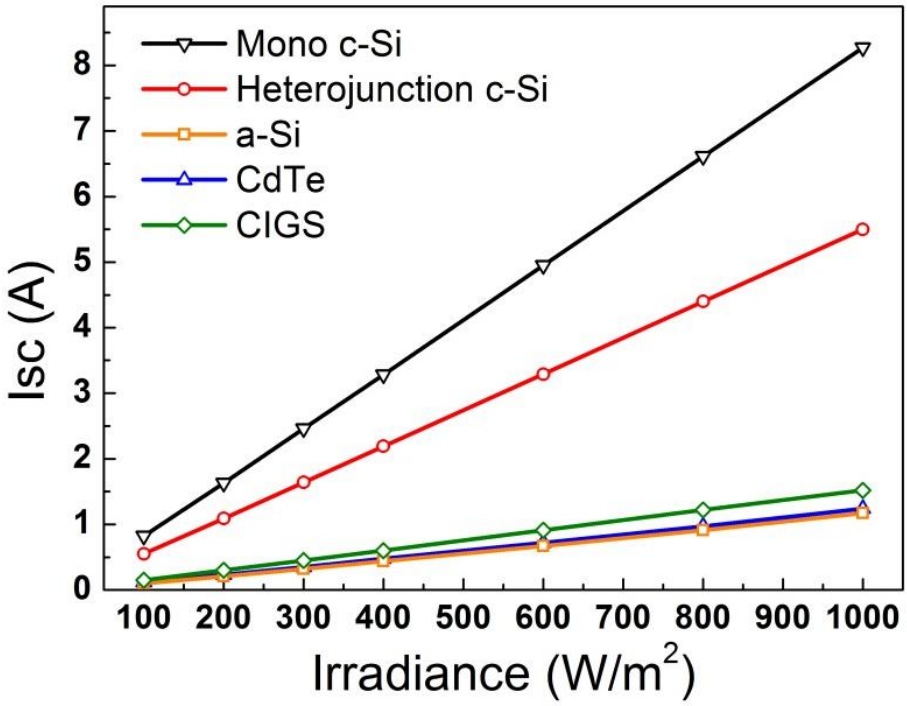

Figure 2.9: Short-circuit current vs. irradiance intensity of studied modules.

In the following, experimental details of the full-area illumination method established at SERIS are outlined.

2.2.3.1 Illumination intensity (time dependence)

The solar simulator for the full-area illumination SR measurement is a large-scale pulsed flash with the time dependent irradiance as shown in Figure 2.10. The stable irradiance plateau lasts for about 12 ms. The data acquisition,

which requires about 10 ms, occurs during the plateau period, whereby the light intensity varies by less than ± 1%.

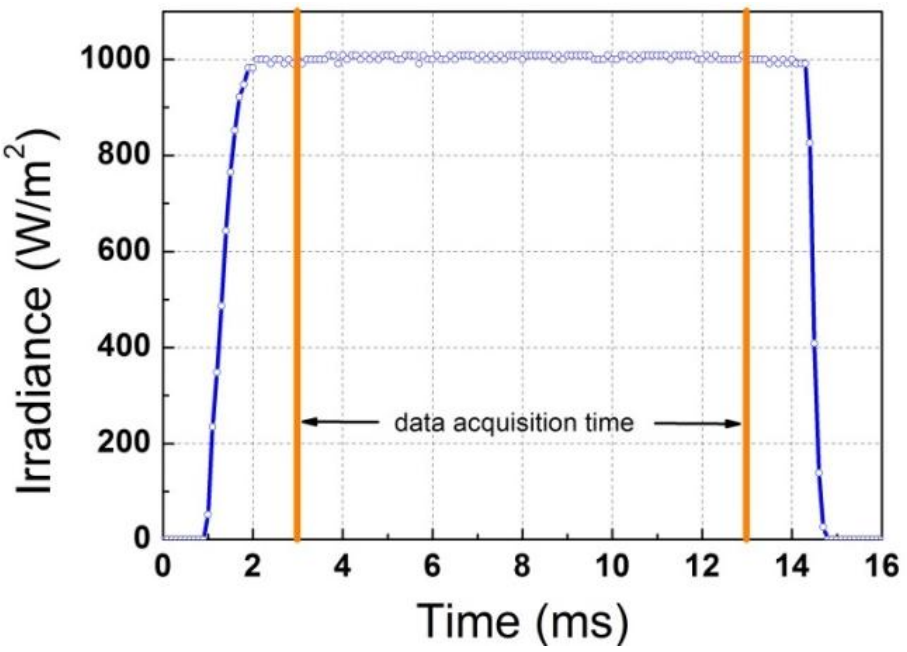

Figure 2.10: Irradiance of one large-area pulse versus time. During the data acquisition time (10 ms), the irradiance varies by less than ± 1%.

2.2.3.2 Spectral distribution

A spectroradiometer (Ocean Optics QEB1034 & NQ51A0200), which can accurately measure irradiance in the wavelength range from 300 to 1700 nm, was used to measure the spectral distribution of the light source and the spectral transmission of the 15 filters. The corresponding measured spectrum of the solar simulator with and without filters is shown in Figure 2.11. The spectral irradiance of the light source (flash) is close to the standard AM1.5G spectrum, as can also be seen from Figure 2.11. In order to ensure a high enough light intensity, the used quasi-monochromatic filters have a comparatively large bandwidth (defined as full width at half maximum (FWHM)) of around 50 nm, which corresponds to a spectral range of around 100 nm associated to each filter, see Figure 2.11. This bandwidth is much broader compared to the bandwidth of filters which are typically used for spectral

response measurements of solar cells (10 to 25 nm). In the following section it is discussed how this will affect the measured SR of the module (uncertainty analysis).

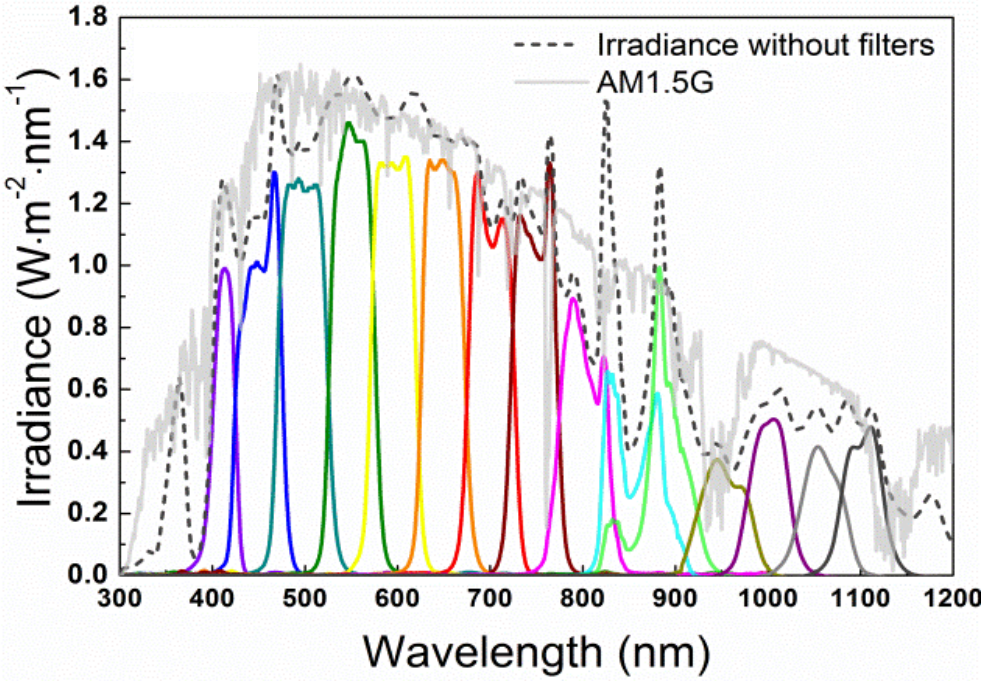

Figure 2.11: Spectral characteristics of the light source of the solar simulator (with and without quasi-monochromatic filters). The global AM1.5 spectrum is also shown for comparison.

Figure 2.12 shows the integrated irradiance from the light source passing through the filters compared to an ideal case where the standard AM1.5G spectrum and "ideal" rectangular on/off filters with a bandwidth of 50 nm are assumed. As can be seen, the integrated irradiance of the measured quasi-monochromatic flashed radiation is close to the ideal case at most wavelengths, except for 400, 450, 1000 and 1050 nm.

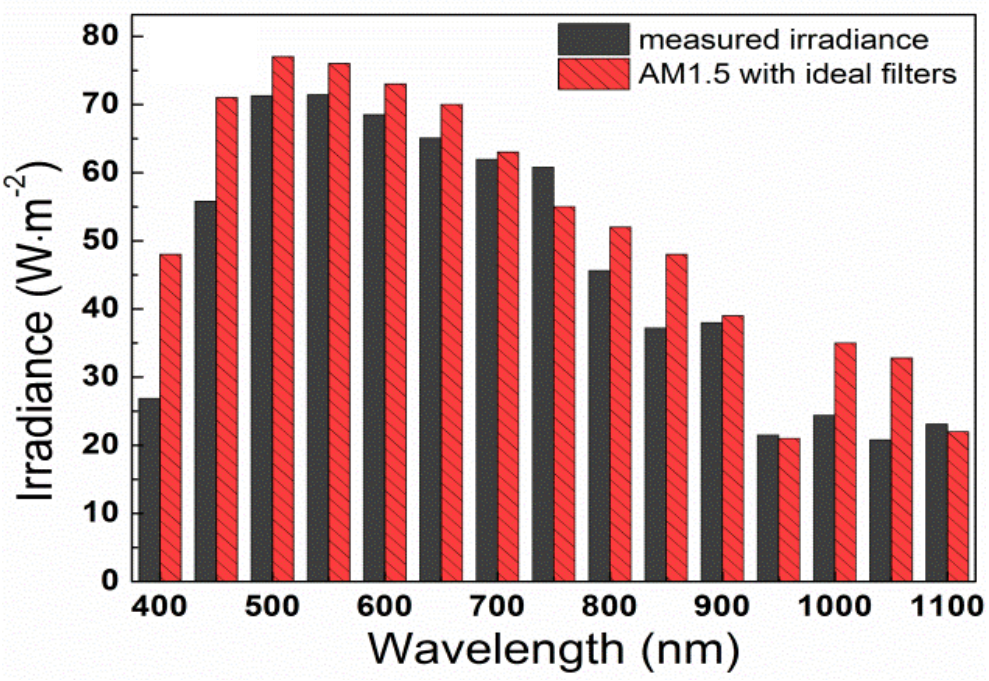

Figure 2.12: Integrated irradiance passing through the filters. The black bars represent the measured irradiance from the solar simulator using the actual filters. The red bars represent the ideal case (AM1.5G spectral irradiance with ideal rectangular on/off filters with 50 nm bandwidth).

2.2.4 Uncertainty calculations

An uncertainty analysis was conducted for the full-area illumination method established at SERIS. The calculation was conducted according to the "Guide to the Expression of Uncertainty in Measurement" [163]. The SR of the module under test is calculated from the measured short-circuit current of the tested module and the calibrated reference cell according to Eq. (2.4). Thus the relative uncertainty of the absolute SR measurement for the module under test is:

$$u\left(SR^{Test}(\lambda)\right) = \sqrt{u\left(\frac{I_{sc}^{Test}(\lambda)}{I_{sc}^{Ref}(\lambda)}\right)^2 + u(SR^{Ref}(\lambda))^2} = \sqrt{{U_{I_{sc}}}^2 + {U_{SR}^{Ref}}^2} \quad (2.5)$$

Two main contributions are involved in this equation: (1) a contribution stemming from the quotient of the short-circuit current measurements,

$U_{I_{sc}} \coloneqq u\left(\frac{I_{sc}^{Test}(\lambda)}{I_{sc}^{Ref}(\lambda)}\right)$, and (2) a contribution stemming from the known uncertainty of the calibrated SR of the reference solar cell $U_{SR}^{Ref} := u(SR^{Ref}(\lambda))$. $U_{I_{sc}}$ itself has a component that is derived from the spatial non-homogeneous irradiance (spatial uncertainty of I_{sc}), and another one from the different spectral responses of the test module and the reference cell in the finite bandwidth of the applied filters (spectral uncertainty of I_{sc}), as shown in (2.6). A monocrystalline Si cell calibrated in Fraunhofer ISE was used as the reference cell for this study. The SR calibration of the reference cell was based on the differential spectral response method, using a primary calibrated reference cell (traceability: PTB, Germany) to determine the irradiance level. The relative uncertainty of the calibrated SR of the reference cell is listed in Table 2.2.

Table 2.2: Standard uncertainty of the SR calibration of the reference cell [%].

Wave-length [nm]	**400**	**450**	**500**	**550**	**600**	**650**	**700**	**750**	**800**	**850**	**900**	**950**	**1000**	**1050**	**1100**
U_{SR}^{Ref}	**4.5**	**1.0**	**1.0**	**1.0**	**1.0**	**1.0**	**1.0**	**1.5**	**1.5**	**1.5**	**1.5**	**1.5**	**1.5**	**5.0**	**9.5**

$U_{I_{sc}}$ itself has three components: electrical, temperature, and optical [164]. In the following, the uncertainty components are calculated as the standard (k = 1) uncertainties expressed in %. The divisor of $\sqrt{3}$ is used for components with a rectangular probability distribution (temperature).

2.2.4.1 Electrical uncertainty

The short-circuit current for the calibrated c-Si reference solar cell are measured using the same instrument under the quasi-monochromatic

illumination. Due to the different magnitude of signal, different channels (0.1/0.3/1/3/10/30 A) were assigned for the I_{sc} measurement, for which the manufacturer guarantees the accuracy for each channel to be within ±0.2%. The reference cell measurement is using the 0.3 A channel, while modules are measured with either the 3 A or the 10 A channel. The accuracy transfers to a standard uncertainty of 0.077% assuming a 99% confidence level (k = 2.586), and thus the resulting standard electrical uncertainty for the I_{sc} ratio is within ±0.15%.

2.2.4.2 Temperature uncertainty

The temperature range during the SR measurement is 25.0 ± 0.5 °C. This results in the standard uncertainty of 0.289°C. Assuming the temperature coefficient for current to be 0.05%/°C at 25°C, the resulting uncertainty for current is calculated as follows:

$$0.5\%/°C \times \pm 0.289°C = \pm 0.14\%$$

Thus, the resulting standard temperature uncertainty is within ±0.28%.

2.2.4.3 Optical uncertainty

The optical uncertainty arising from the wide-bandwidth filters is discussed from two sides: the spatial non-homogeneous irradiance (spatial uncertainty of I_{SC}), and the different spectral responses of the test module and the reference cell in the finite bandwidth of the applied filters (spectral uncertainty of I_{SC}), as shown in (2.6):

$$U_{I_{sc}} = \sqrt{\left(U_{I_{sc}}^{spatial}\right)^2 + \left(U_{I_{sc}}^{spectral}\right)^2} \tag{2.6}$$

1) Uncertainty due to spatial non-homogeneous irradiance

Due to the different sizes of the reference cell and the module under test, spatially non-homogeneous irradiance will alter the quotient $\frac{I_{sc}^{Test}(\lambda)}{I_{sc}^{Ref}(\lambda)}$. To analyse the corresponding measurement error resulting from the spatial irradiance non-homogeneity, the irradiance intensity $U_{\emptyset}^{spatial}$ through each filter were measured with a c-Si reference cell at 9 positions (3×3) in the test area. Results are shown in Figure 2.13. The spatial uniformity of the flash light without filters at those 27 positions in the test area was also measured, and the uniformity is within ± 1%, indicating very good spatial uniformity of the light source itself.

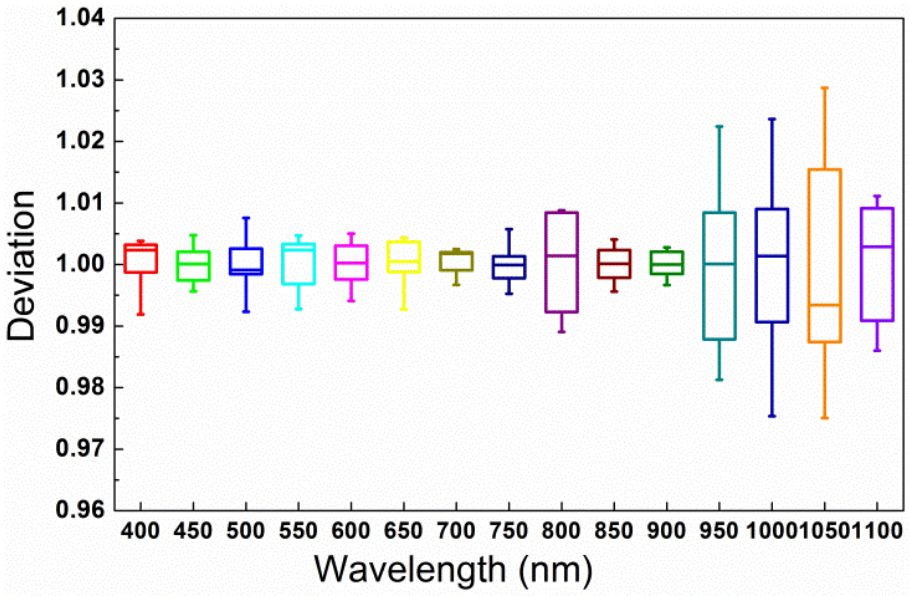

Figure 2.13: Measured spatial irradiance uniformity over the module testing area for all 15 filters. The whiskers denote the 10% and 90% values of the deviation. The 25% and 75% values are used as the bottom and top edges in the box charts, and the lines inside the boxes denote the median.

Slightly different photocurrents, corresponding to the measured spatial irradiance distribution, are assigned to 60 otherwise identical silicon wafer solar cells. The resulting short-circuit current of the module is then simulated

with the LTSPICE simulation software to calculate the uncertainty $U_{I_{sc}}^{spatial}$ according to Eq. (2.7):

$$U_{I_{SC}}^{spatial} = \left.\frac{I_{SC}^{Test}}{I_{SC}^{Ref}}\right|_{\lambda_o}^{homo} - \left.\frac{I_{SC}^{Test}}{I_{SC}^{Ref}}\right|_{\lambda_o}^{inhomo} \tag{2.7}$$

The above mentioned uncertainty quotient is evaluated under spatially homogeneous and inhomogeneous conditions. Simulation is conducted for different R_{Shunt} conditions and the largest uncertainty obtained is taken for $U_{I_{sc}}^{spatial}$.

2) Uncertainty due to finite bandwidth of filters

In spectral regions where the slope of the reference cell's SR is different to that of the module under test, absorbed photons within the finite bandwidth of the filters contribute differently to the measured short-circuit currents I_{SC}^{Ref} and I_{SC}^{Test}, thus the quotient $\frac{I_{sc}^{Test}(\lambda)}{I_{sc}^{Ref}(\lambda)}$ will be altered. The corresponding uncertainty stemming from the finite bandwidth of the applied filters $U_{I_{SC}}^{spectral}$ is calculated according to

$$U_{I_{sc}}^{spectral} = u\left(\frac{i_{sc}^{Test}(\lambda)}{i_{sc}^{Ref}(\lambda)}\right) = \left|\frac{\Delta\left(i_{sc}^{Test}(\lambda)\right)}{i_{sc}^{Test}(\lambda)} - \frac{\Delta\left(i_{sc}^{Ref}(\lambda)\right)}{i_{sc}^{Ref}(\lambda)}\right|$$

$$= \left|\frac{\frac{\partial SR_{Test}(\lambda)}{\partial\lambda}|_{\lambda_0}}{\int SR_{Test}(\lambda)\, E_{mono}^{filter}(\lambda)\, d\lambda} - \frac{\frac{\partial SR_{Ref}(\lambda)}{\partial\lambda}|_{\lambda_0}}{\int SR_{Ref}(\lambda)\, E_{mono}^{filter}(\lambda)\, d\lambda}\right| \int E_{mono}^{filter}(\lambda) d\lambda \;\; \Delta\lambda \tag{2.8}$$

$$\approx \left|\frac{\frac{\partial SR_{Test}(\lambda)}{\partial\lambda}|_{\lambda_0}}{SR_{Test}(\lambda_0)} - \frac{\frac{\partial SR_{Ref}(\lambda)}{\partial\lambda}|_{\lambda_0}}{SR_{Ref}(\lambda_0)}\right| \Delta\lambda$$

where $\Delta\lambda$ refers to the whole spectral range of the filters. $E_{mono}^{filter}(\lambda)$ is the measured quasi-monochromatic light intensity with the wide bandwidth filters as per Figure 2.11.

2.2.4.4 Total uncertainty of the full-area measurement method

The final expanded (k = 2) combined uncertainty of the SR measurement is listed in Table 2.3.

Table 2.3: Total uncertainty of SR measurement, with 95% confidence level [%].

Wave-length [nm]	**400**	**450**	**500**	**550**	**600**	**650**	**700**	**750**	**800**	**850**	**900**	**950**	**1000**	**1050**	**1100**
U_{c-Si}^{SR}	**9.0**	**2.0**	**2.0**	**2.0**	**2.0**	**2.0**	**3.0**	**3.0**	**3.0**	**3.0**	**3.0**	**3.0**	**3.0**	**10.0**	**19.0**
$U_{Het\ c-Si}^{SR}$	**9.6**	**2.5**	**3.3**	**2.1**	**2.1**	**2.1**	**2.1**	**3.1**	**3.1**	**3.1**	**3.1**	**3.1**	**3.1**	**10.1**	**21.2**
U_{a-Si}^{SR}	**9.0**	**2.0**	**2.0**	**2.0**	**2.0**	**2.1**	**3.6**	**4.5**	**7.0**	**8.3**					
U_{CdTe}^{SR}	**9.1**	**2.1**	**2.8**	**2.1**	**2.1**	**2.1**	**2.1**	**3.1**	**3.1**	**22.0**	**3.2**				
U_{CIGS}^{SR}	**9.7**	**2.5**	**3.3**	**2.1**	**2.1**	**2.1**	**2.1**	**3.1**	**3.1**	**3.1**	**3.1**	**3.1**	**3.1**	**10.1**	**21.2**

2.2.4.5 Results and discussion

Using the full-area illumination method with calibrated reference solar cell as outlined above, the absolute SR (in A/W) of the five types of PV modules under investigation were measured. The results are shown in Figure 2.14, together with the SR of the c-Si reference solar cell.

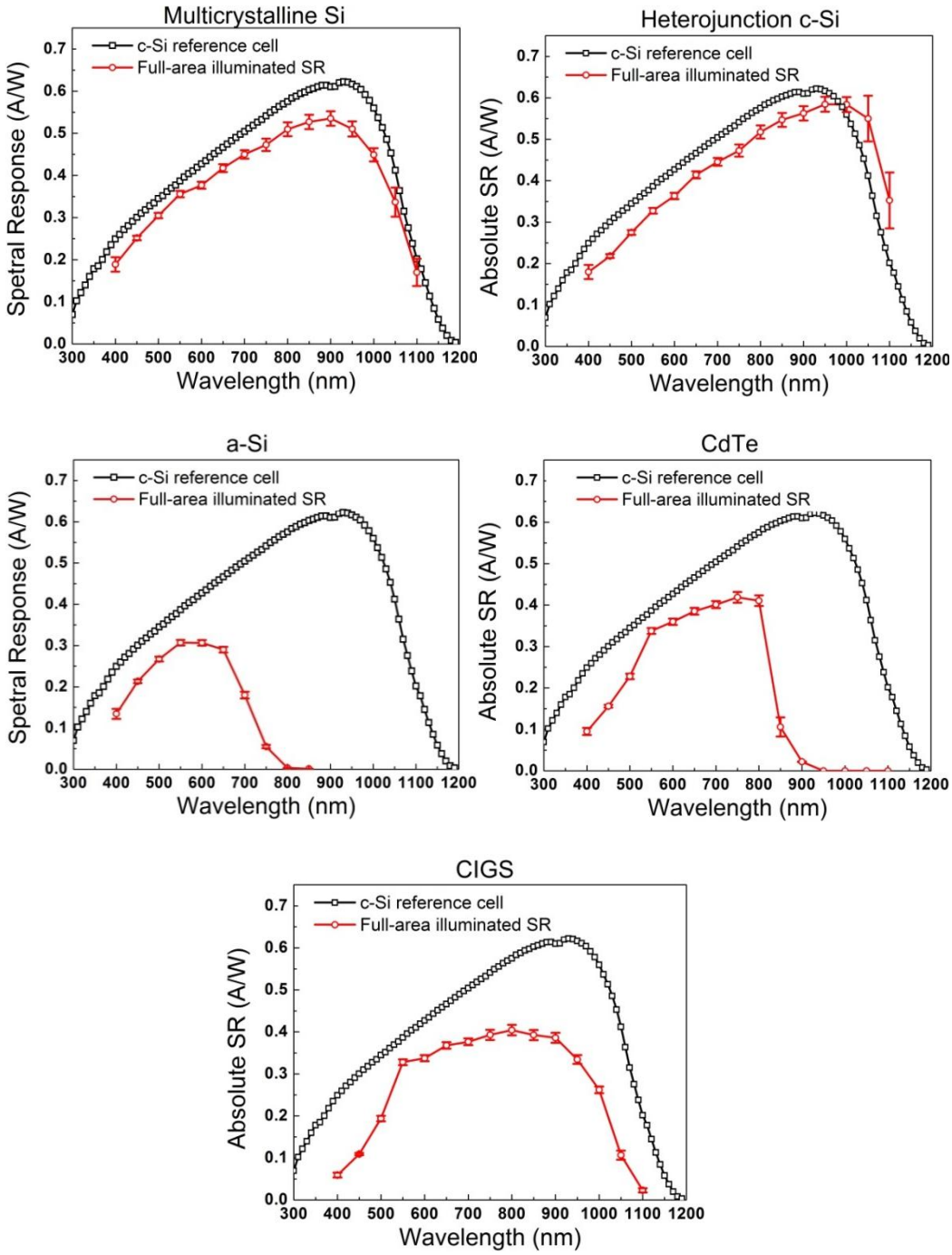

Figure 2.14: Absolute SR measurements of the five modules measured at SERIS with full-area illumination, together with the calibrated SR curve of the used c-Si reference solar cell. The error-bars were calculated as described in the previous sections.

Since a calibrated c-S- wafer solar cell was used as a reference cell in this study, if a wafer-based PV module is measured, the SR mismatch between the reference cell and the module under test is small (see Figure 2.14), as is the uncertainty caused by the wide bandwidth of the quasi-monochromatic filters.

The resulting total measurement uncertainty is then mainly determined by the uncertainty of the calibrated SR of the reference cell.

In contrast, if a thin-film module is measured, the SR mismatch between the c-Si reference cell and the measured module can be quite large at long wavelengths. This large difference leads to large measurement uncertainties related to the finite bandwidth of the quasi-monochromatic radiation. The more different the slopes of the SR of the calibrated reference cell and the SR of the measured module are, the larger is the error introduced by the band-width of the filters, see also Eq. (2.8). As a result, if the used calibrated reference cell has a SR that is similar to that of the module under test, the uncertainty caused by the wide bandwidth of the quasi-monochromatic filters can then be significantly reduced. For example, in case of measuring thin-film a-Si modules, a calibrated crystalline silicon reference cell covered with an additional band-pass filter (KG-3 or KG-5) could be used in order to adjust the reference cell's SR to that of the tested module. However, because of the small value at the tail after the steep decrease, the error introduced is not significant, and thus it is acceptable to use mismatched cells in this case.

2.3 Application of spectral response

This section discusses the application of spectral response for spectral mismatch correction. The correction to AM1.5G spectrum for solar simulator is presented.

2.3.1 Spectral mismatch

The spectral mismatch is a common source of error in irradiance measurements for PV. A spectral mismatch occurs when a PV device is rated

with respect to a standardized reference spectral irradiance [104, 143, 165-167]. The standard AM1.5G spectrum, which is commonly used to calibrate irradiance sensors, is seldom met in real-life conditions. This affects the irradiance measurements, as these are based on the spectral response of the sensor. For example, if the reading of a sensor measuring radiation with a non-standard spectral distribution is 1000 W/m^2, it means that the sensor generates the same output as it does under the standard spectrum of that intensity. However, a module with a different spectral response (such as a-Si) might not generate the same short-circuit current under these two spectra, even though the measured light intensity is the same. The short-circuit current of a PV module depends on both the spectral response of the module and the spectral distribution of the light within the module's active wavelength range. Therefore it is necessary to correct the irradiance intensity for the spectral mismatch. This requires for the calculation of the so-called mismatch factor (MMF). The following formula describes the MMF and all values that need to be measured (Taken from IEC standard 60904-7 [152]).

$$MMF = \frac{\int_{\lambda_1}^{\lambda_2} E_{AM1.5}(\lambda) SR_{ref}(\lambda) d\lambda \int_{\lambda_3}^{\lambda_4} E_{\lambda}(\lambda) SR_{DUT}(\lambda) d\lambda}{\int_{\lambda_1}^{\lambda_2} E_{\lambda}(\lambda) SR_{ref}(\lambda) d\lambda \int_{\lambda_3}^{\lambda_4} E_{AM1.5}(\lambda) SR_{DUT}(\lambda) d\lambda} \tag{2.9}$$

with:

$E_{AM1.5}$	AM1.5G spectral distribution
SR_{ref}	spectral response of reference cell
E_{λ}	realistic spectrum (solar simulator or real solar spectrum)
SR_{DUT}	spectral response of module under test
λ_1, λ_2	starting and end wavelength of the SR of reference cell
λ_3, λ_4	starting and end wavelength of the SR of module

Spectral mismatch can occur in both outdoor and indoor measurements. For outdoor applications, the MMF is applied to calculate the effective irradiance

intensity for various PV technologies, which will be discussed in Chapter 3. For indoor measurements, the MMF is applied to calibrate the intensity of the solar simulator to obtain the standard irradiance for the test device.

2.3.2 Spectral mismatch correction to AM1.5G for solar simulators

With the spectral responses of the modules and the reference cell (from calibration reports), and the spectrum of the solar simulator (measured by a spectrometer as shown in Figure 2.11), we can calculate MMF based on a c-Si reference cell by Equation (2.9). The derived mismatch factors are shown in Table 2.4.

Table 2.4. Mismatch factor (MMF) for the studied modules

	Multicrystalline Si	Heterojunction c-Si	a-Si	CdTe	CIGS
MMF	1.011	1.011	1.033	1.053	1.027

The intensity of the solar simulator is thereafter adjusted so that the reading of the c-Si reference sensor shows $G_{corrected}$ according to (2.10):

$$G_{corrected} = \frac{G^*}{MMF} \tag{2.10}$$

where $G_{corrected}$ is the irradiance reading of the reference sensor corrected for spectral mismatch, G^* is the standard irradiance reading (1000 W/m^2 for STC) of the reference sensor.

For the present setup used in SERIS, if a non-filtered c-Si reference cell is used for irradiance calibration, the spectral mismatch can introduce an error of 3.3, 5.3 and 2.7% for the a-Si single-junction module, the CdTe module, and the CIGS module, respectively. There are also a GaAs and a KG-3 filtered c-Si reference cell in SERIS, which are recommended for CdTe modules and

a-Si single-junction modules, respectively [169, 170]. Calculations of MMF with these two reference cells were conducted for the CdTe and the a-Si modules. Results show that for a-Si single-junction module, by using the KG-3 filtered reference cell, MMF reduces to 1.00. Although the SR of the GaAs reference cell is closer (compared to the non-filtered c-Si reference cell) to the CdTe module, 2% spectral mismatch remains (MMF = 1.020). The accuracy of power measurement for thin-film modules is improved by about 3% relative with spectral mismatch correction.

2.4 Conclusions

A thorough study was conducted on the spectral response of PV modules. It was found that the spectral response of PV modules depends on (1) the SRs of the individual cells, (2) the shunt resistances of the cells, and (3) the use of bypass diodes. A detailed measurement uncertainty analysis was conducted for the SR measurement setup in SERIS. For c-Si modules, the uncertainty mainly depends on the uncertainty of the calibrated reference cell used. For thin-film modules, the uncertainty depends additionally on the SR mismatch between the reference cell and the measured module. The application of spectral response to correct solar simulator intensity for the AM1.5G spectrum was discussed. For the solar simulator used in SERIS, the spectral mismatch error accounts for 3 to 5 % of the maximum power measurement uncertainty for different thin-film modules.

Chapter 3 Influence of irradiance spectrum on module performance in the tropics[*]

A lot of research work has been carried out to understand the performance of PV modules in outdoor operating conditions [171-176]. These results show that the actual performance often deviates from that at STC. Especially for thin-film modules, their stabilized performance depends significantly on the operating conditions. Starting from this chapter, this thesis will focus on the outdoor performance analysis of PV modules in the tropics. Following the previous chapter on the spectral response of PV modules, this chapter will study the effect of the local solar spectrum on the performance of various thin-film PV module technologies in tropical Singapore.

3.1 Effect of solar spectrum on module performance

Exceptionally high measured performance ratios of above 95% have been reported for amorphous silicon PV systems operating in tropical Singapore, while c-Si based PV systems are usually operating in the 80 - 90 % range [177]. Since the power output of amorphous silicon modules is particularly sensitive to the spectrum of the incident light, the high PR may be partly due to a spectral effect. The seasonal spectral variation under outdoor conditions has been studied widely in mid-latitude regions with various climates [78, 107-109, 178-181]. In regions with high latitude, the spectrum has a bias towards shorter wavelengths (more "blue-rich") in summer and towards longer wavelengths (“red” shift) in winter, compared to the standard AM1.5G

[*] The work described in this chapter is based on the publication “Effect of solar spectrum on the performance of various thin-film PV module technologies in tropical Singapore,” *IEEE Journal of Photovoltaics*, DOI:10.1109/JPHOTOV.2014.2328585

spectrum. Thus, the spectral effect on the energy yield of PV modules over the whole year is partially cancelled out, with the net spectral influence depending on the specific location [182]. However, in tropical regions with low latitude and only little variation of the air mass throughout the year (at solar noon) [183], seasonal variations of the spectrum are negligible. Therefore the spectral distribution can have a significant impact on the module performance, if a constant "blue-shifted" or "red-shifted" spectrum prevails all year round. Hence, this study aims to quantify the spectral effect on the performance of PV modules under the tropical climate conditions of Singapore.

Four different thin-film PV modules (single-junction amorphous Si, CdTe, CIGS, double-junction "micromorph" Si) are investigated. They are all commercial modules bought from the market. Figure 3.1 shows the relative spectral responses (obtained by scaling of the measured SRs (in A/W) so that the maximum SR value is unity) of the four PV modules studied in this work. The SR of a multicrystalline Si (c-Si) sensor for outdoor irradiance measurements is also shown for comparison. The SRs of the single-junction modules were measured with the full-area illumination method as described in Chapter 2. The SR of the micromorph module is taken from the literature [157].

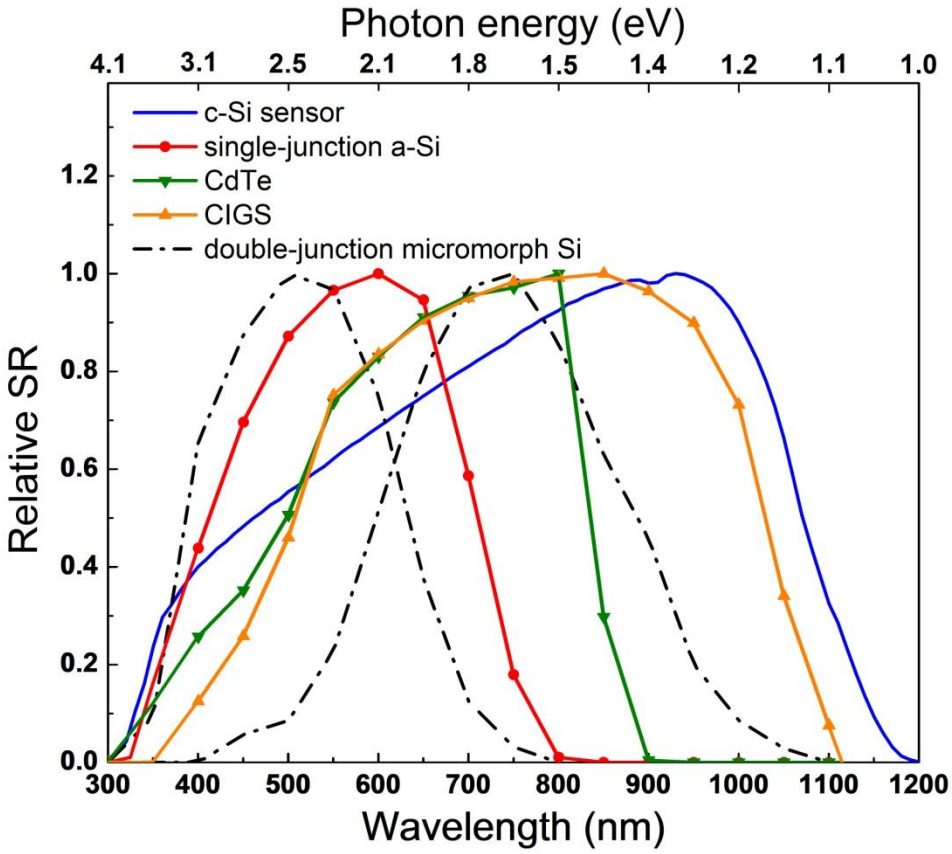

Figure 3.1: Measured relative SRs of the investigated single-junction PV module technologies (single-junction a-Si, CdTe and CIGS). Data before 400 nm and after 1100 nm are obtained with extrapolation. The SR curves for the top and bottom cells of the investigated double-junction micromorph Si technologies (dashed lines) are taken from the literature [184]. Also shown, for comparison, is the SR of a multicrystalline Si sensor.

3.1.1 Effective irradiance

As explained in Section 2.3.1, the non-standard spectrum of a light source can introduces error to the irradiance measurement, and therefore it is necessary to compensate the irradiance reading for the spectral mismatch. There are generally two methods to determine the effective irradiance intensity of the reference spectrum for a module based on either the spectral mismatch factor or the short-circuit current, as outlined below.

3.1.1.1 Spectral mismatch factor calculated from measured SR

The spectral mismatch factor (MMF), which was described in Chapter 2, is applied to adjust the intensity of an irradiance with a non-standard spectrum to the intensity the irradiance would need to have if it was of the standard spec-

trum in order that a test device will produce the same current under both irradiances.

If a pyranometer is used as the irradiance sensor, $SR_{ref}(\lambda)$ is equal to 1 over all wavelengths. The MMF then becomes the spectral factor (SF) according to Refs. [185, 186]. The spectral response of the reference device affects the value of the irradiance reading and the spectral mismatch factor, but the corrected irradiance reading to indicate the intensity of the AM1.5G spectrum is not dependent on the SR of the reference device. However, larger differences in SR between the reference sensor and the test module can lead to higher uncertainty in the calculation of MMF [187]. A c-Si reference cell was used in this study for the irradiance measurement.

Assuming a negligible effect of the operating conditions on the relative SR of each module, the real-time MMF can be calculated with the spectrum measured outdoors (every minute from 7:00 till 19:00) and the SRs of the modules and the reference sensor measured indoors. Thus the effective irradiance intensity (G') of the reference AM1.5G spectrum that generates the same short-circuit current in the test device as generated by the outdoor spectrum at the measured irradiance intensity (G) is given by [152, 188]:

$$G'_{MMF} = MMF \cdot G \tag{3.1}$$

where G' is the effective irradiance intensity and $G$is the in-plane irradiance intensity measured by an irradiance sensor, which is a c-Si reference cell in this study.

3.1.1.2 Spectral mismatch from measured short-circuit current

Another way to determine the effective irradiance intensity of the AM1.5G spectrum is based on the short-circuit current (I_{sc}) of the test device. The short-circuit current of a PV module depends on both the spectral response of the module and the spectral distribution of the light within the module's responsive range. When a module operates outdoors, the measured I_{sc} can be further affected by other factors such as the cosine response of the module and the irradiance linearity at low illumination [88, 117]. In this study, the spectral effect is considered in more detail, while the effects of cosine response and irradiance linearity are assumed to be negligible. Thus, the deviation of the irradiance spectrum from the standard spectrum will alter the module's I_{sc}, and the I_{sc} loss (or gain) compared to AM1.5G radiation indicates how the effective irradiance intensity of the non-standard spectrum differs from the AM1.5G spectrum.

Before being compared to the I_{sc} measured at STC, the I_{sc} measured outdoors was corrected for the temperature influences. The temperature coefficient for the short-circuit current (α) from the manufacturer's datasheet is applied to I_{sc}, as follows:

$$I_{sc}(G, T^*) = I_{sc}/[1 + \alpha(T - T^*)] \tag{3.2}$$

where $I_{sc}(G, T^*)$ is the short-circuit current of the module corrected to 25°C module temperature (T^*), and I_{sc} is the short-circuit current measured outdoors. The effective irradiance intensity for a module can then be calculated based on the outdoor-measured I_{sc} as follows:

$$G'_{I_{sc}} = \frac{I_{sc}(G, T^*)}{I^*_{sc}} \cdot G^* = \frac{I_{sc}/[1 + \alpha(T - T^*)]}{I^*_{sc}} \cdot G^* \quad (3.3)$$

The asterisk (*) denotes the STC conditions; thus, I^*_{sc} and G^* are the short-circuit current at STC and the irradiance with the AM1.5G spectrum, respectively.

3.1.2 Effective Irradiance Ratio (EIR)

The effective irradiance ratio (*EIR*) is defined by the present author [189] as the ratio between the cumulative effective irradiance intensity for a module (G') and the cumulative irradiance intensity measured by a c-Si reference cell (G) over a period of time (t):

$$EIR_t = \frac{\sum_t G'}{\sum_t G} \quad (3.4)$$

where t is the summation over the period of interest. For example, to calculate the annual *EIR*, t is 365 days.

The "effective" here refers to the measured irradiance corrected for spectral mismatch. If *EIR* > 1, the effective radiation is higher than the measured radiation, indicating a spectral gain for the module. Similarly, *EIR* < 1 indicates a spectral loss for the module.

Hence, the *EIR* calculated based on the *MMF* is:

$$EIR_t^{MMF} = \frac{\sum_t G'_{MMF}}{\sum_t G} \quad (3.5)$$

while the *EIR* based on I_{sc} is:

$$EIR_t^{I_{sc}} = \frac{\sum_t G'_{I_{sc}}}{\sum_t G} \quad (3.6)$$

3.1.3 Average photon energy (APE):

To quantitatively determine whether a spectrum is “red-shifted” or “blue-shifted” compared to the standard AM1.5G spectrum, the "average photon energy" (*APE*) within a certain wavelength range (λ_1, λ_2) has been proposed [111, 178]. The *APE* includes no information about the PV device and is calculated by:

$$APE = \frac{Integrated\ irradiance}{Total\ photon\ number} = \frac{\int_{\lambda_1}^{\lambda_2} E(\lambda)d\lambda}{\int_{\lambda_1}^{\lambda_2} \phi(\lambda)d\lambda} = \frac{\int_{\lambda_1}^{\lambda_2} E(\lambda)d\lambda}{\int_{\lambda_1}^{\lambda_2} \frac{E(\lambda)}{hc/\lambda}d\lambda} \quad (3.7)$$

where λ_1 and λ_2 are the wavelength range of interest. $E(\lambda)$ is the spectral distribution of a spectrum, and $\phi(\lambda)$ is the photon flux density of the spectrum. *h* and *c* are the Planck constant and the speed of light, respectively. The *APE* value between 305 and 1150 nm (the measurement range of the spectroradiometer used in this work) of the standard AM1.5G spectrum is approximately 1.83 eV.

3.2 Setup for outdoor monitoring of PV modules

The outdoor module testing (OMT) facility is a specialized testing setup for outdoor PV module performance under real-life conditions in tropical Singapore. It is built and operated by the Solar Energy Research Institute of Singapore (SERIS) and located on the main campus of the National University of Singapore (NUS), see Figure 3.2.

Figure 3.2: Outdoor PV module performance testing system at NUS.

All modules studied in this thesis were installed in August 2010 with a fixed tilt angle of 10° facing true south. DC parameters including full I-V curves, V_{OC}, I_{SC}, V_{mpp}, I_{mpp}, P_{mpp} together with module temperature are measured every 10 seconds for each module. While the full I-V curve is recorded every minute to save storage space, the other parameters are logged every 10 seconds. The module temperature is measured at the back of each module with PT1000 temperature sensors. Environmental parameters including in-plane solar irradiance *G*, ambient temperature T_{amb}, wind speed and wind direction are logged simultaneously with the DC parameters.

Between I-V measurements, electrical energy is extracted from the modules at their maximum power point (MPP). This avoids unwanted side effects (such as keeping amorphous modules in open-circuit conditions under illumination, causing significant light-induced degradation) and ensures that the modules are not hotter than they would be in a real system. The uncertainty of all electrical measured parameters is within ±0.1%. The in-plane solar irradiance intensity *G* is measured with a calibrated c-Si reference cell. The calibration

uncertainty of the reference cell at 1-sun condition is within ±2%. The modules under investigation in this study were not cleaned during the data acquisition period, but weekly checking was conducted to remove bird droppings, to ensure minimal external effects on module performance. However, the silicon sensors were cleaned every week and calibrated every two years to ensure accurate irradiance readings. In addition to the c-Si irradiance sensor, an SPN1 pyranometer with shadow mask is used to measure the diffuse/global irradiance, with an uncertainty of ± 5%.

A spectroradiometer (EKO MS-700 grating spectroradiometer) was installed in January 2013 to measure the outdoor spectrum. The device was installed with the same tilt angle as the module plane. The spectroradiometer measures the spectrum from 305 to 1150 nm, with a measurement interval of 3.3 nm. The spectrum is measured and logged every minute, simultaneously with the measurement of the module characteristics. So the MMF and the effective irradiance were calculated every minute.

3.3 Results

The effective irradiance ratios for different PV module technologies under the tropical spectral conditions of Singapore are calculated for the period studied.

3.3.1 Annual Results (EIR_y)

The effective irradiance ratio (EIR_y) for the year 2013 is calculated for the four modules using equations (3.5) and (3.6). The data availability is above 99% for the CdTe, CIGS, and micromorph Si modules, however only 94% for the single-junction a-Si module calculation, because this module was taken out

from the measurement setup for 20 days in June due to a setup rearrangement. This would only affect the EIR_y^{Isc} calculation. The results are shown in Table 3.1.

Table 3.1. Annual effective irradiance ratio (EIRy) for the four thin-film PV modules, calculated based on MMF and I_{sc}.

	Single-junction a-Si	CdTe	CIGS	Double-junction micromorph Si
EIR_y^{MMF}	1.07	1.03	1.00	
EIR_y^{Isc}	1.06	1.02	1.00	0.99

As shown in Table 3.1, the annual *EIR* calculated using the *MMF* and the module I_{sc} are generally consistent. The EIR_y^{MMF} values are generally slightly higher than the EIR_y^{Isc} values. This is because the short-circuit current is affected by other factors (such as soiling losses, reflection, and varying temperature coefficient with irradiance and temperature) besides the spectral effect. For the a-Si module, the EIR^{MMF} of 1.07 indicates that the cumulative effective irradiance intensity is 7% higher than the cumulative measured irradiance intensity over the year 2013. Thus, the module can generate 7% more energy due to the "blue-shifted" spectrum, which helps to explain the observed high performance ratios for a-Si PV systems in Singapore reported in [177], where the a-Si systems was operating at around 95% and c-Si systems in the range of 80 to 90 %. If we subtract the 7% irradiance gain, the a-Si system would operate with a PR value of 88%, which is then comparable to the PR values of the c-Si systems. For the double-junction micromorph Si module EIR_y^{Isc} is less than 1, indicating that the blue-shifted spectrum causes a decrease in the current output due to the current mismatch between the two cells in the stack.

3.3.2 Monthly Results (EIR_m)

Figure 3.3 shows the monthly *EIR* for the modules studied. The seasonal variation of the spectral effect is not as strong as in temperate regions, where the spectrum has a positive influence (up to 14%) on the performance of single-junction a-Si technology in summer and a negative influence (up to -9%) in winter [178, 182, 190, 191].

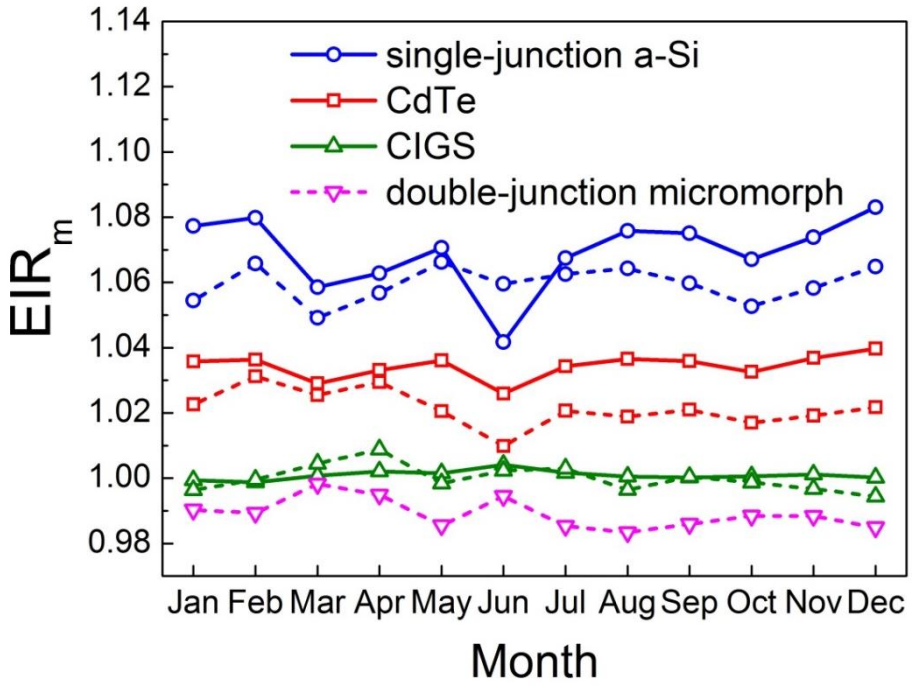

Figure 3.3: Monthly effective irradiance ratios of the investigated thin-film PV modules based on the spectral mismatch factor (EIR_m^{MMF}) (solid lines) and the short-circuit current (EIR_m^{Isc}) (short-dash lines). The EIR_m^{Isc} for the single-junction a-Si module in June was calculated based on data from 1st June to 10th June. The EIR_m^{MMF} for the double-junction micromorph module is missing because the SR of this module was not available.

As a special effect, a severe haze occurred in Singapore in June 2013, increasing the Pollutant Standards Index (PSI) to ~400 during several days [192]. As can be seen from Figure 3.4, the irradiance on one typical day with heavy haze (19 June 2013, PSI in the range of 350) showed a spectrum with higher distribution in the long-wavelength region (red shift). This is because the atmosphere contained additional particles (such as aerosols), causing

enhanced scattering of short-wavelength light [193]. The haze spectrum shows an *APE* value of 1.82 eV, while the *APE* value for the AM1.5G and the averaged day solar noon spectrum is 1.83 and 1.90 eV, respectively. Since the haze caused a red-shift in the spectral irradiance, the spectral distribution was getting closer to that of the AM1.5G spectrum. Thus the spectral effect for the a-Si and the CdTe technologies showed a decrease in June 2013, see Figure 3.3.

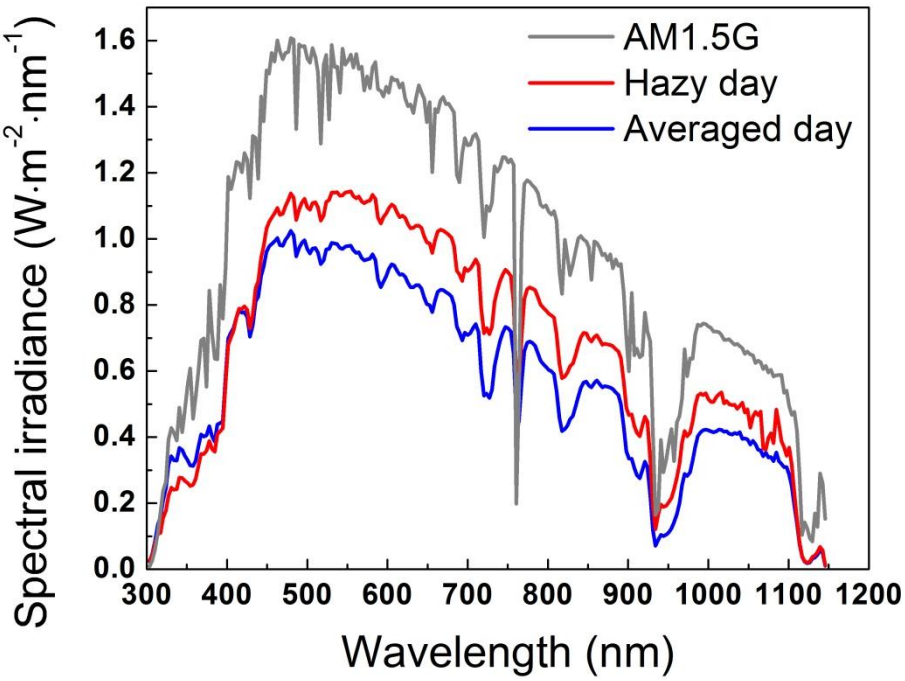

Figure 3.4: Solar noon spectra for a hazy day and an averaged day in Singapore in 2013. The grey line shows the AM1.5G spectrum.

The single-junction a-Si module was taken out from the measurement setup for rearrangement of the setup, which happened to be the time before the haze period. Thus, although only data from 1st June to 10th June were available for the EIR_m^{Isc} calculation, it represents the normal June conditions, i.e., without haze effects. The difference between EIR_m^{MMF} and EIR_m^{Isc} indicates that the

haze decreases the *EIR* for the a-Si module by about 2%. A similar decrease of *EIR* due to the haze can be seen for the CdTe module, in both the EIR_m^{MMF} and the $EIR_m^{I_{sc}}$.

3.3.3 Averaged Day Results (EIR_d)

Further analysis is carried out by studying the *EIR* for an averaged day. An averaged day is obtained by averaging the 1-year measurement results into a single day. Due to the high variations in cloud coverage in Singapore, the intra-day irradiance changes drastically (from 200 - 350 W/m^2 to 900 - 1100 W/m^2) and is highly variable. However, due to the low latitude, neither the length of day nor the "weather" changes significantly throughout the year. Considering these climate characteristics, an averaged day is thus used to represent the average environmental conditions in Singapore. The in-plane irradiance (G_i), diffuse irradiance (G_d), and the *APE* for the averaged day in 2013 in Singapore are shown in Figure 3.5. The *APE* value is higher than that of the AM1.5G spectrum over the whole day, indicating that the spectrum in Singapore is overall more blue-rich. The *APE* is higher in the afternoon than in the morning because Singapore is, on average, sunnier in the morning than in the afternoon. Since the fraction of shorter-wavelength photons in diffuse solar irradiance is larger than that in direct solar irradiance, *APE* is higher in cloudy conditions.

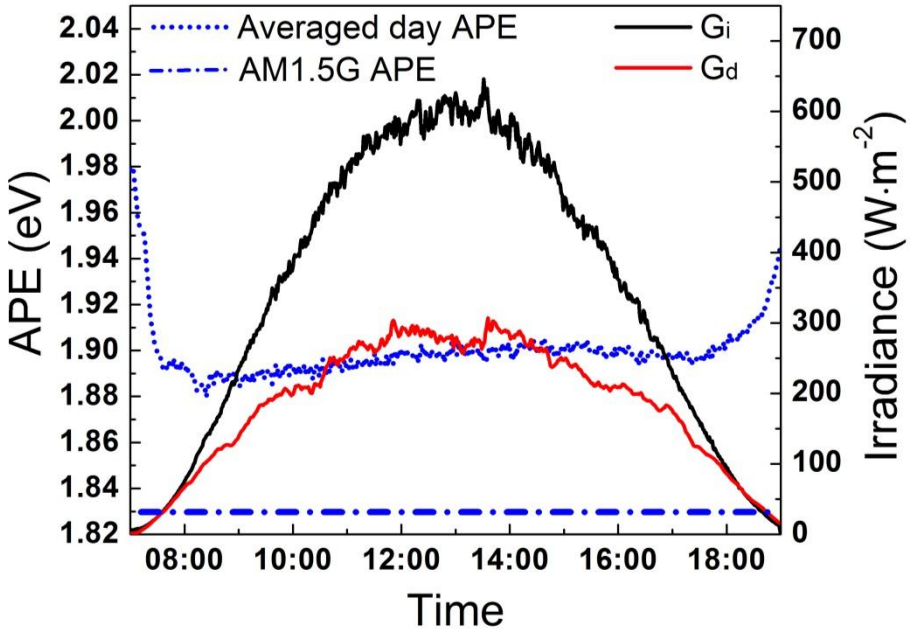

Figure 3.5: In-plane (G_i), diffuse irradiance (G_d) and average photon energy (APE) of the outdoor spectrum for an averaged day in Singapore. An averaged day is obtained by averaging the 1-year results into a single day. The APE of the standard AM1.5G spectrum from 305 to 1150 nm (1.83 eV) is also shown for comparison.

Figure 3.5 shows that the *APE* is highest in the early morning and the late afternoon, when the irradiance is low and mainly diffuse. Light scattering due to the high air mass enhances the blue diffuse irradiance [106] and thus the *APE*.

The EIR over an averaged day for the four thin-film modules is shown in

Figure 3.6, calculated hourly based on both the MMF and the I_{sc}. From Figure 3.6 it can be seen that the single-junction a-Si module has a consistently high *EIR* of 1.06 - 1.08. CdTe shows an *EIR* of around 1.03. The *EIR* for CIGS is around 1.00 over the whole averaged day, with a slight decrease in the early morning and late afternoon.

Figure 3.6 also shows that the EIR_d^{MMF} of the a-Si and CdTe module is higher in the afternoon than in the morning. This asymmetry of the spectral

effect between the morning and afternoon is due to typically more cloudy conditions in the afternoon in Singapore, as mentioned previously.

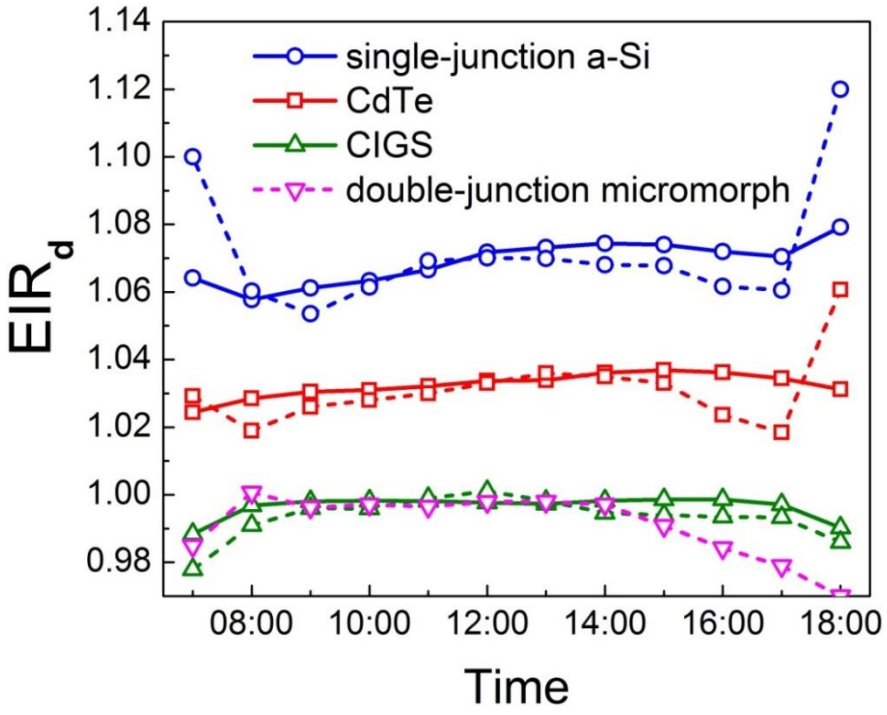

Figure 3.6: Averaged day effective irradiance ratio based on the *MMF* (EIR_d^{MMF}) (solid lines) and the I_{sc} ($EIR_d^{I_{sc}}$) (short-dash lines) for the thin-film PV modules studied on an averaged day in Singapore.

The two methods give similar results, except for early morning and late afternoon when $EIR_d^{I_{sc}}$ shows sharp increases for the single-junction a-Si module and the CdTe module. This is possibly due to the fact that we assumed the cosine effect and irradiance linearity effect to be negligible, while these effects become more pronounced during early morning and late afternoon, hence surfacing in $EIR_d^{I_{sc}}$. The $EIR_d^{I_{sc}}$ of the micromorph Si module decreases slightly with increasing *APE* in the afternoon, because the more "blue-shifted" the spectrum gets, the more serious the current mismatch between the two cells becomes.

3.4 Conclusion

The effective irradiance ratio (EIR) has been defined in this work to indicate the ratio between the cumulative effective irradiance of AM1.5G spectrum and the cumulative measured irradiance, for a specific time and location. Its value in tropical Singapore was quantified experimentally for four different thin-film PV module technologies, using two different methods (one based on the MMF, the other based on the I_{SC}). Specifically, the annual EIR, monthly EIR, and hourly EIR over an averaged day were determined. It was found that the spectrum in Singapore is constantly blue-rich compared to the standard AM1.5G spectrum, which results in the EIR of 1.07 and 1.03 for the single-junction a-Si module and the CdTe module, respectively. EIR larger than 1 indicates energetic irradiance gain. The blue-rich spectrum does not significantly affect the CIGS module, while causing around 1% loss to the double-junction micromorph Si module. On a monthly basis, the spectral variation is not significant throughout the year due to Singapore's low latitude. A haze event, which occurred in the middle of the investigation period, caused a red-shift of the spectrum and thus affected the effective irradiance intensity, especially for the a-Si and the CdTe modules. The constantly blue-rich spectrum in Singapore allows the wide-bandgap PV modules to better utilize the solar spectrum and generate extra energy relative to AM1.5G conditions, which (together with their lower temperature coefficient) explains the observed overperformance of a-Si systems in tropical Singapore.

Chapter 4 Influence of irradiance intensity on module performance in the tropics*

Tropical climate regions (such as in Singapore) are characterized by fast-changing irradiance conditions due to high variations in cloud coverage. Different PV technologies possibly react differently to these variations of irradiance conditions, which in turn will influence the module power output. This chapter analyses and discusses the effects of the fast-changing irradiance on the module performance in tropical Singapore.

4.1 Fast-changing irradiance conditions

In tropical areas, besides the constant high temperature and humidity, the weather is also characterised by fast-changing irradiance conditions. In fact, for the case of Singapore (1° north of the equator), clear-sky conditions over the course of a full day were only observed on one single day in a 1-year observation period based on SERIS meteorological data. Typically, the irradiance in Singapore is highly variable with cloud coverage. The effect of fast-changing irradiance on the electrical parameters and performance of PV modules has not been investigated for tropical regions. In this work, a method is proposed that allows to quantify the level of irradiance fluctuation and to investigate its effect on the performance of different module technologies.

4.1.1 Methodology

Figure 4.1 (black curve) shows the measured irradiance of a typical day (03-Apr-2011) in Singapore with fast-changing irradiance conditions and a clear

* The work described in this work is based on the publication "Outdoor PV module performance under fluctuating irradiance conditions in tropical climates", *Energy Procedia* **33**, pp. 238-247, 2012. DOI:10.1016/j.egypro.2013.05.064

distinction between low irradiances (200 - 350 W/m^2) and high irradiances (900 - 1100 W/m^2). In this chapter, a method to distinguish fast-changing irradiance into "low" and "high" irradiances, with a clear-sky model as reference, is proposed.

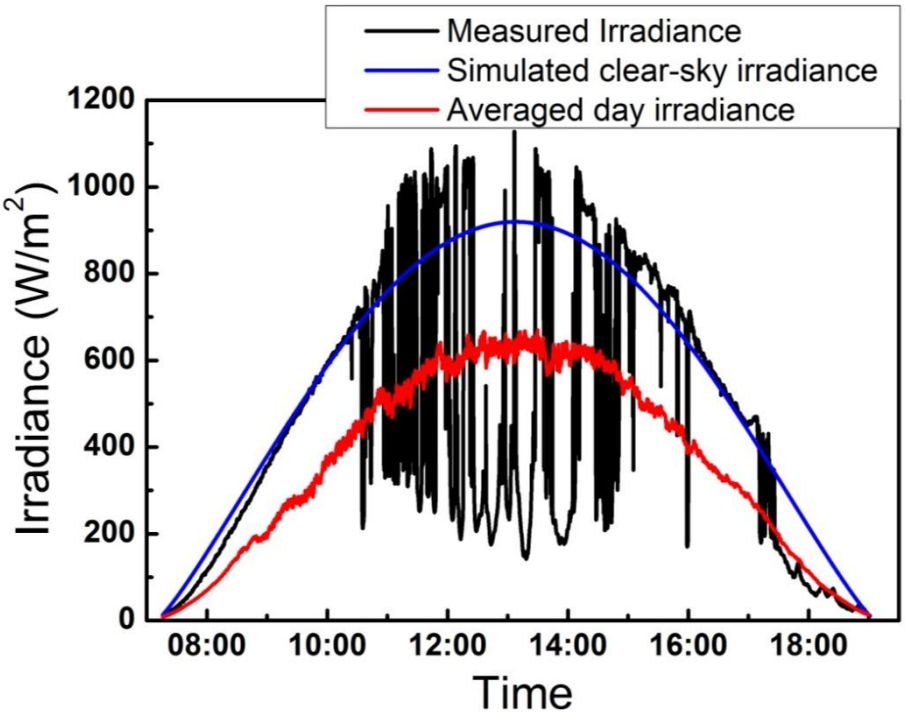

Figure 4.1: Measured irradiance on a typical day in Singapore (03-Apr-2011) characterised by a high level of variability (in black), compared with simulated clear-sky irradiance (in blue) and the 2011 averaged day irradiance (in red) [194].

A number of models have been proposed to simulate the horizontal irradiance under clear-sky conditions [195, 196]. Based on the calculation of the Pearson correlation coefficient using two years' data from Singapore [197], the Adnot model, which is a function of the solar zenith angle, was found to fit the Singapore irradiance best:

$$G_C = G_o \times cos^{1.15}(\theta_z)\,;\, G_o = 951\ W/m^2 \tag{4.1}$$

where θ_z denotes the solar zenith angle. Equation (4.1) results in the global irradiance received horizontally on a clear day. It can be adjusted to simulate

the irradiance on a titled surface by changing the solar zenith angle to the incident angle on the tilted plane (θ), as shown in Equation (4.2):

$$G_I = G_o \times cos^{1.15}(\theta);\ G_o = 951\ W/m^2 \tag{4.2}$$

The solar incident angle on a tilted surface can be obtained from an NREL online solar position algorithm calculator [145, 168].

It is noted that under clear-sky conditions the maximum irradiance over the whole year in Singapore is around 951 W/m^2, hence not even reaching the 1000 W/m^2 used in the Standard Test Conditions (STC) to rate PV modules. The solar noon zenith angle for Figure 4.1 (April-03-2011) is 3.8°, so the zenith angle for the tilted surface is 13.8°, and thus the calculated irradiance peak is 919.5 W/m^2. Irradiance values above that (as seen in Figure 4.1) result from the albedo effect of the ground and reflections from clouds.

The simulated in-plane irradiance using the Adnot model was verified with measured irradiance on a clear-sky day (05-Aug-2011) from a silicon sensor with the same orientation as the studied modules. The comparison is shown in Figure 4.2. The solar noon zenith angle on 05-August-2011 is 15.75°, and the zenith angle for the tilted surface is 25.75°, resulting in the peak irradiance of 825 W/m^2. The results from Equation (4.2) and the empirical data have a Pearson's correlation coefficient of 0.999.

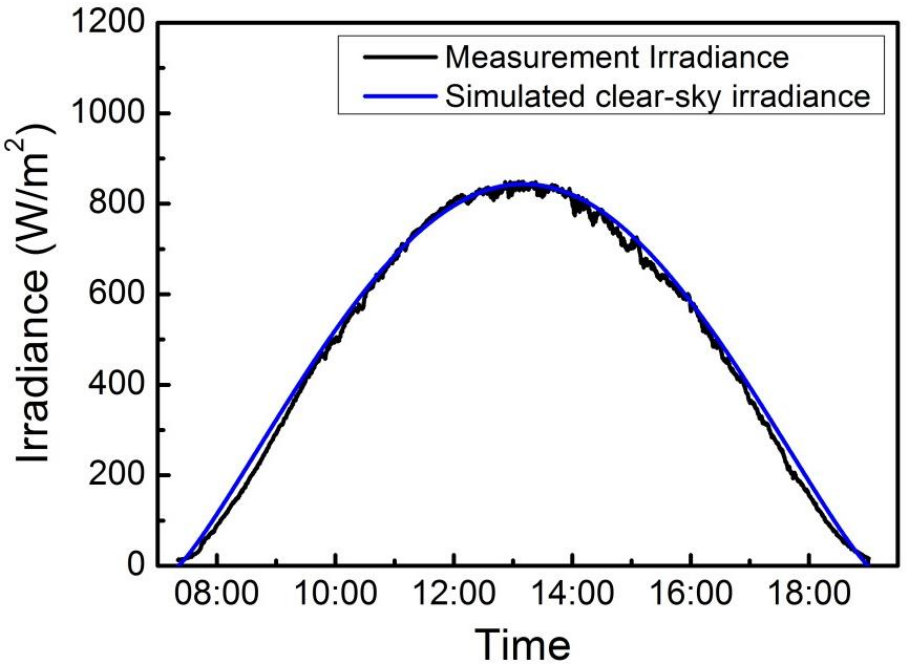

Figure 4.2: Comparison of simulated irradiance with measured irradiance during an exceptional day with clear-sky conditions in Singapore (05-Aug-2011).

Figure 4.1 also shows the average irradiance values (red line) for every 10 seconds over the course of a full year (here: 2011). This is equivalent to the averaged day in-plane irradiance. The definition of the averaged day is given in Section 3.3.3. The maximum of the averaged day irradiance is around 69% of the clear-sky model. This value was used in the following to separate the irradiance values into: "low irradiance" (irradiance lower than 69% of the simulated clear-sky irradiance) and "high irradiance" (irradiance higher than 69% of the simulated clear-sky irradiance). To see if there is an influence on module performance from fast-changing irradiance, the two categories (high and low irradiance) were further classified into six groups based on the number of minutes with relative stable irradiance. The six groups are: (1) less than or equal to 2 minutes; (2) longer than 2 minutes, less than or equal to 5 minutes; (3) longer than 5 minutes, less than or equal to 10 minutes; (4) longer

than 10 minutes, less than or equal to 20 minutes; (5) longer than 20 minutes, less than or equal to 30 minutes; and (6) longer than 30 minutes. These categories are chosen with the consideration of possible time scales for irradiance forecasting.

4.1.2 Distribution of fast-changing irradiance

Measured irradiance over a whole year from January to December 2011 in Singapore was separated and classified with respect to different energy radiation levels and different stable irradiance durations. Figure 4.3 shows the distribution of cumulative radiation energy with different irradiance levels and duration ranges (number of minutes with stable irradiance conditions). The irradiance was measured with the same Si sensor mentioned above. Considering irradiance of less than 30-minute duration as fast-changing irradiances, these contributed more than half of the total radiation energy (1465 kWh/m^2). It can be seen from Figure 4.3 that the share of fast-changing irradiance increases with higher irradiance levels. As mentioned earlier, the peak irradiance (from the Adnot clear-sky model) in Singapore should have its maximum value at around 951 W/m^2, hence irradiance values above that are attributed to reflection from clouds, and would mostly occur during times of partly cloudy skies.

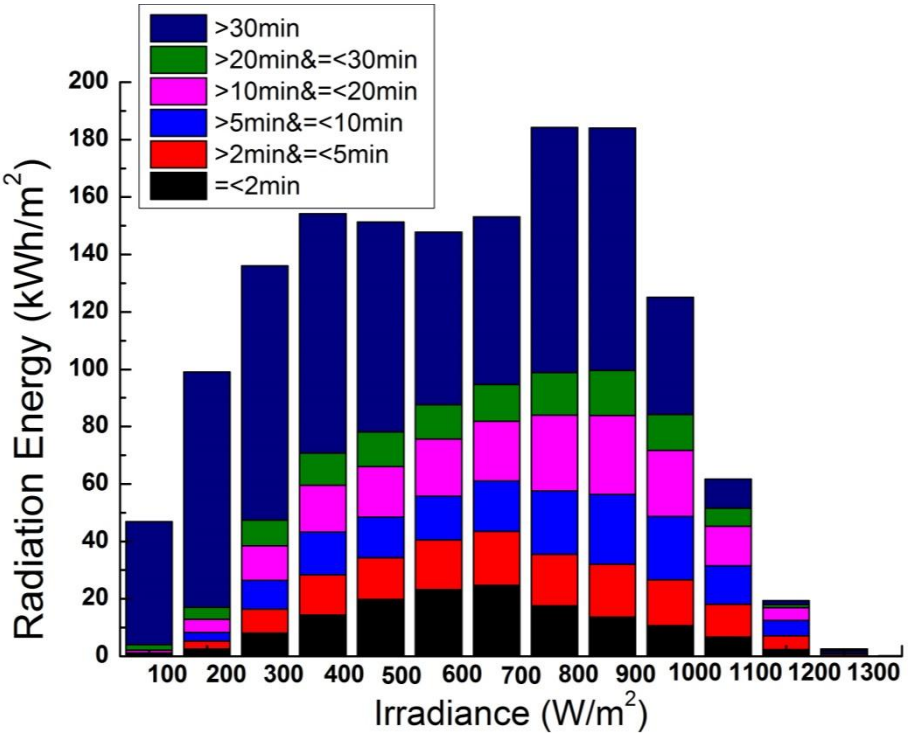

Figure 4.3: Radiation energy distribution with respect to irradiance level and time range of variability in Singapore (2011 data).

4.2 PV module performance under fast-changing irradiance

Four different PV technologies were selected to investigate the impact of fast-changing irradiance on PV performance. For equal comparison and to avoid influences from the thermal behaviours of different module constructions, only modules with the same glass-cell-backsheet encapsulation structure were selected for this analysis. The data sheet information of the studied modules is listed in Table 4.1.

Table 4.1. Specifications of PV modules under investigation for the influence of irradiance intensity on the module performance in Singapore.

PV module	Technology	Nominal power (Wp)	Temperature coefficient of I_{SC} (%/°C)
1	Mono c-Si	180	+0.050
2	Single-junction a-Si	60	+0.075
3	Double-junction a-Si	95	+0.080
4	Micromorph Si	110	+0.056

4.2.1 Short-circuit current of PV modules under fast-changing irradiances

The short-circuit current (I_{SC}) of a PV module is proportional to the solar irradiance and practically insensitive to the PV module temperature [198]. Therefore it is used as a gauge to analyse the response of the various PV technologies to fast-changing irradiances. The normalized I_{SC}/G ratio was calculated via

$$\left(\frac{I_{sc}}{G}\right)_{Normalized} = \frac{\frac{I_{sc}}{G}}{\frac{I_{sc}^*}{G^*}} \times 100\% \tag{4.3}$$

where

I_{sc}: Measured short-circuit current of a module

G: Measured instant in-plane irradiance

I_{sc}^*: Short-circuit current of a module under STC

G^*: Reference irradiance under STC, which is 1000 W/m^2

The normalized I_{SC}/G ratio is then plotted as box chart with percentage against the time intervals of stable irradiance duration, at both high and low irradiances (see Figure 4.4).

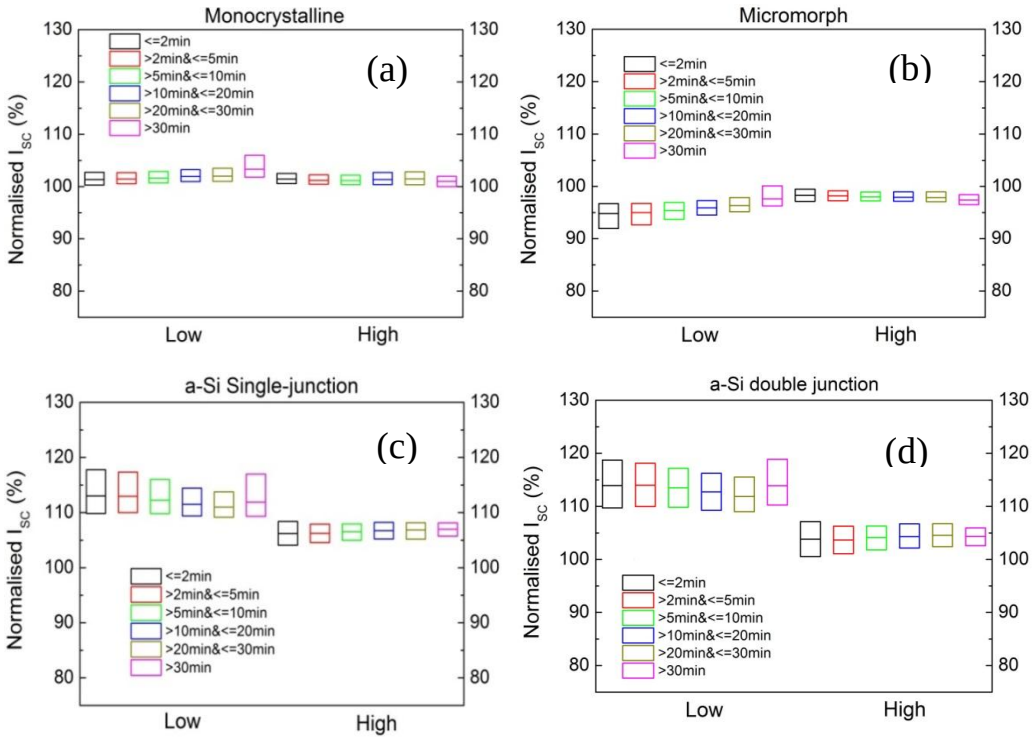

Figure 4.4: Box charts of relative I_{SC}^{Norm} of selected PV modules: (a) monocrystalline Si; (b) micromorph Si; (c) a-Si single junction; (d) a-Si double junction. "Low" and "High" represents the irradiance conditions "sun covered by clouds" (low irradiance) and "direct sun exposure" (high irradiance) according to irradiance levels lower and higher than the 69% of the modelled clear-sky irradiance.

The 25% and 75% values were used as the bottom and top edges in the box charts, and the lines inside the boxes denote the median. The results indicate that the I_{SC} of the monocrystalline Si module varies only little around its average value and is independent of irradiance fluctuations. However, the data of the thin-film Si modules (a-Si single-junction, a-Si double-junction, and micromorph Si) show a large range of variability, especially at low irradiances. The normalised I_{SC} of the a-Si modules (both single-junction and double-junction) were 5 - 7 % higher at low irradiances compared to high irradiance conditions, and also exhibit wide variations (larger boxes). The normalised I_{SC} was less scattered at high irradiances and more stable conditions. For the micromorph Si module, in contrast, its normalised I_{SC} values under low

irradiance conditions were around 2% lower than that under high irradiance conditions, with wider variations under low irradiances.

As discussed in Chapter 3, such change in I_{SC} for Si based thin-film modules is most likely attributed to the spectral variation. The outdoor spectra on a fast-changing day (17-Oct-2011) were measured with an Ocean Optics spectroradiometer (NQ51A0200 & QEB1034), which can accurately measure spectral irradiance from 300 to 1700 nm. Spectra were measured within 30 minutes around noon time so that the air mass influence can be neglected. They were normalized by the total energy of AM1.5G between 300 and 1200 nm. The normalized spectra are shown in Figure 4.5.

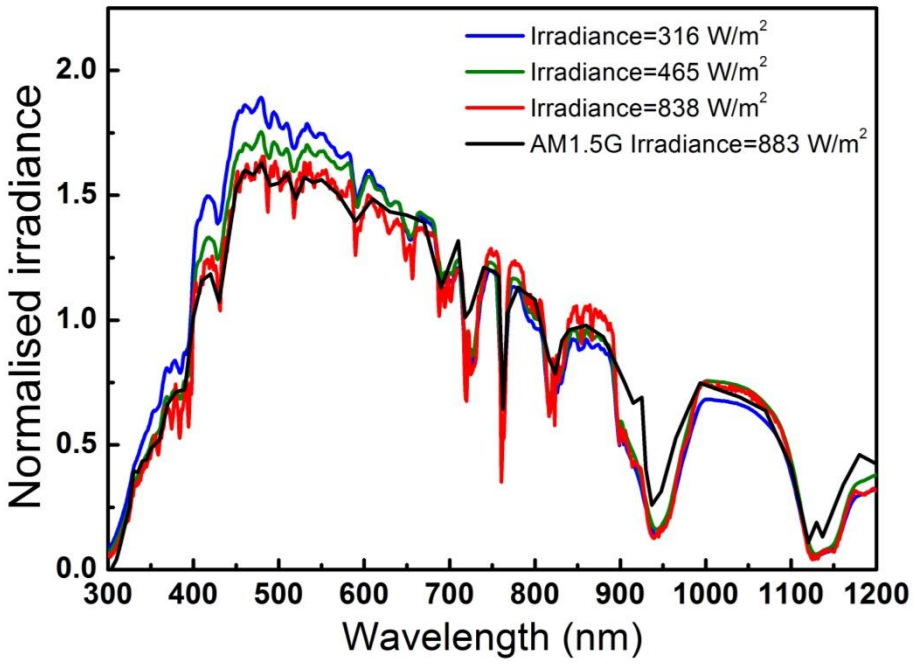

Figure 4.5: Measured spectra at various irradiance levels on 17th October 2011, normalised with the AM1.5G reference spectrum.

Spectra with low irradiances were measured when the sun was covered by clouds, while the high irradiance spectra were measured when the sun was not covered. It can be seen that the lower the irradiance gets, the higher is the normalized irradiance in the range of 350 - 600 nm. The average photon

energy (APE), as described in Section 3.1.3, is thus also higher, which is favourable for a-Si modules. In contrast, spectral distribution deviating from the standard spectrum leads to a current mismatch between the top cell and the bottom cell for micromorph Si modules since this kind of tandem solar cell is optimized for the AM1.5G spectrum. The higher the APE gets, the larger the current mismatch becomes - unless the module stack is specifically designed for that (e.g., through varying the thicknesses of the individual layers).

Thus the spectral variation during fast-changing irradiance conditions is the main reason leading to the variation of the normalised I_{SC} of PV modules. The lower the irradiance gets during irradiance variation, the higher the APE becomes. As a result, a-Si modules show a higher normalised I_{SC} under low irradiance, while micromorph modules perform worse due to the current mismatch between the top and bottom cells. Crystalline Si modules do not show significant changes in the normalised I_{SC} under variable irradiance conditions.

4.2.2 Temperatures of PV modules under fast-changing irradiance

Figure 4.6 shows the temperature distribution of the monocrystalline Si PV module during January to December 2011 (the other investigated PV module technologies show a similar behaviour and hence are not shown here). At low irradiances, the module temperature decreases with longer duration of stable irradiance, allowing the PV modules to gradually approach equilibrium with the ambient air temperature. The decrease is smaller initially (i.e., at higher variability) due to the smoothing effect of the thermal inertia of the PV modules, which typically follows an exponential curve [46]. In contrast, at

high irradiance, the module temperature increases with increasing duration of the irradiance, due to the continuous absorption of direct solar radiation and the relatively large heat capacity of a solar module, which is in the range of (1.5 - 3.0)×10^4 J/K for standard PV modules [199]. As can be seen from Figure 3.2, the test setup facilitates good ventilation of the PV modules. Since there is only little contact area between the PV modules and the frame, the influence of heat conduction is negligible. The main heat exchange portions are therefore radiation and convection. Quantitative studies on the heat transfers require dynamic experimental data in short time scale, which were unfortunately not available. Therefore, the module temperature could only be qualitatively analysed here.

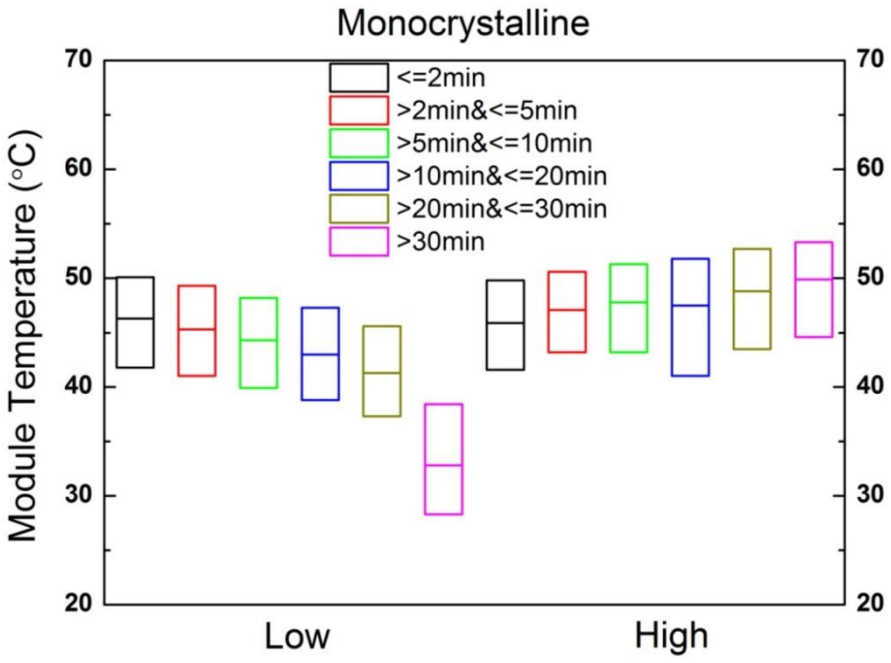

Figure 4.6: Mono c-Si module temperature vs. duration of the stable irradiance, for low and high irradiance levels.

4.2.3 Outdoor average efficiencies of PV modules under fast-changing irradiance

As the open-circuit voltage (V_{OC}) of a PV module is significantly influenced by the module temperature, and is only marginally affected by irradiance when irradiance levels are above 100 W/m^2 [88], the impact of irradiance variation on the V_{OC} is correlated with the impact on PV module temperatures. Instead of analysing V_{OC} alone, the efficiency, which depends on both V_{OC} and the module temperature, is characterised under fast-changing irradiance here. Figure 4.7 shows the outdoor average efficiencies with increasing number of minutes of stable irradiance for low and high irradiance conditions. For the mono c-Si module, as the duration of stable irradiance increases, the average efficiency increases for low irradiances and decreases for high irradiances. This trend is inversely proportional to the module's temperature (see Figure 4.6), as expected. In contrast, the a-Si technologies (both single-junction and double-junction) show little change in efficiency with duration of the stable irradiance, indicating that the effect of module temperature on the efficiency is not so significant for these technologies. However, they show a considerable difference between the efficiencies at high and low irradiances, which is equivalent to the effect seen in the normalised I_{SC} distribution (see Figure 4.4). Therefore the efficiency of a-Si modules is less dependent on the irradiance variability, but more on the irradiance level, with spectral variation as the main reason. For the micromorph Si module, its efficiency trend is similar to mono c-Si, indicating that the μc-Si cell dominates. At low irradiances, the efficiency is lower at fast-changing conditions, where there is a negative impact from the current mismatch

between the bottom (μc-Si) and the top (a-Si) cell, which is again due to a different spectral distribution under different irradiance levels.

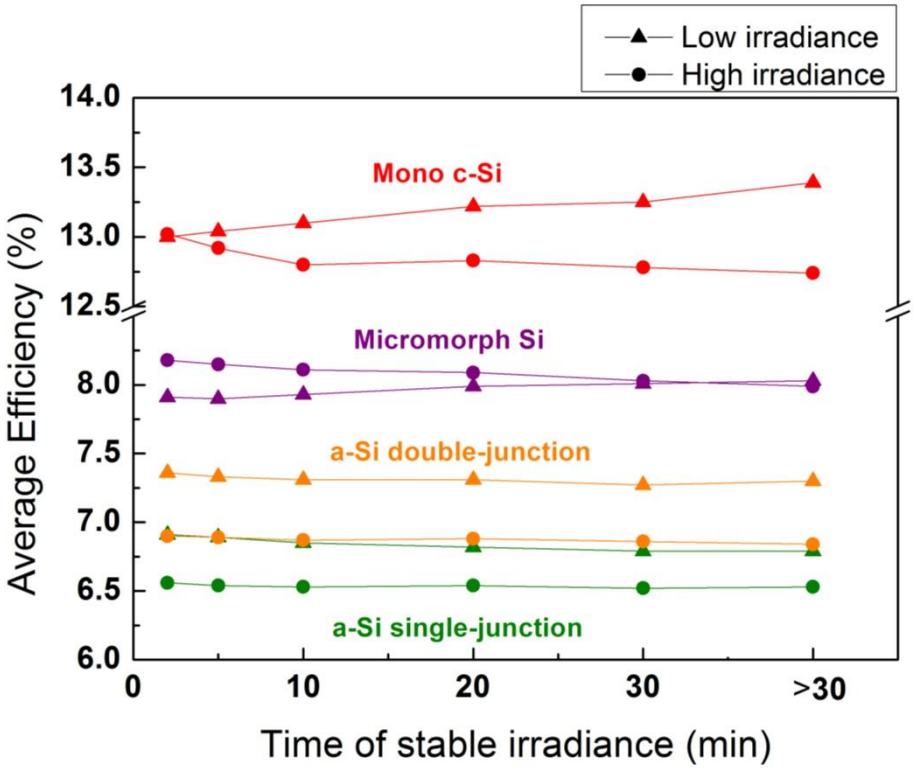

Figure 4.7: Average annual efficiencies of the four investigated PV module technologies versus the increasing duration (in minutes) of stable irradiance, for low-irradiance and high-irradiance conditions. Lines are guides for the eye. The value at 2 min shows the readings for < 2 min; the value of 5 min shows the readings for 2 - 5 min, etc.

4.3 Conclusion

A method was introduced to study fast-changing irradiance and its influence on PV module performance in tropical Singapore, separating measured unstable irradiance into high and low irradiance using a clear-sky irradiance model as basis. The distribution of fast-changing irradiance (defined as stable irradiance with duration of less than 30 minutes) in Singapore is presented. More than half of the radiation energy in Singapore can be classified as fast-changing irradiances. The normalised I_{SC} of wafer-based modules were found to be independent of the irradiance changes, but the I_{SC} distribution of a-Si and micromorph Si modules revealed relevant

dependences on the irradiance levels and the variation frequency. The average efficiency of the mono c-Si modules was found to be mainly affected by the module temperature, while the efficiency for a-Si thin-film modules showed a much stronger dependence on the irradiance level than on its variability or the module temperature. Higher efficiencies at low irradiances for a-Si modules are attributed to the "blue-shifted" spectrum. The micromorph Si module showed similar characteristics as mono c-Si for high irradiances (including temperature dependence), but a relatively lower efficiency for low irradiances, caused by the internal current mismatch between the top and bottom cells.

Chapter 5 Influence of temperature on PV module performance in the tropics[*]

Temperature is one of the most important parameters affecting the power output of PV modules. Tropical regions are characterized by constantly high ambient temperature throughout the year. Hence, the power loss due to high module temperature can be significant. In order to correct for the temperature effect and compare with the STC efficiency, temperature coefficients are applied to various electrical parameters such as voltage, current and maximum power [102]. However, the dependence of temperature coefficient on irradiance and temperature is still controversially discussed [99, 200, 201]. In this study, a model is derived to extract the temperature coefficient of the modules' maximum power and to understand its dependence on irradiance and temperature. Later, the PV module temperatures and the resulting losses due to high operating temperatures in tropical Singapore are discussed.

5.1 Temperature coefficient

The temperature coefficient of the maximum power (γ hereafter) is widely used to predict energy yield and performance ratio (PR) of PV systems [86, 97, 98]. The temperature coefficient γ is obtained by measuring the module power either indoors or outdoors under controlled conditions [121, 202]. Although it is stated in the IEC standard [121] that the coefficient determined is valid only at the irradiance at which the measurements were made, there is only one γ on the datasheet provided by the manufacturers. Usually the γ provided was

[*] The work described in this chapter is based on the publication "Determination of PV module temperature coefficient from outdoor testing data in the tropics," *International Journal of Photoenergy* (submitted).

measured under 1000 W/m^2, and it is then applied to all irradiance intensities during yield and PR predictions. In this section, an expression is derived based on the one-diode model to extract γ from outdoor monitoring data, and I-V data measured under STC conditions. Thereafter the dependence of γ with irradiance and module temperature can be studied. To exclude spectral and other technology-related effects, two monocrystalline Si modules from the same manufacturer but with different constructions (standard with frame and glass-glass without frame) are used for this study.

5.1.1 Theory

Emery *et al.* and Kurnik *et al.* have discussed the dependence of γ on irradiance measured through indoor controlled experiments with continuous illumination [99, 200]. Polynomial fitting of efficiency with temperature by Garg and Agawal showed that γ is proportional to the reciprocal of operating temperature and the γ for the studied crystalline silicon module at 25°C was calculated to be around -0.4 %/°C [203]. Reindl *et al.* used a linear model to regress power on temperature within a limited band of irradiance and found that the γ for c-Si modules decrease with irradiance in real operating conditions [96]. King *et al.* extracted γ using clear sky I_{mpp} and V_{mpp} data and reported the dependence of γ on irradiance and temperature for c-Si and a-Si modules [102]. So far the reported methods are all based on clear-sky or quasi-stable irradiance conditions [201, 204]. Considering the unique weather characteristics in the tropics (highly variable during a day and little seasonality throughout the year), data from the averaged day (obtained by averaging the 1-year measurement results into a single day, refer to Section 3.3.3 for a detailed explanation) is used to extract the γ.

The power at the maximum power point, P_{mpp}, of a PV module is a function of both irradiance *G* and module temperature *T*. In accordance with IEC61215 [121], the maximum power P_{mpp} under arbitrary *G* and *T* delivered by a PV module can be written with the temperature coefficient as:

$$P_{mpp}(G,T) = P_{mpp}(G,T^*)\,[1+\gamma(T-T^*)] \tag{5.1}$$

where (*) denotes the STC conditions (i.e., module temperature T^*= 25°C and G^* = 1000W/m^2). γ is the temperature coefficient of the module's power output.

To be precise, γ should be measured separately at each level of irradiance, but this is not done in practice. Instead, the temperature coefficient is measured at 1000 W/m^2, and then this value is used in Equation (5.1) to find the effect of temperature on the module power at all irradiance levels.

The form of Equation (5.1) implies that the diode parameters (ideality factor *n* and reverse saturation current I_o) are constant with temperature, and all the temperature dependence of module power is incorporated into γ. Given the fact that γ measured at STC irradiance is applied at all irradiance levels, it also implies that the diode parameters (*n* and I_o) are constant with irradiance. In this study, we extract γ from outdoor testing data based on Equation (5.1) and study how γ behaves with varying irradiance and temperature in real outdoor operating conditions.

By using the three parameters of the I-V curve (short-circuit current I_{SC}, open-circuit voltage V_{OC}, and fill factor FF), Equation (5.1) can be written as:

$$P_{mpp}(G,T) = I_{SC}(G,T^*)\,V_{OC}(G,T^*)\,FF(G,T^*)\left(1+\gamma(T-T^*)\right) \tag{5.2}$$

Note that the I_{SC}, V_{OC}, and FF in Equation (5.2) are values at 25°C, which seldom occur in real-life operating conditions. To derive the temperature coefficient from outdoor data, we need to calculate these parameters from outdoor operating conditions. In the following, we will find an expression for each of the $I_{SC}(G,T^*)$, $V_{OC}(G,T^*)$, and $FF(G,T^*)$ based on indoor and outdoor measurements and certain assumptions.

Short-circuit current I_{SC}

I_{SC} can be considered proportional to the solar irradiance G [35, 83]. Since a c-Si sensor was used to measure the irradiance, the spectral effect for the c-Si module under investigation can be neglected. So we have:

$$\frac{I_{SC}(G,T^*)}{I_{SC}(G^*,T^*)} = \frac{G}{G^*} \tag{5.3}$$

Rearranging the terms in Equation (5.3), we get:

$$I_{SC}(G,T^*) = I_{SC}(G^*,T^*)\ \frac{G}{G^*} \tag{5.4}$$

Open-circuit voltage V_{OC}

From the one-diode model describing solar cell characteristics [205], we have:

$$I = I_L - I_0\left[\exp\left(\frac{q(V+IR_S)}{nkT}\right) - 1\right] - \frac{V+IR_S}{R_{Shunt}} \tag{5.5}$$

where I_0, n, k, T are the reverse saturation current, the ideality factor, the Boltzmann constant and the cell temperature, respectively. R_S and R_{Shunt} are the series and shunt resistances.

Assuming a high-quality solar cell with high shunt resistance, which is

usually the case for commercial c-Si modules, $I_L \approx I_{SC}$, and the open-circuit voltage V_{OC} is given as

$$V_{OC} = \frac{nkT}{q} \ln\left(\frac{I_{SC}}{I_0} - 1\right) \tag{5.6}$$

n and I_0 are assumed to be the same as in the STC conditions. Dividing $V_{OC}(G, T^*)$ by $V_{OC}(G^*, T^*)$, we get:

$$\frac{V_{OC}(G, T^*)}{V_{OC}(G^*, T^*)} = \frac{\ln\left(\frac{I_{SC}}{I_0^*} - 1\right)}{\ln\left(\frac{I_{SC}^*}{I_0^*} - 1\right)} \tag{5.7}$$

For any practically relevant light intensity, the "-1" in the logarithmic term can be neglected. Rearranging leads to:

$$\frac{V_{OC}(G, T^*)}{V_{OC}(G^*, T^*)} = \frac{\ln\left(\frac{I_{SC}}{I_0^*}\right)}{\ln\left(\frac{I_{SC}^*}{I_0^*}\right)} \tag{5.8}$$

Fill Factor *FF*

Fill factor is defined as the ratio of maximum output power to the product of open-circuit voltage and short-circuit current. It represents the rectangularity of the I-V curve and is dependent on the series resistance and shunt resistance of a module. Large series resistance and low shunt resistance result in low fill factor and thus low power output. The temperature effect on fill factor is negligible under moderate illumination levels (below 1.2 suns) [206]. So we have:

$$FF(G, T^*) = FF(G, T) \tag{5.9}$$

Dividing (5.9) by a common denominator of $FF(G^*, T^*)$ and rearranging gives:

$$FF(G,T^*) = FF(G^*,T^*)\frac{FF(G,T)}{FF(G^*,T^*)} \tag{5.10}$$

Temperature coefficient γ:

Substituting (5.4), (5.8) and (5.10) into (5.2), results in:

$$P_{mpp}$$

$$= \left[I_{SC}(G^*,T^*)\frac{G}{G^*}\right]\left[V_{oc}(G^*,T^*)\frac{\ln\left(\frac{I_{SC}}{I_0^*}\right)}{\ln\left(\frac{I_{SC}^*}{I_0^*}\right)}\right]\left[FF(G^*,T^*)\frac{FF(G,T)}{FF(G^*,T^*)}\right]$$

$$\cdot\,[1+\gamma(T-T^*)] \tag{5.11}$$

$$= \frac{G}{G^*}\,\frac{\ln\left(\frac{I_{SC}}{I_0^*}\right)}{\ln\left(\frac{I_{SC}^*}{I_0^*}\right)}\,\frac{FF(G,T)}{FF(G^*,T^*)}\,P_{mpp}(G^*,T^*)\,[1+\gamma(T-T^*)]$$

Making γ in (5.11) the subject:

$$\gamma = \frac{1}{(T-T^*)}\left[\frac{P_{mpp}(G,T)\;G^*\;\ln\left(\frac{I_{SC}^*}{I_0^*}\right)\;FF(G^*,T^*)}{P_{mpp}(G^*,T^*)\;G\;\ln\left(\frac{I_{SC}}{I_0^*}\right)\;FF(G,T)} - 1\right] \tag{5.12}$$

This is an expression for γ which depends on values at STC (T^*, G^*, $P_{mpp}(G^*,T^*)$, I_{SC}^*, I_0^*, $FF(G^*,T^*)$) and values from outdoor measurement (T, G, $P_{mpp}(G,T)$, I_{SC}, $FF(G,T)$).

Determination of I_0^*

The I_0^* in Equation (5.12) was determined from the I-V curve measured under STC conditions, using the partial fitting method proposed by Yordanov [207]. This method is based on the one-diode model. When studying the higher voltage part of an I-V curve, the model can be shown as:

$$\ln\left(\frac{I_L - I}{I_L}\right) = \ln\left(\frac{I_0}{I_L}\right) + \frac{q(V + IR_S)}{N_S nkT} \quad (5.13)$$

where N_S denotes the number of cells in a module.

By choosing the R_S resulting in the best linearity (based on least-squares residual) of $\ln[(I_L - I)/I_L]$ versus $(V + IR_S)/N_S$, the vertical axis intercept of the linear fit (equalling to $\ln(I_0/I_L)$) can be determined and I_0 is derived.

5.1.2 Data for study

Measured data from the outdoor module testing (OMT) facility at SERIS was used for the study. Measured data over a 1-year period from 1-Jan-2011 till 31-Dec-2011 were used. As discussed in Section 3.3.3, the averaged day is defined to characterize the average environmental conditions in Singapore. Thus the extraction of the temperature coefficient γ was conducted on the averaged day for 2011. The averaged day irradiance of 2011 is shown in Figure 5.1 (black solid line), together with the module temperatures of the two modules in the study. The same averaging method was applied to the measured data of the studied modules in 2011 to obtain the averaged day values of P_{mpp}, I_{SC} and FF , for the extraction of γ.

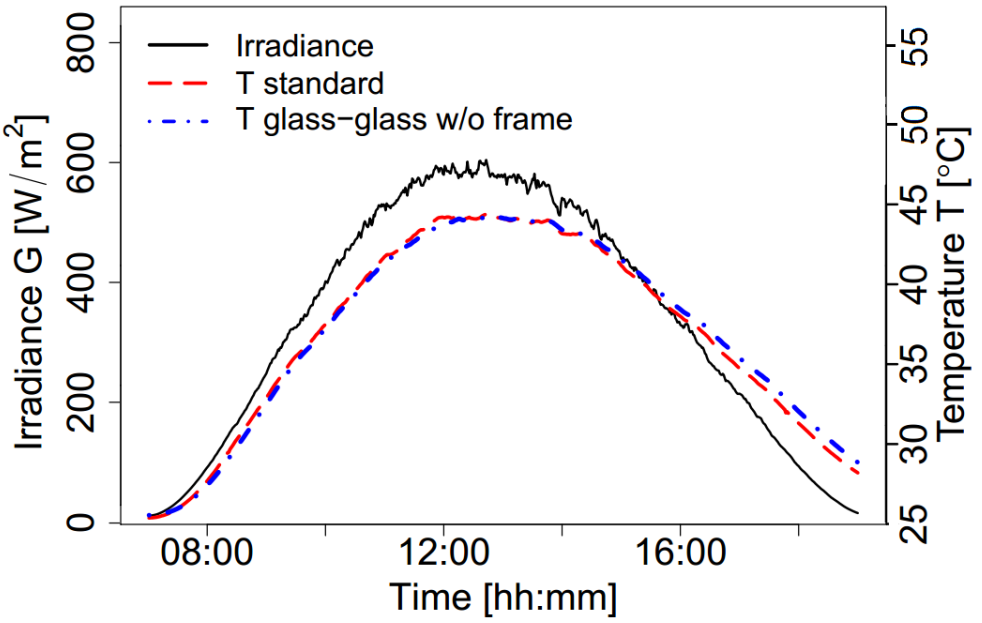

Figure 5.1: Temperature of the two studied modules and irradiance on the averaged day of 2011 in Singapore.

5.1.3 Results and discussion

Following Equation (5.12), Figure 5.2 shows the extracted temperature coefficient as a function of irradiance and module temperature. The nameplate γ are denoted as blue planes. Data with irradiances below 200 W/m^2 were omitted because angular loss and large air mass at these irradiances may violate earlier assumptions. The projections of Figure 5.2 on y-z and x-z planes are shown in Figure 5.3.

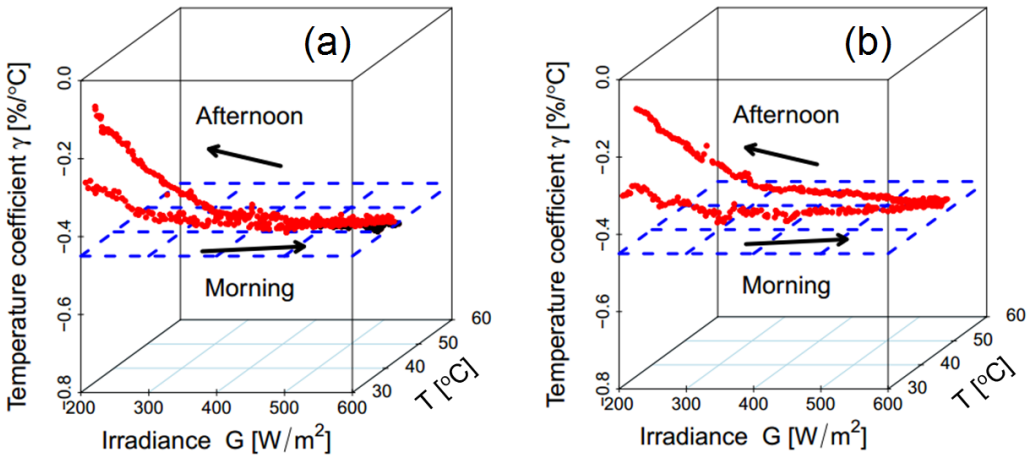

Figure 5.2: Temperature coefficient γ as a function of irradiance and module temperature for the module with (a): standard glass-backsheet construction and (b): glass-glass construction on the 2011 averaged day. The blue plane shows the datasheet value of γ.

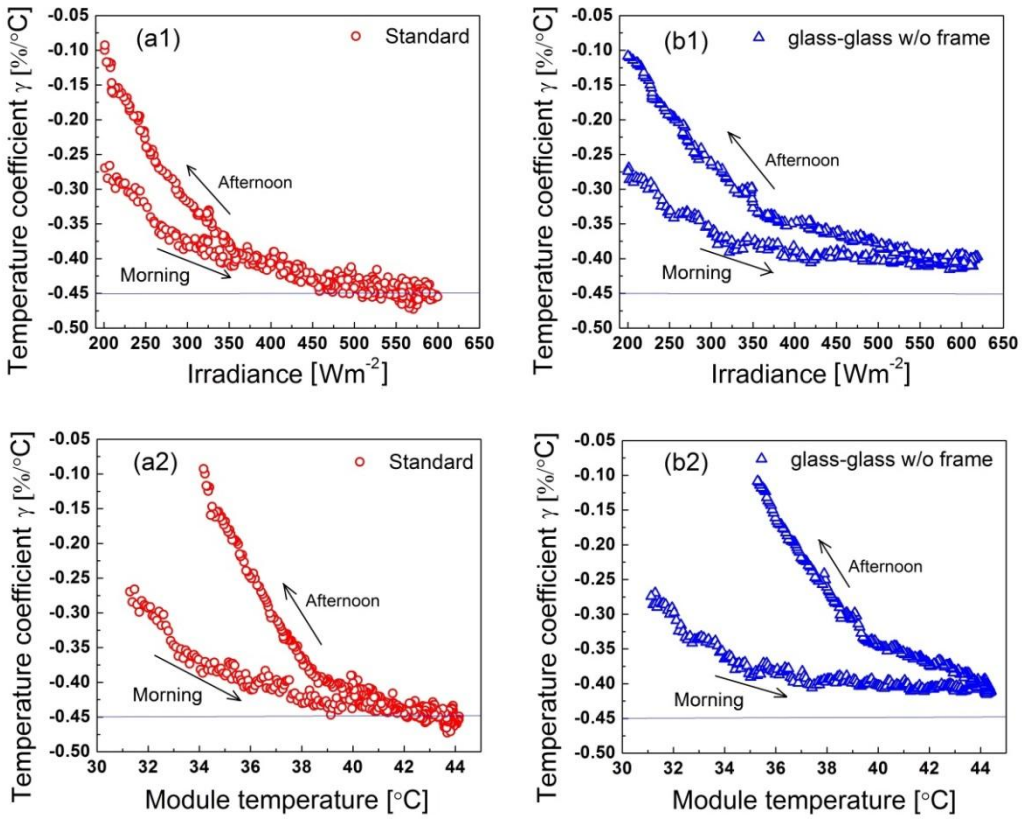

Figure 5.3: Projection of Figure 5.2 on y-z and x-z planes for the module with (a) standard glass-backsheet construction and (b) glass-glass construction.

We observe a split of data points for the morning and afternoon, which is due to higher module temperatures (about 3°C) in the afternoon than in the

morning under the same irradiance (see Figure 5.4). It is evident that both the module temperature and the irradiance affect the temperature coefficient.

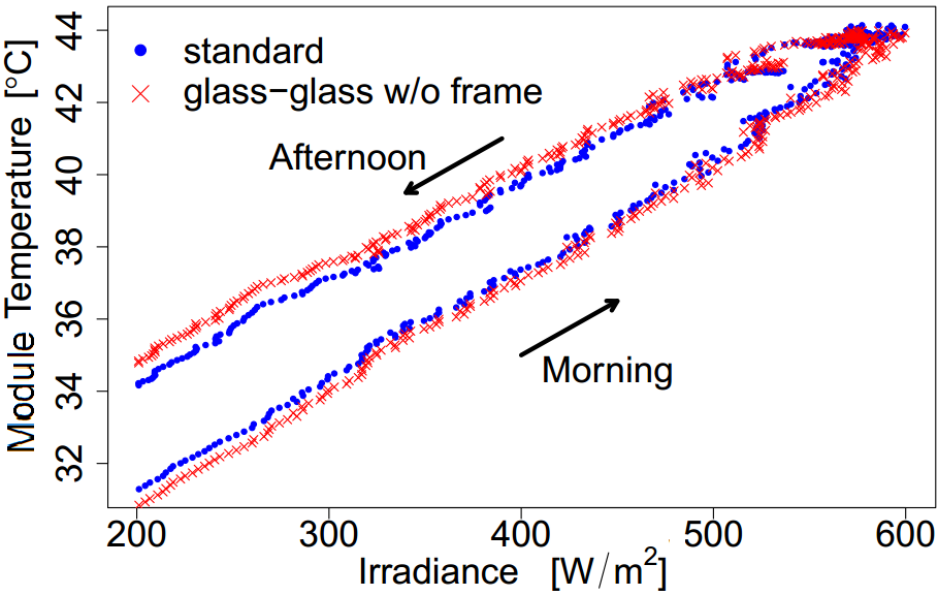

Figure 5.4: Module temperatures of the two modules vs irradiance for different times of the day.

It can be seen from Figure 5.2 and Figure 5.3 that the temperature coefficient increases with decreasing irradiance, especially when irradiance is relatively low (< 300 W/m^2). For moderate irradiance values (> 400 W/m^2), γ remains fairly constant. The saturated values of γ are -0.45%/°C and -0.41%/°C for the glass-backsheet module and the glass-glass module, respectively (see Figure 5.2). Under the same irradiance, γ is higher in the afternoon than in the morning (see Figure 5.3 (a1) and (b1)), indicating that γ increases with increasing module temperature.

Figure 5.4 shows the module temperature of the two modules versus irradiance on the 2011 averaged day. The temperatures of the two modules are found to be very similar. However, slower heat absorption/dissipation can still be observed for the glass-glass construction as compared to the glass-

backsheet construction because of its larger thermal mass [46]. As the temperature of the glass-glass module is lower in the morning but higher in the afternoon, the temperature effect is more evident for the glass-glass module, showing a bigger split between morning and afternoon for γ in Figure 5.2. The larger thermal mass of the glass-glass module affects its temperature behaviour and thus γ.

In the theory section, we explained that due to the form and usage of Equation (5.14), we held n and I_0 constant in the extraction of the temperature coefficients from the outdoor data. In reality, n and I_0 are themselves functions of both temperature and irradiance. By holding them constant, the dependence of these parameters on irradiance and temperature surfaces in γ instead. For example, the reason why γ increases at low irradiance is because n increases at low irradiance [84]. And the reason why γ is higher in the afternoon than in the morning is because I_0 increases with increasing temperature [208].

Of course, it would have been possible to allow n and I_0 to vary with irradiance and temperature, but that would have prevented any reasonable outcome at all. Even $\gamma = 0$ could have resulted. The problem with the temperature coefficient is that it is an abstraction, not a physical solar cell parameter. The module behaviour is already fully described by the ideal diode equation, but the temperature coefficient does not appear here. The temperature coefficient as defined by Equation (5.14) may be a convenient way to describe a module's temperature behaviour, but it is an over-simplification. This is probably also the reason for the controversy surrounding temperature coefficients in the literature [96, 99, 102, 201].

5.2 Operating temperatures of PV modules in Singapore

The PV module temperature is reported to be highly sensitive to irradiance and wind speed, and practically insensitive to the ambient temperature [209]. The mean daily wind speed in Singapore is relatively small, in the range from 1.3 to 2.5 m/s, according to 69 years of data recording [119]. Our measurement of wind speed at the outdoor module testing (OMT), as described in Section 3.2, confirms that mean wind speed over a 3-year monitoring period from January 2011 to December 2013 was only 1.5 m/s, with a standard deviation of 1.1 m/s. Thus, the effect of wind speed on the PV module temperature can be considered small in Singapore [120].

The ambient temperature in Singapore is constantly high over the whole year, as shown in Figure 5.5, a comparison of the average ambient temperature between Singapore and Frankfurt.

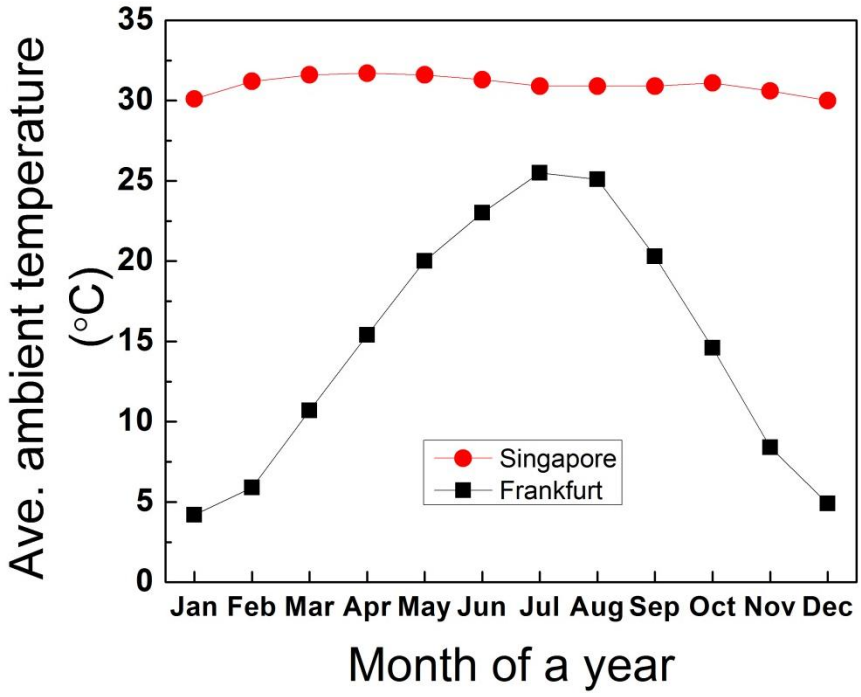

Figure 5.5: Average ambient temperature comparison between Singapore and Frankfurt. [234]

The dependence of module temperature on ambient temperature and irradiance can be studied for different PV modules by extracting the Ross coefficient k from the following model [210]:

$$T_{mod} = T_{amb} + kG \tag{5.14}$$

where T_{mod} and T_{amb} are module and ambient temperatures, respectively. The slope k is called the Ross coefficient which expresses the temperature rise above ambient with increasing irradiance [211].

Measurement data of 10 various PV modules from OMT from 01-Jan-2012 to 31-Dec-2012 were used for such temperature analysis. Only irradiance values above 400 W/m^2 which remain stable (variation within $\pm$80 W/m^2) for more than 2 min were selected for the modelling. The relevant information of the studied modules and the calculated k values are listed in Table 5.1.

Table 5.1: Information of modules for temperature comparison using the Ross coefficient k.

PV module	Technology	Nominal power (W)	Module area (m^2)	Rear material	Frame	k
1	monocrystalline Si	180	1.28	Backsheet	Yes	0.016
2	monocrystalline Si	170	1.70	Glass	No	0.015
3	hetero-junction c-Si	210	1.26	Backsheet	Yes	0.016
4	monocrystalline Si back-contact	95	0.55	Backsheet	Yes	0.016
5	multicrystalline c-Si	230	1.63	Backsheet	Yes	0.016
6	Double-junction micromorph-Si	110	1.22	Backsheet	Yes	0.017
7	single-junction a-Si	60	0.95	Backsheet	Yes	0.017
8	double-junction a-Si	95	1.45	Backsheet	Yes	0.018
9	CIGS	70	0.76	Glass	Yes	0.016
10	CdTe	75	0.72	Glass	No	0.016

Since all the modules are installed on the same racks at the same site with good ventilation (see Figure 3.2), the Ross coefficients are in a relatively small range from 0.015 to 0.018. Most of the studied modules show k of 0.016. The Si based thin-film modules show slightly higher values of 0.017 to 0.018, which might be attributed to their lower efficiency, so more absorbed energy turns into thermal energy. The reported k value for a setup with similar characteristics (concrete rooftop material and with more than 1-meter distance from the ground) extracted from PV systems in Singapore is around 0.022 [120], which is significantly higher than the result from the OMT. This discrepancy might be attributed to the fact that only one module in a string is measured for the case of PV systems, and very often the one in the middle of the string is measured. Therefore the ventilation might not be as good as an individual free-standing module (like at the OMT setup) and hence the module temperature increases at a higher rate.

Figure 5.6 shows the dependence of the temperature difference between module and ambient environment on the irradiance level. The module temperatures were measured at the backside using a PT1000 thermocouple. The thermocouples were calibrated by the manufacturer with an uncertainty within ±0.7% for the measurement range. As can be seen, the temperature difference among the various PV modules is within 3°C for the same irradiance intensity.

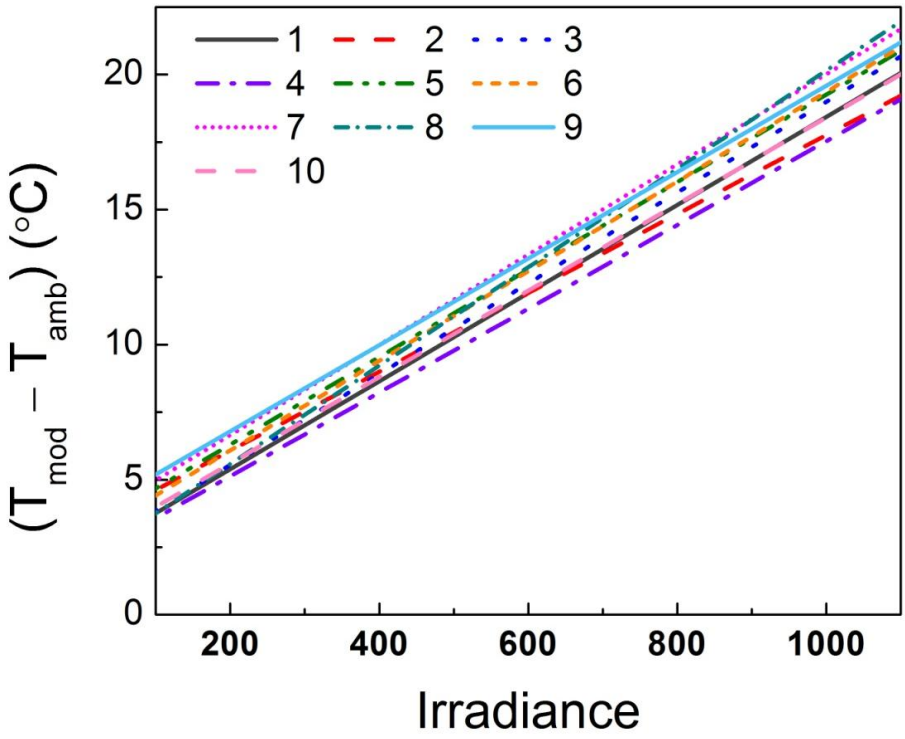

Figure 5.6: Dependence of module temperature above ambient temperature on irradiance intensity for the 10 modules in this study. The module type corresponding to each number is listed in Table 5.1.

Compared to summer in temperate climate regions, the module temperature in the tropics is not significantly higher [212]. However, due to little variation of the module temperatures throughout a year, higher thermal loss for crystalline Si modules is expected. On the contrary, for a-Si modules, the constantly high module temperature has positive effect to their performance since they are continuously annealed, healing dangling bonds caused by the Staebler-Wronski effect [44, 45].

Figure 5.7 shows the distribution of module temperature during daytime period (irradiance above 20 W/m^2) for the monocrystalline Si with the standard glass/cell/backsheet construction with aluminium frame. The temperature distribution has two peaks. The one in the range of 31 to 35 °C is mainly attributed to irradiance below 400 W/m^2. The other in the range of 45 to 51 °C is mostly contributed by irradiance between 600 and 900 W/m^2.

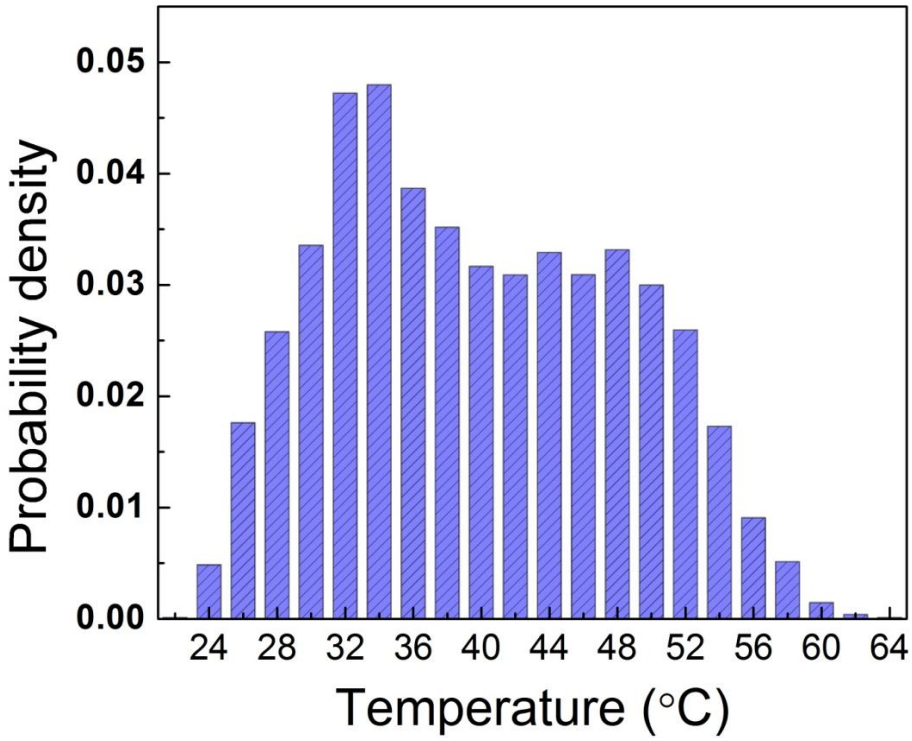

Figure 5.7: Distribution of module temperatures (monocrystalline Si module with standard glass-backsheet construction) over a 1-year period from 1-Jan-2013 till 31-Dec-2013. Data with irradiance below 20 W/m^2 was filtered out to exclude night time conditions.

5.3 Thermal loss of PV modules working in the tropics

As discussed in Section 5.1, the temperature coefficient of P_{mpp} is not a physical parameter and its value in reality is dependent on irradiance, temperature, and possibly the material status of the module. A full understanding of the thermal behaviour of various PV module technologies would require continuous power measurement under temperature-controlled environments. These experiments are not covered in this work but are recommended as future work.

To estimate the loss of the module power due to relatively high operating temperature in Singapore throughout the year, the γ from the datasheet is applied. The relative thermal loss (TL) over a period of time can be calculated as:

$$TL = \frac{\sum P_{mpp}/[1+\gamma(T-T^*)] - \sum P_{mpp}}{\sum P_{mpp}/[1+\gamma(T-T^*)]} \quad (5.15)$$

The annual thermal loss for the 10 PV modules listed in Table 5.1 is shown in Figure 5.8. The error bars account only for the measurement uncertainty of the setup, which is ±2%.

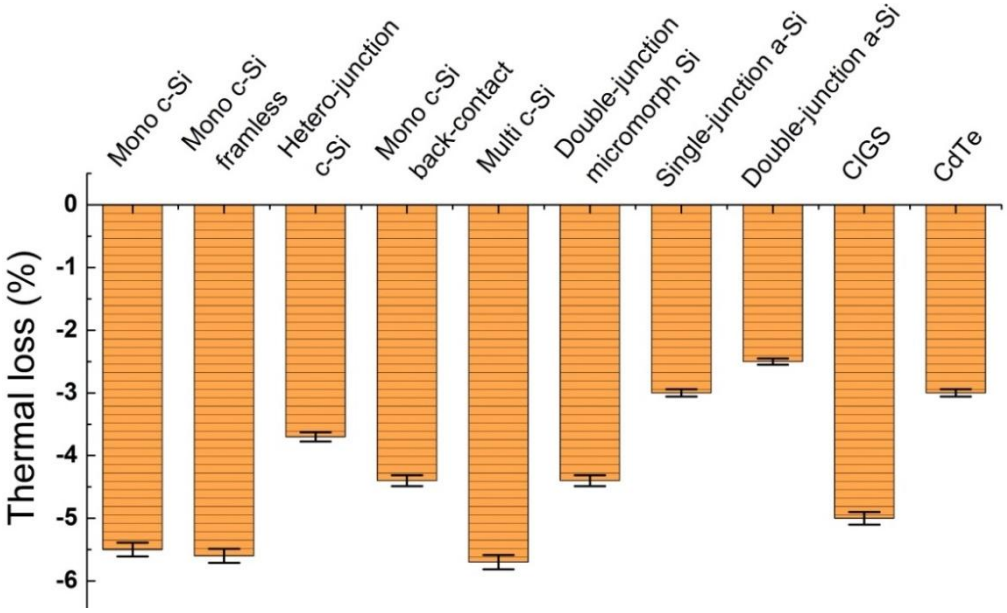

Figure 5.8: Thermal loss of the 10 PV modules, calculated based on the temperature coefficient from datasheet.

The correspondingly calculated annual thermal loss of the conventional c-Si modules (mono c-Si and multi c-Si) is around -5.5%, while the high-efficiency c-Si modules (hetero-junction c-Si and back-contact c-Si) show 1 to 2 % lower losses. Amorphous Si modules show the least thermal losses, of less than -3% per year. The annual thermal loss percentage is correlated to the absolute reduction of the Performance Ratio of the studied modules.

5.4 Conclusions

An expression was derived, based on the one-diode model, to extract the temperature coefficient from outdoor monitoring data and STC measured I-V characteristics. It was found that the temperature coefficient of the maximum

power for the studied modules depends on both irradiance and module temperature. The distribution of module temperature in tropical Singapore was presented and the difference between module and ambient temperatures for various module technologies under the same operating conditions was shown to be around 3°C. The annual thermal loss of power for various module types was calculated to be between 2.5 and 5.5 %.

Chapter 6 Long-term outdoor performance of PV modules in tropical Singapore[*]

This chapter focuses on the long-term performance of PV modules operating in tropical Singapore, including a degradation study and the discussion on the seasonal performance variation. The performance of ten PV modules with nine different solar cell technologies (and one different module construction) was monitored over a 3-year period. The statistical method applied for the long-term performance study is first introduced. Then the degradation and seasonality are discussed. The module degradation rates are found to be relatively high compared to those reported in temperate climates. The seasonality of the PV module performance is shown to be small for c-Si modules, and insignificant for thin-film modules.

6.1 Methodology

The degradation of PV modules is usually studied with regression fitting to continuous data (i.e., monthly or daily performance ratio (PR) as defined in IEC standard 61724 [79]), assuming a linear degradation over the long-term operation [118, 213-215]. Other methods include comparing the annual PR [216], periodic indoor evaluations [214, 217-219], or regular outdoor measurements under similar meteorological conditions [133, 213, 220]. Although the degradation of PV modules is often regarded as linear for long-term operation, thin-film modules tend to show a steeper degradation during the initial months of exposure to sunlight [3, 6]. In addition, linear regression is sensitive to data

[*] The work described in this chapter is based on the publication "Performance degradation of various PV module technologies in tropical Singapore," *IEEE Journal of Photovoltaics*, DOI:10.1109/JPHOTOV.2014.2338051

outliers and neglects the possible seasonality of the data, so several complete cycles (typically five years) are needed to obtain reasonably accurate degradation rates [221]. Statistical decomposition, in contrast, is known as a robust way to determine both degradation rates and seasonal trends at the same time, with smaller uncertainties, even for shorter observation periods compared to linear fitting [222]. Therefore, in this work, a statistical decomposition method is used to extract the degradation rates and seasonality from the data. Degradation rates for the performance ratio (see Section 1.2.3.2), as well as I-V characteristics, V_{OC}, I_{SC} and FF are obtained for 10 PV modules with 9 different technologies over a 3-year period.

The statistical decomposition method applied in this study is based on the locally weighted scatterplot smoothing (LOWESS) [197, 223] to extract the degradation trend of the PR. 'LOWESS' allows more flexible regression than some other smoothers like linear regression or polynomial regression. It effectively fits a complex curve driven by the local properties of the data. The time series is decomposed into seasonal, trend and irregular components by applying a sequence of LOWESS. It is an interacting process of filtering to look for the optimized seasonal and trend components by assigning robustness weights to data depending on the remainders calculated from the previous pass. The seasonal component was found by LOWESS smoothing the seasonal sub-series (i.e., the series of values at each month across the years of observation, the first sub-series being the January values), which assumes that the seasonal index variation is the same for each year of observation. The trend was then obtained by subtracting the seasonal component from the original data, followed by LOWESS smoothing. The irregular component is the remaining

variation in the data beyond that in the seasonal and trend components. Depending on the remainder, weights are assigned to each data point and the decomposition process is repeated until the trend and seasonal components converge. Supposing that the data, the seasonal component, the trend component, and the remainder component are denoted by *Y*, *S*, *T*, and *R*, respectively, then the decomposition can be written as:

$$Y = S + T + R \tag{6.1}$$

The trend component is the low-frequency (lower than seasonality) variation in the data together with non-stationary, long-term changes in level. Since robustness weight is considered during the LOWESS smoothing, outliers are assigned with small weights during the regression and cause only small uncertainties to the decomposition. Figure 6.1 shows an example of the decomposition of the monthly PR values for the investigated double-junction micromorph Si module.

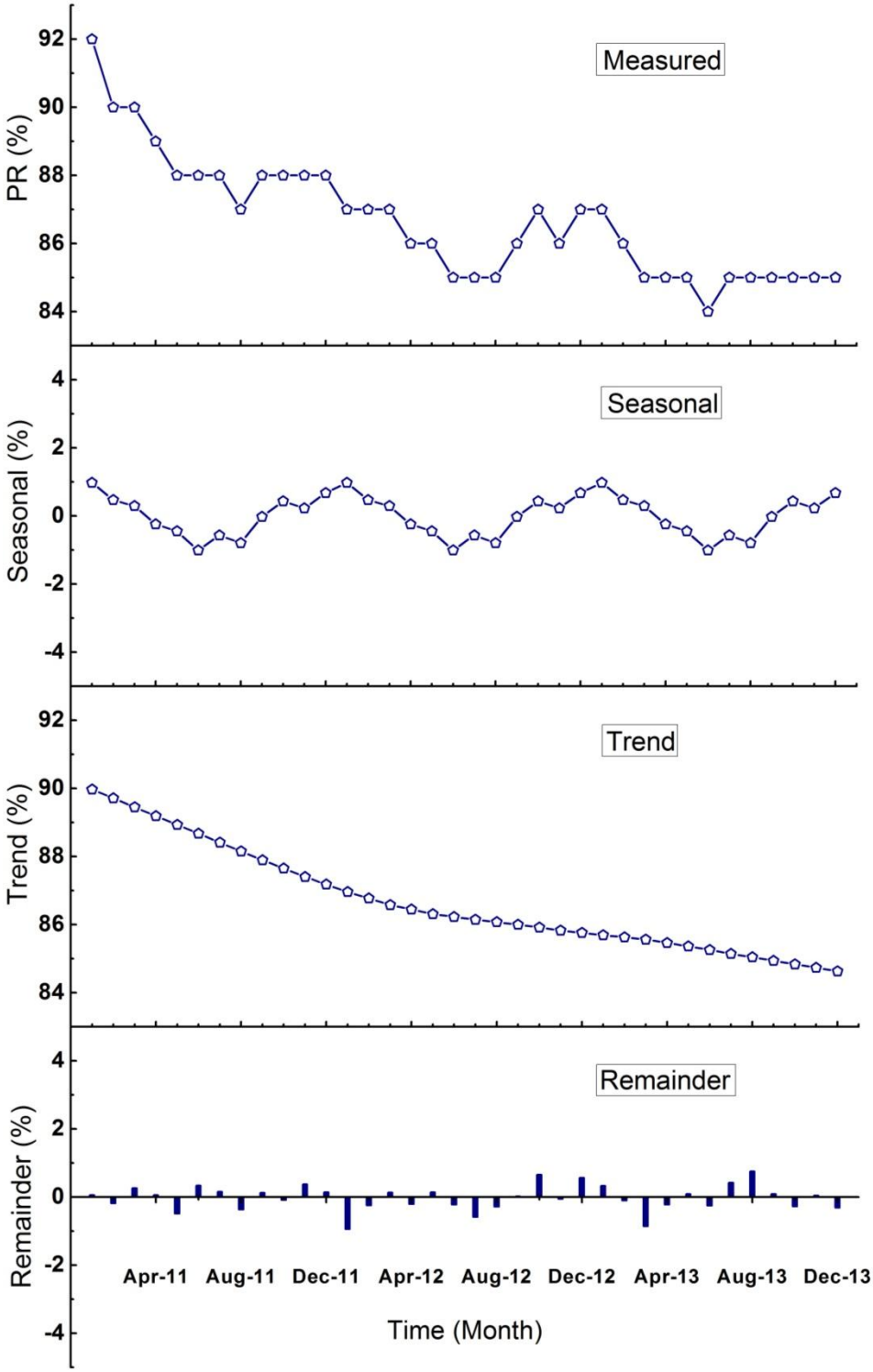

Figure 6.1: The decomposition of monthly performance ratio (PR) for the double-junction micromorph Si module from 01-Jan-2011 till 31-Dec-2013.

6.2 Data for the study

In this study, measurement data from the outdoor module testing (OMT) facility at SERIS (as described in Section 3.2) from 1st January 2011 to 31st

December 2013 were used for the long-term performance analysis. All of the modules studied were installed in August 2010 and had been exposed to outdoor solar radiation for more than 4 months before the data analysis period; hence it is reasonable to assume that this study is not influenced by the initial light-induced degradation processes. For the parameters of these modules, please refer to Table 5.1 on page 95.

6.3 Degradation

Although the degradation of PV modules has been studied widely [118, 133, 216, 218, 220, 224], very few reports are found for the tropics [217, 225]. While the warranties from manufacturers are usually 20 to 25 years regardless of operating conditions, evidence indicates that the degradation mechanisms and degradation rates of PV modules are location dependent [118, 217]. In temperate regions where the ambient temperature changes considerably from summer to winter, the degradation of the interconnections attributed to thermo-mechanical fatigue is one of the dominant factors [226]. In Singapore, the ambient temperature varies daily between 25 to 33 °C, with little variation over the year. The humidity is constantly high with the mean annual relative humidity of 84.2% and annual average rainfall of 2156 mm [119]. Thus, high humidity combined with high temperature quite likely contributes to enhanced moisture ingress into modules, leading to a faster corrosion of solder bonds in c-Si modules, or of the transparent conductive oxide layer of thin-film PV modules [130, 227].

6.3.1 Degradation trend

6.3.1.1 Performance ratio (PR)

In this study, the DC performance ratio (PR), which is described in Section 1.2.3.2, is used as an indicator of the module performance.

Figure 6.2 shows the measured monthly PR of the studied modules from 1st January 2011 to 31st December 2013. A decreasing trend is obvious, especially for the thin-film modules. After applying the decomposition, the trend of the PR is shown in Figure 6.3. The a-Si, micromorph Si and the CdTe modules show a higher degradation rate in the first year, and tend to decrease more slowly from the second year onwards. The degradation rate of the GIGS module, however, seems to increase after month 9 (i.e., September 2011).

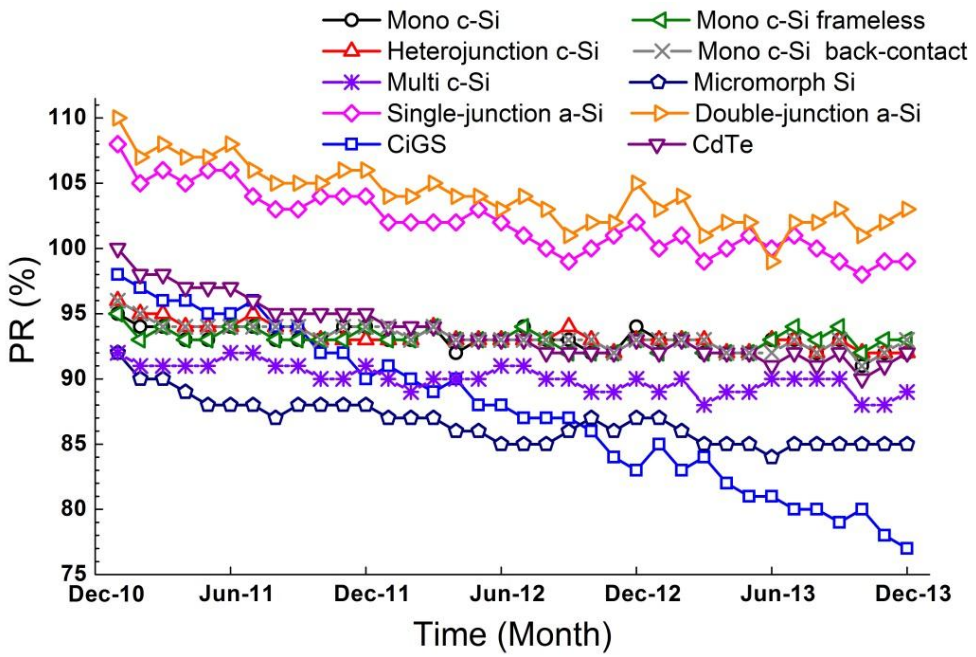

Figure 6.2: Measured monthly performance ratios (PR) of the 10 module types under investigation in this study.

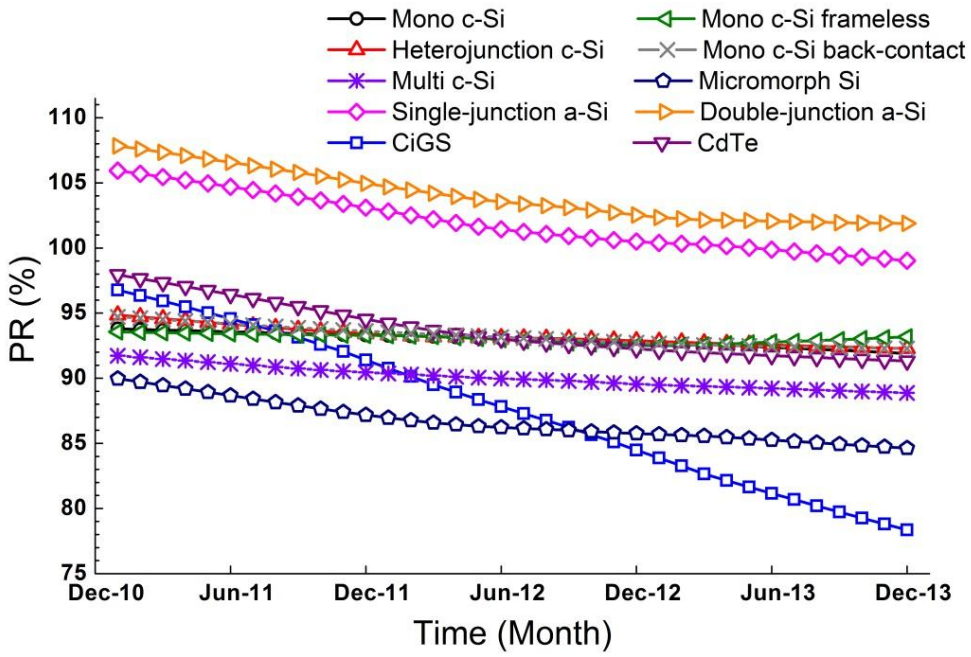

Figure 6.3: The decomposed trend of performance ratios (PR) of the 10 module types under investigation in this study.

6.3.1.2 Analysis of the degradation of individual components

To understand the reasons leading to the degradation of the PR, the degradation trend of the three parameters from the outdoor-measured I-V curves (short-circuit current I_{SC}, open-circuit voltage V_{OC}, fill factor FF) are studied. For a better comparison, only data at irradiance intensities within 900 ± 10 W/m^2 and which remained stable for at least 2 minutes were selected. The reason to choose 900 W/m^2 instead of 1000 W/m^2 is that irradiances above 1000 W/m^2 are mainly attributed to cloud reflection and are usually not stable, as discussed in Chapter 4. The parameters were then averaged monthly for long-term comparison purposes. Thereafter the decomposed trends of these three parameters (I_{SC}, V_{OC}, FF) were extracted with the same decomposition method as described earlier.

Figure 6.4 shows the degradation rates of the decomposed trends of the I-V curve components (I_{SC}, V_{OC}, FF) for the various modules. Based on these

results, the average annual degradation rates calculated from the decomposed trends of the monthly PR and the I-V curve parameters can be seen in Figure 6.5.

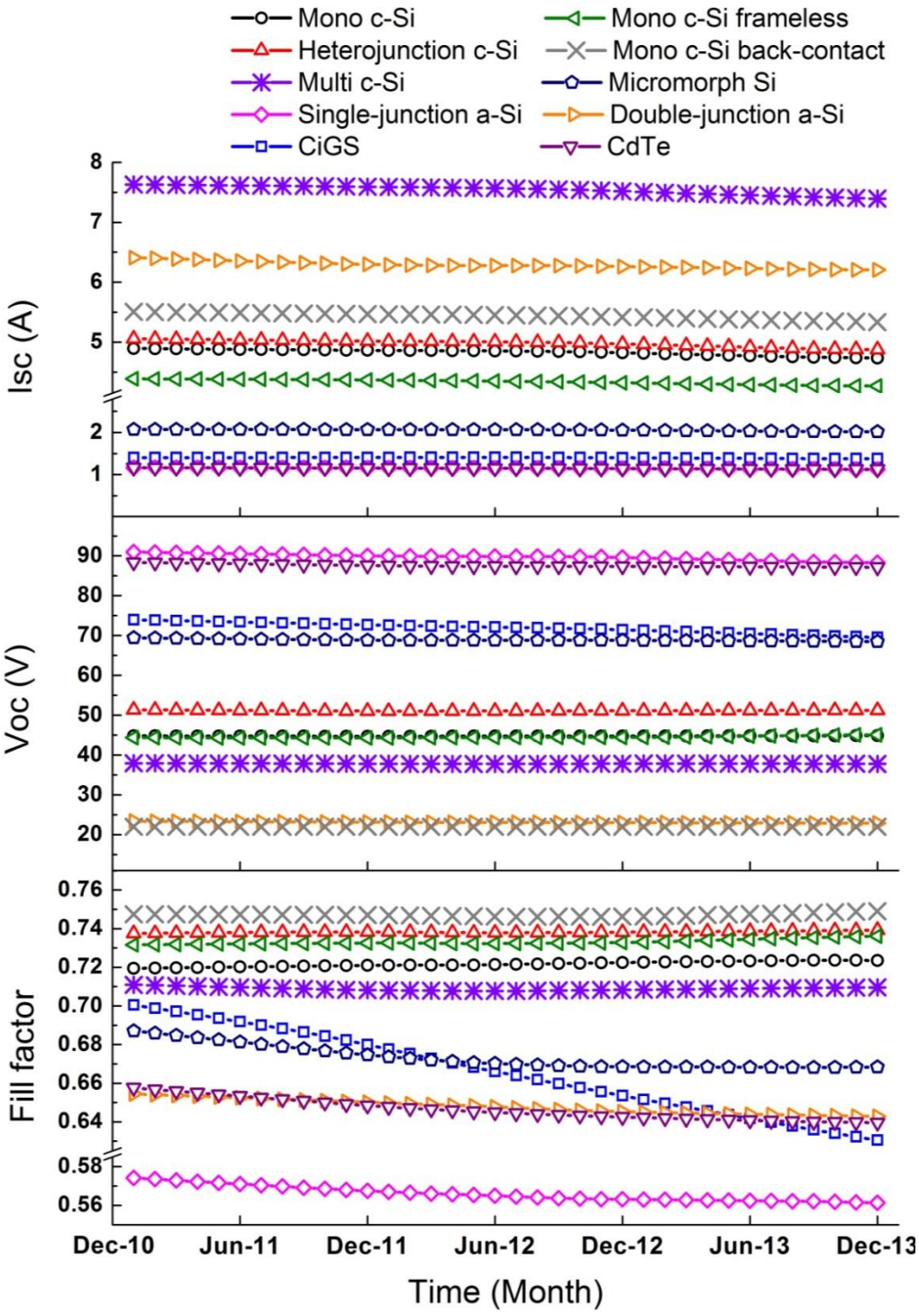

Figure 6.4: Decomposed trend of short-circuit current (I_{SC}), open-circuit voltage (V_{OC}), and fill factor of the 10 modules under investigation in this study.

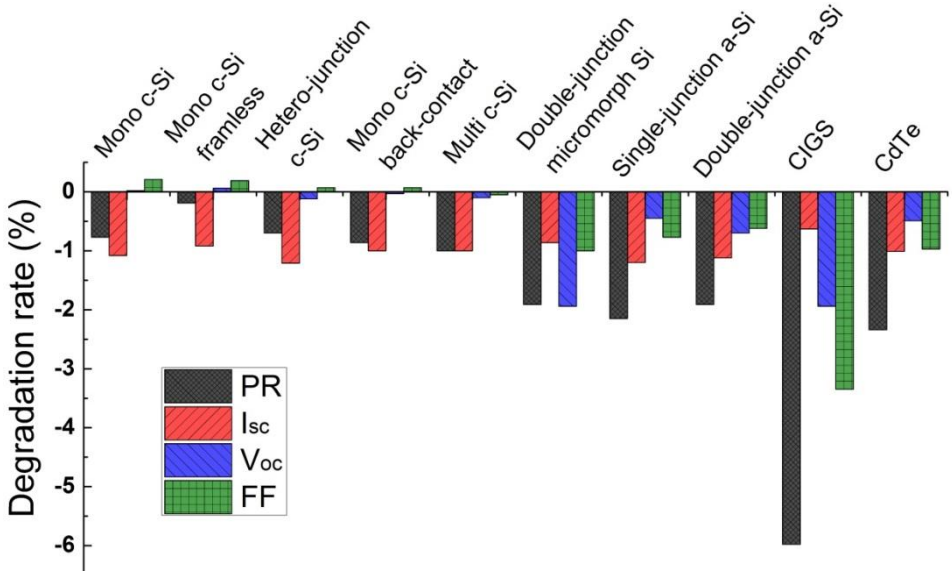

Figure 6.5: Average annual degradation rate (%) of performance ratio (PR) and the I-V curve components: short-circuit current (I_{SC}), open-circuit voltage (V_{OC}), fill factor (FF) for the 10 module types under investigation in this study.

The average degradation rates of the monocrystalline Si modules (monocrystalline Si, monocrystalline Si frameless, hetero-junction c-Si, mono-crystalline Si back-contact) are less than -0.8%/year, which is within the range to meet the 20-25 year power output warranty. The glass-glass mono-crystalline Si module (labelled "frameless" in the graphs) shows exceptionally low degradation over the 3-year period. The multicrystalline Si module shows a slightly higher degradation rate of around -1.0%/year. The CIGS module showed the - by far - highest degradation rate of the PR of around -6%/year, which is related to significant decreases in V_{OC} and fill factor. The degradation rate of the a-Si (single-junction and double-junction), micromorph Si, and CdTe modules is around -2%/year.

6.3.2 I-V characteristics

In order to provide a familiar visual representation of the degradation, we compare the I-V curves measured outdoors on two days in separate years under similar operating conditions. Figure 6.6 shows the outdoor-measured

I-V curves of the 10 different modules on 01-Jan-2011 and 01-Jan-2013 at around the same time (11:30 am) with the same irradiance of ~900 ± 10 W/m^2 (stable for > 2 min). Since the I-V curves were measured at the same day of the year and around the same time of the day with stable irradiance conditions, differences in air mass and spectrum can be considered minimal [213]. The differences in module temperatures for all studied modules were within ±1.5^oC when the two measurements were conducted. Therefore, it is reasonable to assume that the differences in the I-V curves indeed result from the degradation of the modules rather than differences in the measurement conditions.

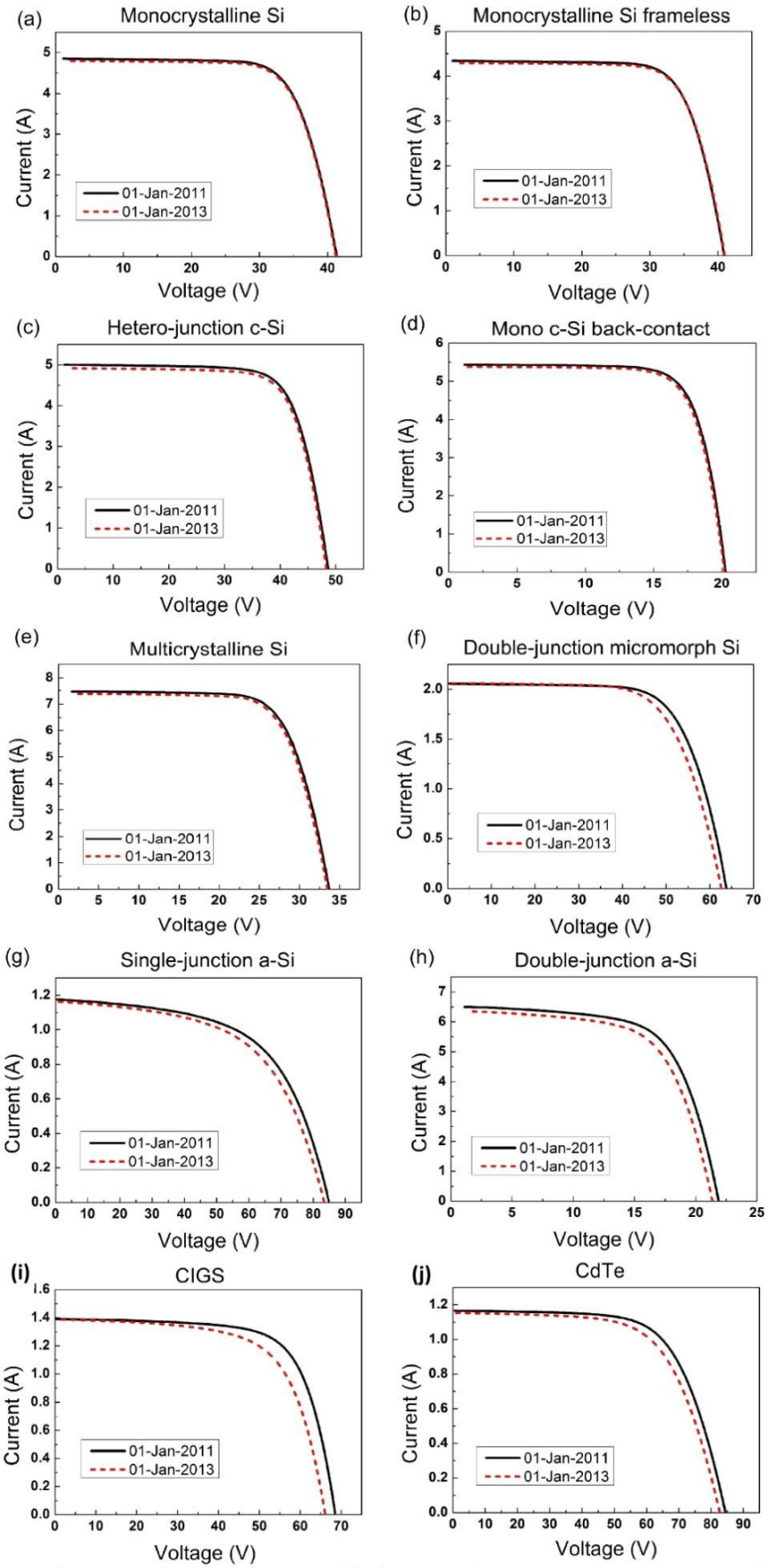

Figure 6.6: I-V curves of the 10 module types under investigation in this study on 01-Jan-2011 and 01-Jan-2013, at around 11:30 with irradiance of 900 ± 10 W/m^2 (stable for > 2 min).

For the five crystalline Si modules (monocrystalline Si, monocrystalline Si frameless, hetero-junction c-Si, monocrystalline Si back-contact, and multi-crystalline Si modules), the short-circuit current decreases slightly, while the open-circuit voltage remains almost the same. For the double-junction micromorph Si module and the CIGS module, the short-circuit currents decreased very little, but both the open-circuit voltage and fill factor decreased significantly, leading to the strong decrease of the maximum power. The single-junction a-Si module, the double-junction a-Si module, and the CdTe module show a reduction in I-V curve parameters at a similar rate. The results are consistent with the degradation rates shown in Figure 6.5.

6.3.3 Discussion

6.3.3.1 Decrease in short-circuit current I_{SC}:

Since the PV modules were not cleaned during the outdoor exposure, the soiling effect is naturally incorporated into the degradation results. Soiling will affect the I_{SC} of modules (by reducing the irradiance passing through the front glass), but not the other parameters. Since all the modules are installed on the same rooftop with the same tilt angle, all modules received the same amount of soiling, while framed modules tend to have more soil accumulation at the lower frame edge. Besides soiling, there are other factors which decrease the I_{SC} of the modules, depending on the module type and technology, such as EVA discoloration or decreased transmission of the short-wavelength photons [133, 220]. Hence, the maximum soiling rate should be less than the decrease rate of I_{SC}, which is around -1%/year, as shown in Figure 6.5. Further

investigations are needed to quantify the contributions leading to the decreased I_{SC}.

6.3.3.2 Decrease in open-circuit voltage V_{OC}:

For all the thin-film modules in this study, the decrease in V_{OC} was significant. In contrast, for all c-Si modules the variation in V_{OC} was negligible. The decrease in V_{OC} is related to the deterioration of the diode quality, such as an increase in the saturation current or the ideality factor, or both [228]. Different technologies have different failure mechanisms. In the case of a-Si modules, their degradation is mainly attributed to the quasi-stable characteristics under illumination (the so-called "Staebler-Wronski effect") [44]. Exposure to light increases the defect density inside the solar cells and hence decreases V_{OC} [229]. However, other than cell technology, difference in module construction can also impact the reliability of the underlying PV cells, which will be discussed later.

6.3.3.3 Fill factor (FF):

For the four monocrystalline Si modules studied, no significant variation in fill factor was observed. From this, we can assume that the series and shunt resistances of these modules did not change significantly. If the series resistance remains the same and I_{SC} decreases, then the power loss resulting from the series resistance will decrease and thus the fill factor will actually increase slightly. As a result, the degradation of the monocrystalline Si modules is partially compensated by the fill factor gain.

The a-Si (single-junction and double-junction), micromorph Si, CdTe, and CIGS modules suffered from fill factor degradation due to either increased

series resistance and/or decreased shunt resistance. No noticeable electrical connector degradation was observed for all the ten modules studied.

6.3.3.4 Possible reasons for the observed degradation rates

All the thin-film modules in this study have one or no bypass diode. It has been reported that the external bypass diode of modules with monolithic panel fabrication and long-thin-stripe cells only start operation when a large area (>40%) of the module is shaded, while the shaded cells can experience high reverse bias with small shadows [230]. If the shadow is only on one or a few cells, significant reverse bias stresses occur. The monolithic modules with frames used in this study are tilted with the cells vertical, so that the shading induced by dust accumulation at the lower frame edge is symmetric for all cells and not causing highly reverse-biased cells. Without appropriate bypass diode design, monolithic panels are more susceptible to reversed stresses induced by partial shadowing, compared to c-Si wafer-based modules with integrated bypass diodes. It has been reported that saturation current increases significantly after negative-bias stress, causing a decrease in both V_{OC} and FF [231]. This might contribute partially to the degradation rates seen in this study for thin-film modules but should not be the main cause, because installation was designed for minimal shading.

The CIGS module in this study showed a particularly severe degradation rate of -6%/year (see Figure 6.5). Some CIGS modules are reported to show high sensitivity to moisture ingress, with significant decrease in V_{OC} and FF due to increased leakage current [232, 233]. The observed high degradation rate might be related to the constantly high humidity (above 80%) in

Singapore, in addition to the reverse-bias behaviour as discussed above. However, since only one module for each technology was monitored, the result is not statistically significant enough to draw general conclusions about particular technologies. It is possible that the CIGS module in this study was an outlier.

Different module constructions (e.g. encapsulant material, rear material, use of edge sealing) employed by different manufacturers can strongly influence the performance degradation. Research on the impact of construction to performance degradation is thus highly necessary.

6.3.4 Summary

The degradation of the c-Si modules is mainly due to the decrease in I_{SC}. The thin-film modules showed a significant reduction in V_{OC} and fill factor. While the fill factor of the monocrystalline Si modules increased with the decreasing I_{SC}, the fill factor of all thin-film modules decreased due to the increased series resistances and the decreased shunt resistances.

6.4 Seasonality

In tropical regions near the equator like Singapore (1° north), which show no distinctive “seasons” and are characterized by constant high ambient temperatures, it is logic at first to assume that the performance of PV modules would not show any seasonal variations. However, the decomposed seasonal element of the monthly PR (Figure 6.7) indicates a small seasonality of less than $\pm$2%, compared to temperate climates where performance variation can be as high as 25% [182].

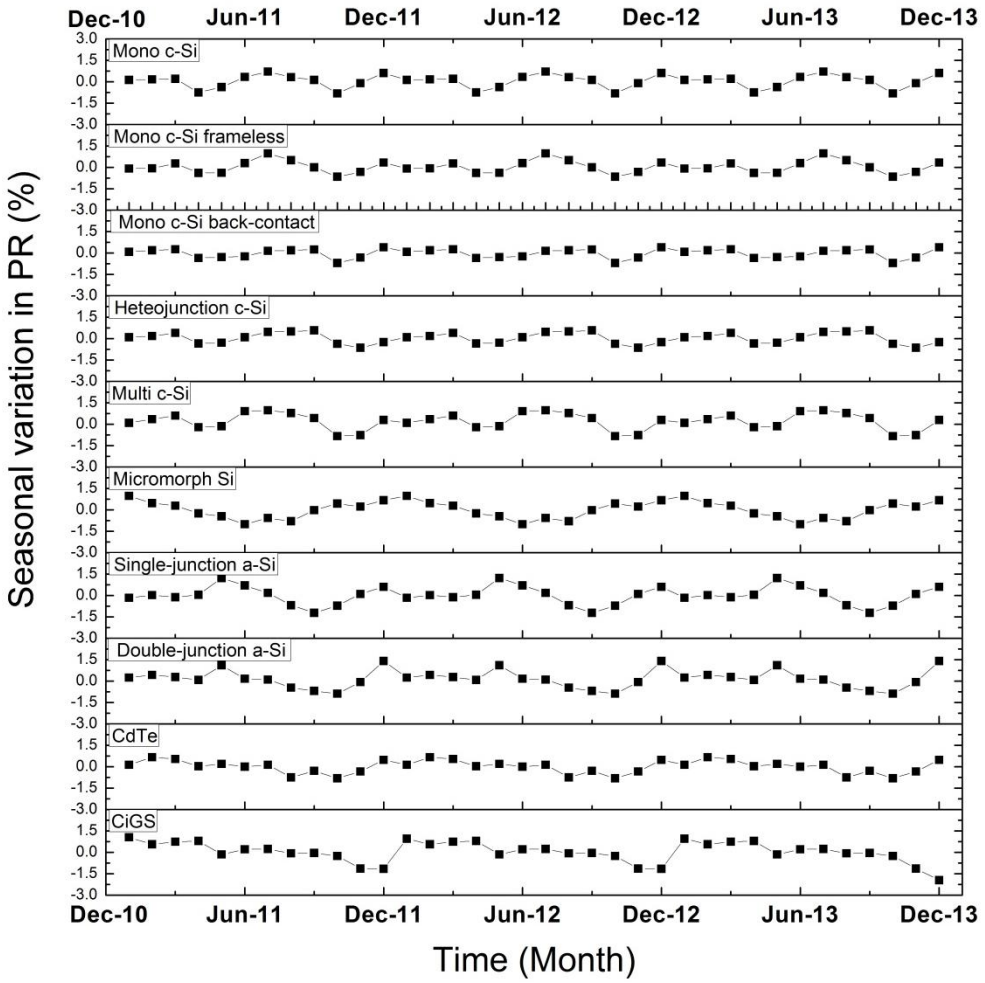

Figure 6.7: Decomposed seasonality of different PV technologies from 1-Jan-2011 to 31-Dec-2013.

The c-Si modules shows similar trends of seasonal variation, which follows the variation of the air mass at solar noon as shown in Figure 6.8 [183]. By calculating the correlation coefficient between the daily average module temperature and the daily performance ratio, it is found that the performance variations of the c-Si modules are mainly related to the module temperature variations [183]. The air mass at solar noon is correlated to the radiation energy arriving on the ground; hence the module temperature is directly proportional to the incident irradiance (see Section 5.2 on page 94). Since the efficiency of c-Si modules is highly dependent on the module temperature, their performance varies correspondingly.

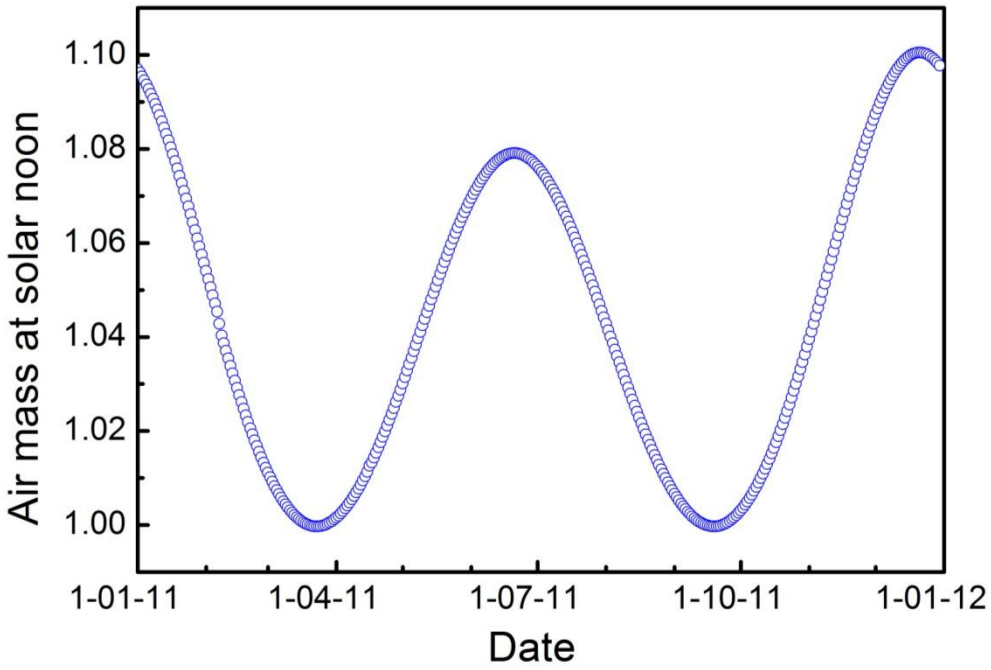

Figure 6.8: Variation of air mass in Singapore at solar noon over a year [183].

However, for the thin-film modules, the seasonal variations in performance ratio vary differently for each technology. Besides module temperature, the performance of thin-film modules depends additionally on the spectral distribution or the history of illumination and annealing. The significance of each factor also varies depending on technologies. Hence the seasonal variation is not as pronounced as for the c-Si modules.

6.5 Conclusion

The performance of 10 different types of PV modules was continuously monitored over 3 years in tropical Singapore. A statistical decomposition method was applied to extract the degradation trend and the seasonal component. The degradation rate of the monocrystalline Si module in this study was less than -0.8%/year, while the multicrystalline Si module degraded at around -1.0%/year. The studied thin-film modules showed degradation rates of around -2%/year, with an exceptionally high degradation rate of -6%/year

for the investigated CIGS module. However, the results are not statistically significant enough to draw general conclusions about particular PV technologies, since only one module for each technology was monitored. The mono c-Si frameless module with the glass/glass construction showed the lowest degradation rate, demonstrating the suitability of this module construction for deployment in the tropics.

The seasonality of PV module performance was shown to be small for c-Si modules, which is mainly corresponding to the temperature variation. For thin-film modules, the seasonality is insignificant.

Chapter 7 Tropical test conditions (TTC)

The existing standard test conditions (STC) reflect more the environmental conditions in temperate regions. As discussed in the previous chapters, the tropical conditions (irradiance intensity, spectrum, module temperatures) are much different from the STC and they can result in significant deviations of the effective module efficiency and energy yield. The performance ratio comparison across different technologies based on STC therefore leads to inconclusive results, even though they are part of an identical measurement setup (see Figure 7.1).

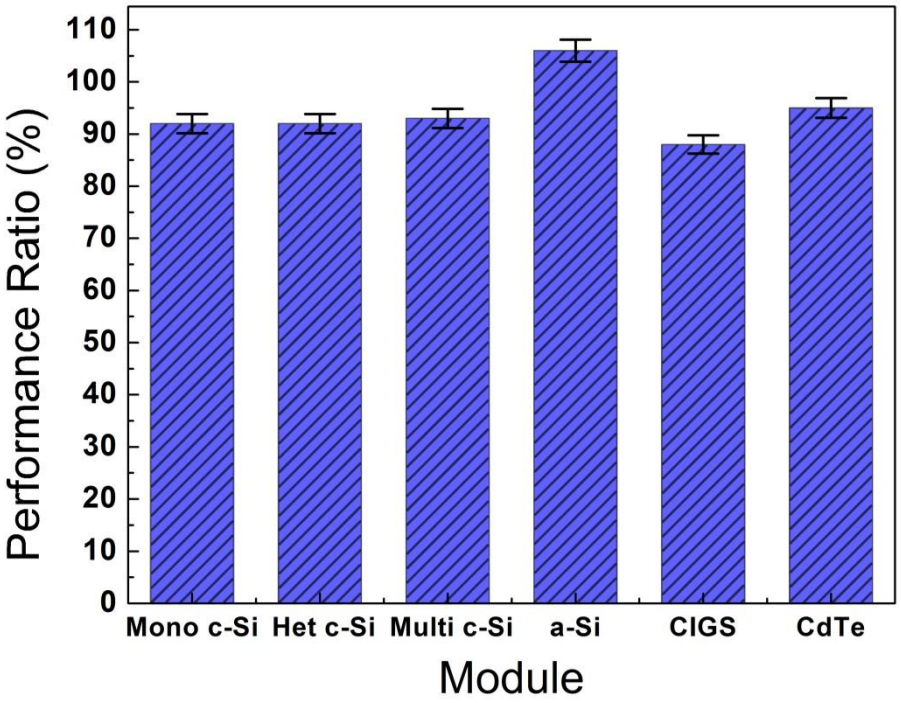

Figure 7.1: DC performance ratio (PR) based on STC power for individual modules. Data from 01-Jan-2013 till 31-Dec-2013 were used for the calculation.

Hence, it would be desirable to have a set of test conditions which can be used for either indoor or outdoor measurements and reflect the tropical PV module working conditions, to enable a standardized performance comparison across different PV technologies under these conditions. This chapter

summarizes the typical operating conditions of PV modules in tropical Singapore. Thereafter, so-called “Tropical Test Conditions” (TTC) are proposed. The power rating under TTC is demonstrated to serve as a benchmark for outdoor module performance comparison.

7.1 Defining the new tropical test conditions (TTC)

In order to define the tropical test conditions, representative values for the irradiance, the module temperatures, and solar spectrum need to be defined.

7.1.1 Irradiance

In Chapter 4, the radiation distribution with respect to time range of variability and irradiance level for year 2011 was discussed. Correspondingly, Figure 7.2 shows the radiation energy distribution with irradiance level for the year 2013, which shows a similar trend as 2011. The distribution of solar radiation peaks at irradiance between 700 to 900 W/m^2 and contains substantial portions of stable irradiance (see Figure 4.3 on page 74) in this range. Considering that the TTC should also be compatible with convenient outdoor measurements, stable irradiance conditions are necessary. Thus, 800 W/m^2 is chosen for the irradiance intensity. To define the spectrum and the module temperature part of the TTC, the range of 700 to 900 W/m^2 is considered as initial input parameters.

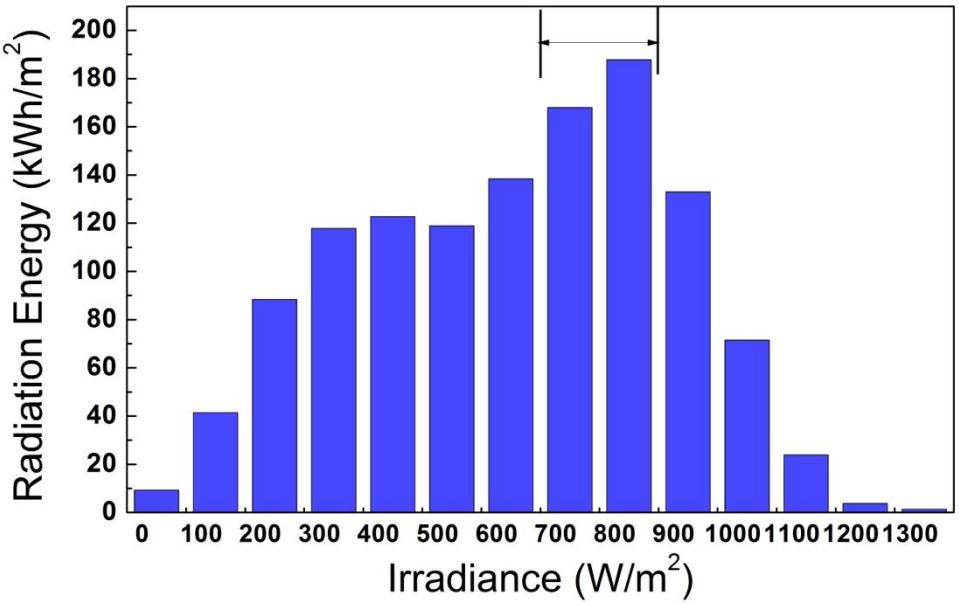

Figure 7.2: Distribution of radiation energy with respect to irradiance level over year 2013.

7.1.2 Spectrum

Chapter 4 showed that the spectrum in tropical regions is constantly blue-rich compared to AM1.5G. This is a combined effect of the low latitude (i.e., the low air mass), the high humidity, and the high diffuse/direct irradiance ratio. Figure 7.3 shows the distribution of the solar radiation against the average photon energy (APE) (as explained in Section 3.1.3, calculated for the range of 305 - 1150 nm) for all irradiance levels over the 1-year period of 2013. The radiation energy peaks at the APE of 1.87 eV, while the APE value for the standard AM1.5G spectrum is 1.83 eV.

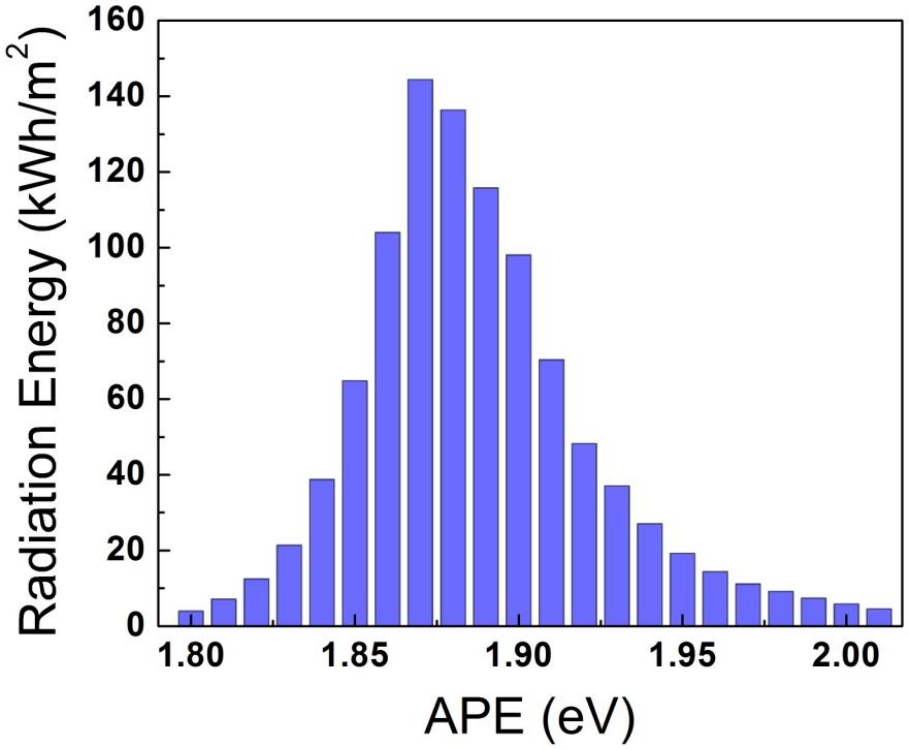

Figure 7.3: Histogram of APE for all irradiance levels over the whole year of 2013.

For irradiances between 700 and 900 W/m^2, the APE is mainly around 1.88 eV, as shown in Figure 7.4.

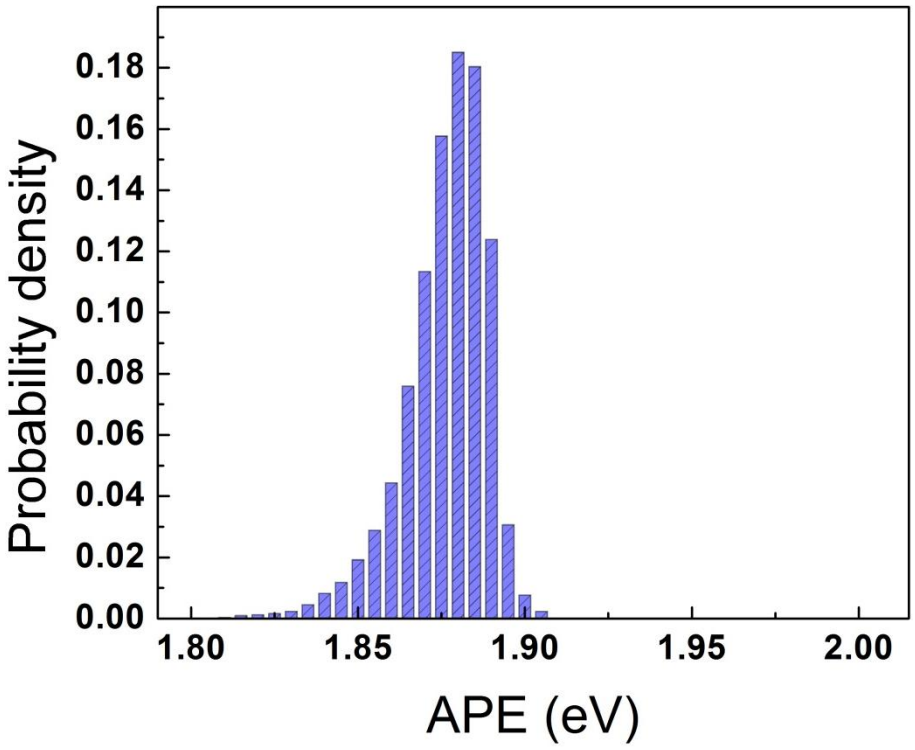

Figure 7.4: Histogram of APE with irradiance within the 700 - 900 W/m^2 range.

To choose the APE value for the spectrum, the average irradiance weighted APE is calculated by applying Equation (7.1), using the one-year data from 01-Jan-2013 till 31-Dec-2013 and the irradiance band 700 - 900 W/m^2.

$$APE_{Irr-weighted} = \frac{\sum_{700}^{900} G \cdot APE}{\sum_{700}^{900} G} \quad (7.1)$$

The resulting annual average irradiance-weighted APE is 1.879 eV. Thus 1.88 eV is chosen for the tropical test conditions. The spectral distribution was obtained by averaging the spectra with 1.880 $\pm$ 0.005 eV and irradiance 700 - 900 W/m^2 of every wavelength into a single spectrum. The tabulated value of the spectrum is attached in Appendix 2.

7.1.3 Module temperature

In Section 5.2, the actual operating temperature of PV modules installed in Singapore was discussed, with Figure 5.7 showing the distribution of module temperatures for the monocrystalline Si standard construction (glass/cell/ backsheet with aluminium frame) for all relevant irradiance levels. The other investigated PV module technologies show a similar distribution and hence are not shown additionally. To define a representative module temperature for the tropical test conditions, Figure 7.5 zooms into the irradiance range of 700 - 900 W/m^2.

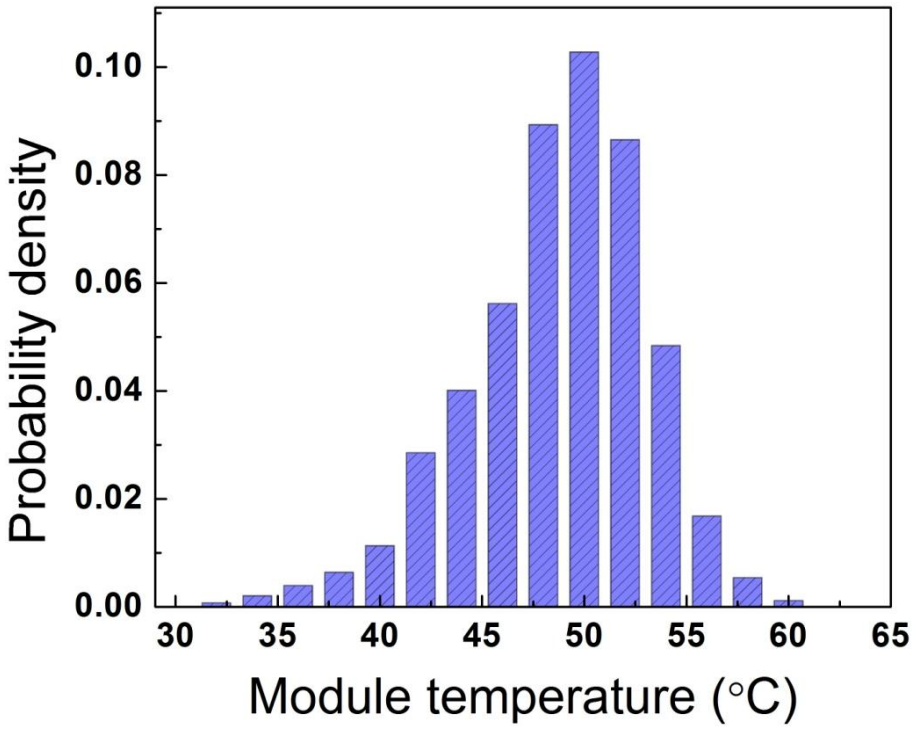

Figure 7.5: Histogram of module temperature over a one-year period from 01-Jan-2013 to 31-Dec-2013, with irradiances between 700 and 900 W/m^2.

Similarly, average irradiance weighted module temperature is calculated by applying Equation (7.2), using the same data set for the average irradiance-weighted APE.

$$T_{Irr-weighted} = \frac{\sum_{700}^{900} G \cdot T_{mod}}{\sum_{700}^{900} G} \tag{7.2}$$

The resulting annual average irradiance-weighted module temperature is 49.5°C Hence we define the Tropical Test Conditions (TTC) module temperature as 50°C.

7.2 TTC-based performance ratio (PR)

To verify the validity of the tropical test conditions (TTC), six PV modules with different technologies (mono c-Si, hetero-junction c-Si, multi c-Si, a-Si single-junction, CIGS and CdTe) were measured indoors with the newly defined conditions. Multi-junction modules (micromorph Si and a-Si double-

junction) were excluded from this study since the spectral responses of these modules are not available for spectral mismatch correction. The intensity of the solar simulator was corrected for spectral mismatch as discussed in Section 2.3.2 by applying the spectral mismatch factor:

$$G_{corrected} = \frac{G^{standard}}{MMF} \tag{7.3}$$

where $G_{corrected}$ is the corrected irradiance reading of the reference sensor, $G^{standard}$ is the standard irradiance reading (800 W/m^2 for TTC) of the reference sensor. MMF here is calculated based on the TTC spectrum.

The annual performance ratio (PR) (see Section 1.2.3.2 for the definition) of these 6 PV modules were calculated based on the TTC rated power. When calculating PR with the TTC rated power, Equation (1.2) on page 12 needs to be modified to

$$PR = \frac{E_{AC} \times G_{TTC}}{E_i \times P_{mpp}^{TTC}} \tag{7.4}$$

where G_{TTC} is the irradiance level at TTC, which is 800 W/m^2.

Data from 01-Jan-2013 till 31-Dec-2013 were used for this study. Results are shown in Figure 7.6.

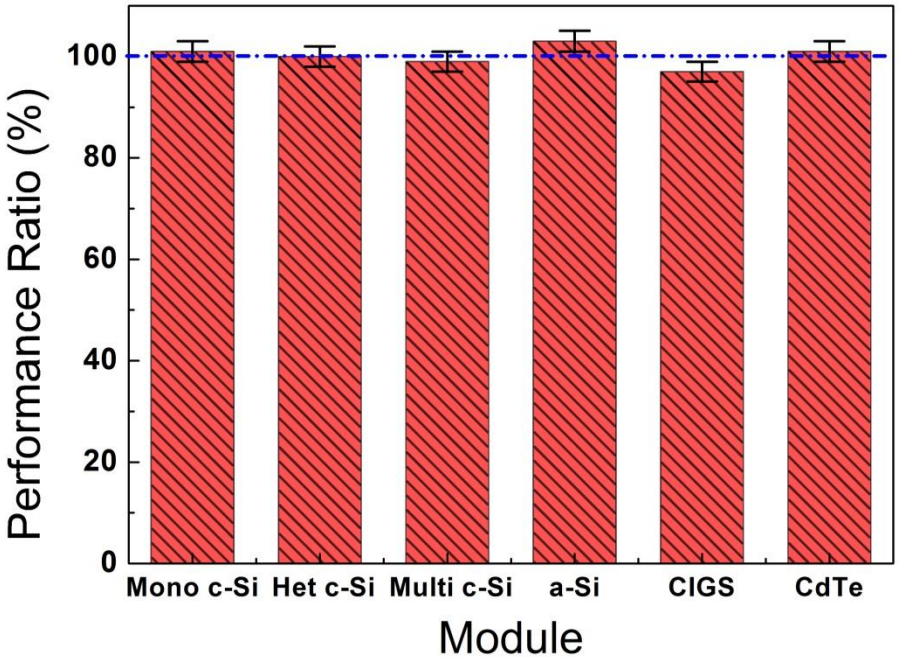

Figure 7.6: Performance ratio (PR) based on newly defined Tropical Test Conditions (TTC), as proposed in this work.

As discussed at the beginning of this Chapter (see Figure 7.1), the PR calculated based on the STC power shows a wide spread across different technologies. The biggest difference in PR can be up to 18% (between single-junction a-Si and CIGS). Thus this value cannot provide reference information on whether the installation is good or not. In contrast, the performance ratio calculated based on the TTC power (Figure 7.6) is close to 100% for all the modules studied, indicating that the overall outdoor operating conditions are close to TTC.

The under-performance of the CIGS module is due to its high degradation rate, as discussed in Chapter 6. The over-performance of the a-Si module can be explained by the more blue-rich spectrum at lower irradiances. As discussed in Section 5.1, the temperature coefficient of the maximum power point is a function of irradiance and temperature. Since the TTC temperature is similar to the actual outdoor operating temperatures, applying the temperature

coefficient can be avoided, which eventually reduces the uncertainty of the performance analysis.

7.3 Conclusions

Based on the typical operating conditions in Singapore, Tropical Test Conditions of 50°C module temperature, tropical solar spectrum as tabulated in Appendix 2, and a solar irradiance intensity of 800 W/m^2 are defined. Such defined conditions are representative of the real outdoor operating conditions in tropical Singapore, as demonstrated by the TTC based performance ratio, which is close to 100% for all the studied modules. Thus TTC can provide a suitable benchmark comparison across various technologies in the tropics, and provide an initial estimation on the outdoor performance of the tested module, based on indoor test data.

Chapter 8 Summary

8.1 Main contributions

The main scientific contributions of the present work are as follows:

A thorough study on the module spectral response (SR) was performed by both numerical simulation and experiments. The SR of PV modules was found to depend on (1) the SRs of the individual cells, (2) the shunt resistances of the cells, and (3) the use of bypass diodes. A detailed measurement uncertainty analysis was conducted for the module SR measurement setup at the Solar Energy Research Institute of Singapore (SERIS). For c-Si modules, the uncertainty was shown to mainly depend on the uncertainty of the calibrated reference cell used. For thin-film modules, the uncertainty depends additionally on the SR mismatch between the reference cell and the measured module. For the solar simulator used in SERIS, the measurement accuracy for thin-film modules can be enhanced by 3 to 5 % by applying spectral correction. The finding was presented at the 23rd Photovoltaic Science and Engineering Conference in Taipei in 2013, and a paper on this topic has been published in the journal Measurement Science and Technology.

The effective irradiance ratio (EIR) was defined in this work to quantify the effect of different solar spectra on module performance. It was found that the spectrum in Singapore is constantly blue-rich and with minimal variation over the year due to the low latitude. The constantly blue-rich spectrum in Singapore results in an annual EIR of 1.07 and 1.03 for the single-junction a-Si module and the CdTe module, respectively. These results, together with their lower temperature coefficients, explain the exceptionally high measured

performance ratios of single-junction a-Si modules in tropical Singapore. The blue-rich spectrum does not significantly affect the CIGS module, while causing an annual EIR of less than 1 to the double-junction micromorph Si module due to a current mismatch between the top and the bottom cells. A journal paper summarizing these findings has been published in IEEE Journal of Photovoltaics.

A method was introduced to study fast-changing irradiance and its influence on PV module performance in tropical Singapore. It was found that more than half of the irradiance in Singapore can be accounted to fast-changing conditions (defined as less than 30 min constant), mostly attributed to irradiances of 950 W/m^2 and above. The average efficiency of the mono c-Si modules was found to be mainly affected by the module temperature rather than different irradiance levels, while the efficiency for a-Si thin-film modules showed a much stronger dependence on the irradiance intensity. Higher efficiencies at low irradiances for a-Si modules were attributed to the "blue-rich" spectrum. The micromorph Si module showed similar character-istics as mono c-Si for high irradiances (including temperature dependence), but a lower efficiency at low irradiances, caused by the internal current mismatch between the top and bottom cells. The results were presented in the 2012 PV Asia-Pacific Conference and documented as a conference paper in Energy Procedia.

An expression for the temperature coefficient of the power output at the maximum power point P_{mpp} of PV modules was derived from the one-diode model. The expression depends on outdoor measurement data and parameters measured at STC. It was found that the temperature coefficient depends on

both the irradiance and the module temperature. The results give an improved insight into the temperature behaviour of P_{mpp} and its change with irradiance and module temperature. The annual average loss of power due to the high operating temperature was calculated for various modules and the loss range is between -2.5 to -5.5 %, correlated to the absolute reduction of the Performance Ratio.

The performance degradation in tropical Singapore was studied for 10 different types of PV modules. For the modules studied in this work, the degradation rate of the monocrystalline Si module was less than -0.8%/year, while the multicrystalline Si module degraded at around -1.0%/year. Thin-film modules showed degradation rates of around -2%/year, with the CIGS module showing an exceptionally high degradation rate of -6%/year. The relatively high and constant degradation rate of the CIGS module indicates that this particular module might have some generic shortfalls, which possibly are related to the high humidity in Singapore (some CIGS modules were reported to be very sensitive to moisture). The degradation of the c-Si modules is mainly due to a decrease in I_{SC} (with a slight increase in fill factor). The thin-film modules showed a significant reduction in V_{OC} and fill factor. The latter is due to the increased series resistances and the decreased shunt resistances. A journal paper on the module performance degradation has been published in IEEE Journal of Photovoltaics.

Tropical test conditions (TTC) were defined based on the monitoring data in tropical Singapore, and the Performance ratio based on TTC was verified to serve as a benchmark. Thus a standardized performance comparison across

different PV technologies in tropical regions is possible with the newly defined conditions. Since the newly defined conditions are representative of the actual outdoor operating conditions in tropical regions, the TTC rating can provide an initial estimation on the outdoor performance under real-world tropical conditions, based on indoor measurements.

8.2 Recommended future work:

The Tropical Test Conditions defined here are based on the data monitored in Singapore. To further verify the general applicability of the tropical test conditions, it is important to conduct meteorological measurements and module testing in other tropical locations. Monitoring of the solar spectrum is important, considering its significant impact on module performance.

The study on the performance degradation of PV modules only depends on three years of data, which is far less than the warranty life time (20 to 25 years) provided by manufacturers. Modules should be extensively monitored to further examine the degradation rate and failure modes of PV modules under tropical conditions.

It will be also interesting to study whether the smaller, but higher temperature range experienced in tropical areas, and the absence of frost and snow loading, can translate into lower cost module production methods. Standard tests, such as the mechanical load test, could be designed to be more flexible based on the local operation conditions.

Appendix 1: Publications arising from this work

Journal papers:

[1] **J.Y. Ye**, T. Reindl, A.G. Aberle, and T.M. Walsh, Effect of solar spectrum on the performance of various thin-film PV module technologies in tropical Singapore, *IEEE Journal of Photovoltaics*, vol. 4, pp 1268-1274, 2014. DOI:10.1109/JPHOTOV.2014.2328585

[2] **J.Y. Ye**, T. Reindl, A.G. Aberle, and T.M. Walsh, Performance degradation of various PV module technologies in tropical Singapore, *IEEE Journal of Photovoltaics*, vol. 4, pp. 1288-1294, 2014, DOI:10.1109/ JPHOTOV.2014.2338051

[3] **J.Y. Ye**, S.Y. Guo, T.M. Walsh, Y. Hishikawa, and R. Stangl, On the spectral response of PV modules, *Meas. Sci. Technol.*, vol. **25,** pp. 095007, 2014. DOI:10.1088/0957-0233/25/9/095007

[4] H. Liu, A.M. Nobre, D. Yang, **J.Y. Ye**, F.R. Martins, R. Ruther, T. Reindl, A.G. Aberle, and I.M. Peters, The impact of haze on the performance ratio and the current generation for PV systems in Singapore, *IEEE Journal of Photovoltaic*, vol. 4, pp. 1585-1592, 2014. DOI: 10.1109/JPHOTOV.2014.2346429

[5] L.H.I. Lim, Z. Ye, **J.Y. Ye**, D. Yang, and H. Du, A linear method to extract diode model parameters of solar panels from a single I-V curve, Renewable Energy, vol.76, pp. 135-142, 2015.

Conference papers:

[1] **J.Y. Ye**, T. Reindl, and J. Luther, Seasonal variation of PV module performance in tropical regions, *Proc. 38th IEEE Photovoltaic Specialists Conference*, pp. 2406-2410, Austin, 2012

[2] **J.Y. Ye**, K. Ding, T. Reindl, and A.G. Aberle, Outdoor PV module performance under fluctuating irradiance conditions in tropical climates, *Proc. PV Asia Pacific Conference 2011*, Singapore. *Energy Procedia* **33**, pp. 238-247, 2012

[3] **J.Y. Ye**, S.Y. Guo, T.M. Walsh, and R. Stangl, On the spectral response of PV modules, *Proc. 23rd International Photovoltaic Science and Engineering Conference*, Taipei, 2013

Appendix 2: TTC spectrum

Wavelength (nm)	Spectral irradiance ($\mu W \cdot m^{-2} \cdot nm^{-1}$)	Wavelength (nm)	Spectral irradiance ($\mu W \cdot m^{-2} \cdot nm^{-1}$)
303.5	31.4	442.3	1191.6
306.9	61.0	445.7	1230.2
310.3	111.6	449.1	1291.7
313.7	175.1	452.4	1312.5
317.0	204.0	455.8	1323.7
320.4	265.9	459.2	1334.9
323.8	315.2	462.6	1349.1
327.2	409.6	466.0	1319.9
330.5	442.6	469.4	1319.0
333.9	427.3	472.8	1342.8
337.3	427.1	476.2	1359.5
340.7	477.7	479.6	1381.0
344.1	470.8	483.0	1362.4
347.4	449.2	486.4	1277.1
350.8	432.0	489.8	1310.9
354.2	412.6	493.2	1331.7
357.6	410.7	496.6	1343.1
361.0	431.9	500.0	1307.2
364.3	490.6	503.3	1291.7
367.7	538.2	506.7	1311.9
371.1	530.8	510.1	1313.8
374.5	536.0	513.5	1294.5
377.9	573.7	516.9	1246.5
381.3	535.0	520.3	1261.6
384.7	512.8	523.7	1306.4
388.0	582.2	527.1	1309.4
391.4	588.2	530.5	1334.0
394.8	595.9	533.9	1331.3
398.2	779.7	537.3	1328.8
401.6	931.0	540.7	1313.0
405.0	956.0	544.1	1310.5
408.4	974.5	547.5	1319.3
411.8	1019.3	550.9	1321.8
415.1	1045.9	554.3	1321.9
418.5	1037.8	557.6	1303.2
421.9	1040.9	561.0	1293.3
425.3	1020.1	564.4	1296.3
428.7	942.8	567.8	1275.0
432.1	989.8	571.2	1266.5
435.5	1088.0	574.6	1270.5
438.9	1106.1	578.0	1273.6

581.4	1291.6	740.4	937.2
584.8	1269.7	743.7	969.4
588.2	1192.6	747.1	989.1
591.6	1163.3	750.5	982.3
595.0	1186.0	753.9	969.6
598.4	1206.8	757.2	877.5
601.7	1234.2	760.6	620.2
605.1	1250.9	763.9	604.9
608.5	1245.7	767.3	771.3
611.9	1224.1	770.7	890.6
615.3	1208.6	774.0	924.4
618.7	1211.3	777.4	928.7
622.1	1202.1	780.8	923.3
625.5	1177.4	784.1	912.8
628.9	1161.1	787.5	882.7
632.2	1161.6	790.8	855.2
635.6	1169.0	794.2	843.2
639.0	1168.6	797.5	831.4
642.4	1157.3	800.9	819.0
645.8	1120.2	804.2	813.2
649.2	1095.7	807.6	802.4
652.6	1090.5	810.9	734.8
655.9	1061.9	814.3	626.0
659.3	1109.6	817.6	574.7
662.7	1143.4	821.0	582.4
666.1	1151.1	824.3	596.8
669.5	1149.8	827.7	622.3
672.9	1141.8	831.0	634.9
676.2	1134.8	834.4	669.3
679.6	1123.9	837.7	711.7
683.0	1093.0	841.1	744.8
686.4	1002.8	844.4	764.1
689.8	981.9	847.7	767.9
693.1	949.7	851.1	750.0
696.5	982.5	854.4	743.3
699.9	972.2	857.8	759.8
703.3	979.0	861.1	769.0
706.7	999.2	864.4	753.6
710.0	1014.1	867.8	740.3
713.4	981.6	871.1	744.8
716.8	822.4	874.4	742.8
720.2	724.4	877.8	739.3
723.5	734.0	881.1	732.8
726.9	715.3	884.4	720.0
730.3	747.2	887.7	712.1
733.6	841.9	891.1	675.3
737.0	895.9	894.4	586.3

897.7	489.7	1052.2	492.1
901.0	460.2	1055.4	502.7
904.3	459.1	1058.7	493.9
907.7	422.4	1061.9	470.1
911.0	392.2	1065.2	471.1
914.3	380.1	1068.4	446.6
917.6	413.1	1071.6	462.2
920.9	448.1	1074.9	441.3
924.2	425.6	1078.1	438.5
927.5	305.9	1081.3	422.2
930.8	163.6	1084.6	456.9
934.2	98.1	1087.8	427.3
937.5	124.1	1091.0	420.3
940.8	144.6	1094.3	408.3
944.1	139.7	1097.5	401.1
947.4	146.0	1100.7	369.3
950.7	155.9	1103.9	321.8
954.0	172.2	1107.1	246.9
957.3	196.8	1110.4	179.7
960.6	231.1	1113.6	98.9
963.9	275.1	1116.8	49.5
967.1	350.3	1120.0	30.4
970.4	396.2	1123.2	23.9
973.7	386.5	1126.4	26.8
977.0	400.0	1129.6	43.2
980.3	446.2	1132.8	47.8
983.6	499.8	1136.0	59.5
986.9	542.0	1139.2	77.6
990.2	557.3	1142.4	66.1
993.4	564.9	1145.6	14.1
996.7	564.9		
1000.0	561.4		
1003.3	555.3		
1006.5	550.3		
1009.8	554.0		
1013.1	560.6		
1016.3	558.4		
1019.6	550.0		
1022.9	552.4		
1026.1	540.8		
1029.4	535.8		
1032.7	538.6		
1035.9	535.8		
1039.2	543.3		
1042.4	520.1		
1045.7	518.8		
1048.9	510.9		

References

[1] A. Luque and S. Hegedus, *Handbook of Photovoltaic Science and Engineering*: Wiley, 2003, p. 6-10.

[2] J. Nelson, *The Physics of Solar Cells*: Imperial College Press, 2003, p. 1.

[3] A. Aberle, "Industrial Solar Cells –The Next 10 Years," Solar Energy Research Institute of Singapore (SERIS), Singapore, 2012.

[4] "Energy outlook for Asia and the Pacific (2013)," Asian Development Bank, 2013.

[5] G. Masson, M. Latour, M. Rekinger, I.-T. Theologitis, and M. Papoutsi, "Global market outlook 2013-2017," European Photovoltaic Industry Association, 2013.

[6] S. M. Shafie, T. M. I. Mahlia, H. H. Masjuki, and A. Andriyana, "Current energy usage and sustainable energy in Malaysia: A review," *Renewable Sustainable Energy Rev.*, vol. 15, pp. 4370-7, 2011.

[7] S. May, "The PV Market in South East Asia – South East Asia - 2012," IHS, 2012.

[8] Hans-Christoph, "APVIA 2012: Singapore leads path to grid parity," *PV magazine*, 2012.

[9] (10 June 2014). "Harnessing the power of the sun," Available: http://www.edb.gov.sg/content/edb/en/resources/downloads/articles/harnessing-the-power-of-the-sun.html

[10] (26 January 2014). "Strong Growth Forecast for Solar PV Industry in 2014 with Demand Reaching 49 GW," Available: http://www.solarbuzz.com/news/recent-findings/strong-growth-forecast-solar-pv-industry-2014-demand-reaching-49-gw

[11] S. R. Wenham, M. A. Green, M. E. Watt, and R. Corkish, *Applied Photovoltaics*: Earthscan, 2007, p. 78.

[12] "PV Equipment Quarterly," Solarbuzz, 2013.

[13] R. H. Bube, *Photovoltaic Materials*: Imperial College Press, 1998.

[14] J. Poortmans and V. Arkhipov, *Thin Film Solar Cells: Fabrication, Characterization and Applications*: Wiley, 2006.

[15] M. A. Green, K. Emery, Y. Hishikawa, W. Warta, and E. D. Dunlop, "Solar cell efficiency tables (version 43)," *Prog. Photovoltaics Res. Appl.*, vol. 22, pp. 1-9, 2014.

[16] R. Schindler and W. Warmuth, "Photovoltaics Report," Fraunhofer Institute for Solar Energy Systems ISE, 2013.

[17] A. Goetzberger and V. U. Hoffmann, *Photovoltaic Solar Energy Generation*: Springer, 2005.

[18] M. Schachinger, "Frozen prices," *PV Magazine*, 2013.

[19] L. Kranz, C. Gretener, J. Perrenoud, R. Schmitt, F. Pianezzi, F. La Mattina, *et al.*, "Doping of polycrystalline CdTe for high-efficiency solar cells on flexible metal foil," *Nature Communications*, vol. 4, pp. 1-7, 2013.

[20] NREL,"Best Research-cell Efficiencies," 2013. Available: http://www.nrel.gov/ncpv/images/efficiency_chart.jpg

[21] EMPA, "Thin film solar cells: New world record for solar cell efficiency," 2013. Available: www.sciencedaily.com/releases/2013/01/130118064733.htm

[22] J. Aleksic, P. Zielke, and J. A. Szymczyk, "Temperature and flow visualization in a simulation of the Czochralski process using temperature-sensitive liquid crystals," *Ann. N.Y. Acad. Sci.*, vol. 972, pp. 158-63, 2002.

[23] H. C. Card and E. S. Yang, "Electronic processes at grain boundaries in polycrystalline semiconductors under optical illumination," *IEEE Trans. Electron Devices*, vol. 24, pp. 397-402, 1977.

[24] T. Surek, "Crystal growth and materials research in photovoltaics: progress and challenges," *J. Cryst. Growth*, vol. 275, pp. 292-304, 2005.
[25] Solar PV cell weekly spot price [Online]. Available: http://pvinsights.com/
[26] C. Haase and C. Podewils, "More of everything," *Photon International*, pp. 174-221, 2011.
[27] "TSM-DC01 datasheet," Trina Solar, Available: http://m.trinasolar.com/product_mono_dc01.php
[28] "TSM-PC05 datasheet," Trina Solar, Available: http://pdf.archiexpo.com/pdf/trina-solar-energy/tsm-pc05/62627-31677.html
[29] "REC Peak Energy Series," REC, Available: http://www.recgroup.com/products/recpeakenergyseries/
[30] R. M. Smith, D. C. Jordan, and S. R. Kurtz, "Outdoor PV module degradation of current-voltage parameters," in *2012 World Renewable Energy Forum*, Denver, Colorado (US), 2012, pp. 1-7.
[31] N. Mason, A. Artigao, P. Banda, R. Bueno, J. M. Fernandez, C. Morilla, *et al.*, "The technology and performance of the latest generation buried contact solar cell manufactured in BP Solar's Tres Cantos facility," in *19th European Photovoltaic Solar Energy Conference*, Paris, France, 2004, pp. 2653-5.
[32] M. A. Green, *Silicon solar cells: Advanced principles and practice*: University of New South Wales, 1995, p. 110.
[33] R. Hezel, *High-efficient low-cost photovoltaics*: Springer, 2009.
[34] D. H. Neuhaus and A. Munzer, "Industrial silicon wafer solar cells," *Advances in OptoElectronics*, p. 15, 2007.
[35] P. Wurfel, "Basic Structure of Solar Cells," in *Physics of Solar Cells*: Wiley, 2007, pp. 109-36.
[36] "95W Monocrystalline Photovoltaic Module," Jiawei, Available: http://www.posharp.com/dge-sp95-w-solar-panel-from-jiawei-solar_p1480245397d.aspx
[37] S. Grama, "A Survey of Thin-Film Solar Photovoltaic Industry & Technologies," Master of Science in Engineering and Management, Massachusetts Institute of Technology, USA, 2007.
[38] J. M. Pearce, N. Podraza, R. W. Collins, M. M. Al-Jassim, K. M. Jones, J. Deng, *et al.*, "Optimization of open circuit voltage in amorphous silicon solar cells with mixed-phase (amorphous+nanocrystalline) p-type contacts of low nanocrystalline content," *J. Appl. Phys.*, vol. 101, pp. 4301-3, 2007.
[39] W. C. Tu, Y. T. Chang, C. H. Yang, D. J. Yeh, C. I. Ho, C. Y. Hsueh, *et al.*, "Hydrogenated amorphous silicon solar cell on glass substrate patterned by hexagonal nanocylinder array," *Appl. Phys. Lett.*, vol. 97, pp. 3109-11, 2010.
[40] B. W. Clare, J. C. L. Cornish, G. T. Hefter, P. J. Jennings, C. P. Lund, D. J. Santjojo, *et al.*, "Studies of photodegradation in hydrogenated amorphous silicon," *Thin Solid Films*, vol. 288, pp. 76-82, 1996.
[41] C. P. Lund, K. Luczak, T. Pryor, J. C. L. Cornish, P. J. Jennings, P. Knipe, *et al.*, "Field and laboratory studies of the stability of amorphous silicon solar cells and modules," *Renewable Energy*, vol. 22, pp. 287-94, 2001.
[42] R. Rüther, G. Tamizh-Mani, J. Del Cueto, J. Adelstein, A. A. Montenegro, and B. von Roedern, "Performance test of amorphous silicon modules in different climates: higher minimum operating temperatures lead to higher performance levels," in *3rd World Conference on Photovoltaic Energy Conversion*, Osaka, Japan, 2003, pp. 2011-4.
[43] B. Kroposki and R. Hansen, "Performance and modeling of amorphous silicon photovoltaics for building-integrated applications," in *Solar 99: Growing the Market*, Portland, Maine, 1999, pp. 12-7.
[44] J. Deng, J. M. Pearce, V. Vlahos, R. W. Collins, and C. R. Wronski, "Characterization of the Bulk Recombination in Hydrogenated Amorphous Silicon Solar Cells," in *MRS Spring Meeting*, San Francisco, CA, 2004, pp. 1-7.

[45] J. M. Pearce, J. Deng, M. L. Albert, C. R. Wronski, and R. W. Collins, "Room temperature annealing of fast state from 1 sun illumination in protocrystalline Si:H materials and solar cells," in *31st IEEE Photovoltaic Specialists Conference*, Lake Buena Vista, FL, 2005, pp. 1536-9.
[46] A. D. Jones and C. P. Underwood, "A thermal model for photovoltaic systems," *Sol. Energy*, vol. 70, pp. 349-59, 2001.
[47] R. Rüther and J. Livingstone, "Seasonal variations in amorphous silicon solar module outputs and thin film characteristics," *Sol. Energ. Mat. Sol. Cells*, vol. 36, pp. 29-43, 1995.
[48] W. Luft, B. von Roedern, B. Stafford, D. Waddington, and L. Mrig, "Controlled light-soaking experiment for amorphous silicon modules," in *22nd IEEE Photovoltaic Specialists Conference*, Las Vegas, NV, 1991, pp. 1393-8
[49] J. Yang, R. Ross, T. Glatfelter, R. Mohr, G. Hammond, C. Bernotaitis, *et al.*, "High efficiency multi-junction solar cells using amorphous silicon and amorphous silicon-germanium alloys," in *20th IEEE Photovoltaic Specialists Conference*, Las Vegas, NV, 1988, pp. 241-6
[50] B. Yan, G. Yue, and S. Guha, "Status of nc-Si:H Solar Cells at United Solar and Roadmap for Manufacturing a-Si:H and nc-Si:H Based Solar Panels," *MRS Online Proceedings Library*, vol. 989, pp. 1-4, 2007.
[51] D. Fischer, S. Dubail, J. A. Anna Selvan, N. P. Vaucher, R. Platz, C. Hof, *et al.*, "The "micromorph" solar cell: extending a-Si:H technology towards thin film crystalline silicon," in *25th IEEE Photovoltaic Specialists Conference*, Washington DC, USA, 1996, pp. 1053-6.
[52] H. Morrow, "Cadmium and Cadmium Alloys," in *Kirk-Othmer Encycl. Chem. Technol.*: John Wiley & Sons, Inc., 2000, pp. 234-5.
[53] V. Fthenakis, M. Fuhrmann, J. Heiser, and W. Wang, "Experimental investigation of emissions and redistribution of elements in CdTe PV modules during fires," in *19th European PV Solar Energy Conference*, Paris, France, 2004, pp. 1008-12.
[54] D. H. Rose, R. C. Powell, D. Grecu, and U. Jayamaha, "Technology support for high-throughput processing of thin-film CdTe PV modules," National Renewable Energy Laboratory, 1999.
[55] R. C. Powell, R. Sasala, G. Rich, M. Steele, K. Bihn, N. Reiter, *et al.*, "Stability testing of CdTe/CdS thin-film photovoltaic modules," in *25th IEEE Photovoltaic Specialists Conference*, Washington DC, USA, 1996, pp. 785-8.
[56] S. Demtsu, S. Bansal, and D. Albin, "Intrinsic stability of thin-film CdS/CdTe modules," in *35th IEEE Photovoltaic Specialists Conference*, Honolulu, HI, 2010, pp. 1161-5.
[57] "SF150-170-S datasheet," Solar Frontier, Available: http://www.solar-frontier.com/eng/products/modules/S002210.html
[58] "POWERMAX datasheet," Avancis, Available: http://www.avancis.de/en/cis-solar-modules/powermax-strong/
[59] "SL 1-F datasheet," Q.CELLS, Available: http://www.q-cells.com/en/products/solar_modules.html#25115
[60] "Next Generation CIS," Solar Frontier, Available: http://solar-frontier.com/eng/products/index.html
[61] M. Gostein and L. Dunn, "Light soaking effects on photovoltaic modules: Overview and literature review," in *37th IEEE Photovoltaic Specialists Conference*, Seattle, WA, 2011, pp. 3126-31.
[62] L. Dunn and M. Gostein, "Light soaking measurements of commercially available CIGS PV modules," in *38th IEEE Photovoltaic Specialists Conference*, Austin, TX, 2012, pp. 1260-5.
[63] U. Rau and H. W. Schock, "Electronic properties of Cu(In,Ga)Se2 heterojunction solar cells–recent achievements, current understanding, and future challenges," *Appl. Phys. A*, vol. 69, pp. 131-47, 1999/08/01 1999.

[64] A. E. Delahoy, A. Ruppert, and M. Contreras, "Charging and discharging of defect states in CIGS/ZnO junctions," *Thin Solid Films*, vol. 361–362, pp. 140-4, 2000.
[65] A. E. Delahoy, J. Cambridge, L. Chen, and Z. J. Kiss, "Thin film CIGS photovoltaic technology: Final technical report," National Renewable Energy Laboratory, 2002.
[66] A. Virtuani, D. Pavanello, R. Kenny, M. Nikolaeva-Dimtrova, and E. Dunlop, "Outdoor module performance of single, double and triple-junction silicon based thin film technologies," in *22nd European Photovoltaic Solar Energy Conference*, Milan, Italy, 2007, pp. 2421-6.
[67] D. Willett and S. Kuriyagawa, "The effects of sweep rate, voltage bias and light soaking on the measurement of CIS-based solar cell characteristics," in *23rd IEEE Photovoltaic Specialists Conference*, Louisville, KY 1993, pp. 495-500.
[68] R. P. Kenny, A. Ioannides, H. Müllejans, W. Zaaiman, and E. D. Dunlop, "Performance of thin film PV modules," *Thin Solid Films*, vol. 511-512, pp. 663-72, 2006.
[69] A. R. McKinley, "Performance characterization of thin film PV modules - The first ten months of the University of Agder's new Grimstad test station," Master, Northumbria University, 2011.
[70] K. Emery, "Calibration and rating of photovoltaics," in *38th IEEE Photovoltaic Specialists Conference*, Austin, USA, 2012, pp. 1-4.
[71] Robert P. Kenny, Anatoli I. Chatzipanagi, and T. Sample, "Preconditioning of thin-film PV module technologies for calibration," *Prog. Photovoltaics Res. Appl.*, vol. 22, pp. 166-72, 2012.
[72] H. Zainuddin, S. Shaari, A. M. Omar, Z. M. Zain, J. Soumin, and Z. Surat, "Preliminary investigations on the effect of humidity on the reception of visible solar radiation and the effect of humidity and wind speed on PV module output," American Institute of Physics, 2010.
[73] J. Merten, L. Sicot, Y. Delesse, and A. G. Montgareuil, "Outdoor evaluation of the energy production of different module technologies," in *23rd European Photovoltaic Solar Energy Conference*, Valencia, Spain, 2008, pp. 2841-5.
[74] M. Pravettoni, A. Virtuani, H. Mullejans, and E. D. Dunlop, "Spectral response measurements of multi-junction PV modules at the European solar test installation laboratories and their usage in clear day outdoor characterisation," in *23rd European Photovoltaic Solar Energy Conference*, Valencia, Spain, 2008, pp. 2908-12.
[75] J. Wirth, S. Kratochwill, D. Philipp, K.-A. Weiß, and M. Koehl, "Comparison of indoor and outdoor power measurements of thin film modules," in *24th European Photovoltaic Solar Energy Conference*, Hamburg, Germany, 2009, pp. 3398-401.
[76] H. Müllejans, T. Wagner, F. Merli, A. Jäger-Waldau, and E. D. Dunlop, "Changes in spectral response with temperature and irradiance intensity," *Thin Solid Films*, vol. 451-452, pp. 145-51, 2004.
[77] R. P. Kenny, M. Nikolaeva-Dimitrova, and E. D. Dunlop, "Performance measurements of CIS modules: outdoor and pulsed simulator comparison for power and energy rating," in *4th World Conference on Photovoltaic Energy Conversion*, 2006, pp. 2058-61.
[78] R. Gottschalg, T. R. Betts, S. R. Williams, D. Sauter, D. G. Infield, and M. J. Kearney, "A critical appraisal of the factors affecting energy production from amorphous silicon photovoltaic arrays in a maritime climate," *Sol. Energy*, vol. 77, pp. 909-16, 2004.
[79] IEC 61724 Photovoltaic system performance monitoring - Guidelines for measurement, data exchange and analysis, International Electrotechnical Commission, Geneva, Switzerland, 1998.

[80] N. H. Reich, B. Mueller, A. Armbruster, W. G. J. H. M. van Sark, K. Kiefer, and C. Reise, "Performance ratio revisited: is PR > 90% realistic?," *Prog. Photovoltaics Res. Appl.*, vol. 20, pp. 717-26, 2012.
[81] D. L. King, J. A. Kratochvil, W. E. Boyson, and W. I. Bower, "Field experience with a new performance characterization procedure for photovoltaic arrays," Sandia National Laboratories, 1998.
[82] L. Dunn, M. Gostein, and K. Emery, "Comparison of pyranometers vs. PV reference cells for evaluation of PV array performance," in *38th IEEE Photovoltaic Specialist Conference*, Austin, Texas, 2012, pp. 2899-904.
[83] C. R. Osterwald, "Translation of device performance measurements to reference conditions," *Sol. Cells*, vol. 18, pp. 269-79, 1986.
[84] M. A. Hamdy and R. L. Call, "The effect of the diode ideality factor on the experimental determination of series resistance of solar cells," *Sol. Cells*, vol. 20, pp. 119-26, 1987.
[85] J. Merten, J. M. Asensi, C. Voz, A. V. Shah, R. Platz, and J. Andreu, "Improved equivalent circuit and analytical model for amorphous silicon solar cells and modules," *IEEE Trans. Electron Devices*, vol. 45, pp. 423-9, 1998.
[86] A. Parretta, A. Sarno, and L. R. M. Vicari, "Effects of solar irradiation conditions on the outdoor performance of photovoltaic modules," *Optics Communications*, vol. 153, pp. 153-63, 1998.
[87] N. H. Reich, W. G. J. H. M. van Sark, E. A. Alsema, R. W. Lof, R. E. I. Schropp, W. C. Sinke, *et al.*, "Crystalline silicon cell performance at low light intensities," *Sol. Energ. Mat. Sol. Cells*, vol. 93, pp. 1471-81, 2009.
[88] G. E. Bunea, K. E. Wilson, Y. Meydbray, M. P. Campbell, and D. M. De Ceuster, "Low Light Performance of Mono-Crystalline Silicon Solar Cells," in *4th World Conference on Photovoltaic Energy Conversion*, 2006, pp. 1312-4.
[89] P. Grunow, S. Lust, D. Sauter, V. Hoffmann, C. Beneking, B. Litzenburger, *et al.*, "Weak light performance and annual yields of PV modules and systems as a result of the basic parameter set of industrial solar cells," in *19th European Photovoltaic Solar Energy Conference*, Paris, France, 2004, pp. 2190-3.
[90] H. D. Mohring and D. Stellbogen, "Annual energy harvest of PV systems – advantages and drawbacks of different PV technologies," in *23rd European Photovoltaic Solar Energy Conference*, Valencia, Spain, 2008, pp. 2781-5.
[91] T. Ishii, K. Otani, T. Takashima, and S. Kawai, "Estimation of the maximum power temperature coefficients of PV modules at different time scales," *Sol. Energ. Mat. Sol. Cells*, vol. 95, pp. 386-9, 2011.
[92] PVCDROM, "PVCDROM:diode-equation," 2013. Available: http://www.pveducation.org/pvcdrom/pn-junction/diode-equation
[93] E. Maruyama, A. Terakawa, M. Taguchi, Y. Yoshimine, D. Ide, T. Baba, *et al.*, "Sanyo's challenges to the development of high-efficiency HIT solar cells and the expansion of HIT business," in *4th World Conference on Photovoltaic Energy Conversion*, Hawaii, US, 2006, pp. 1-5.
[94] (02 June 2014). "PVsyst 6 Help: Temperature behaviour correction," Available: www.valentin-software.com/sites/default/files/.../manual-pvsol-en.pdf
[95] *PV*SOL Expert Manual*. Available: www.valentin-software.com/sites/default/files/.../manual-pvsol-en.pdf
[96] T. Reindl, J. Ouyang, A. M. Khaing, K. Ding, Y. S. Khoo, T. M. Walsh, *et al.*, "Investigation of the Performance of Commercial Photovoltaic Modules under Tropical Conditions," *Jpn. J. Appl. Phys.*, vol. 51, pp. 10NF1-NF1-4, 2012.
[97] D. L. Evans, "Simplified method for predicting photovoltaic array output," *Sol. Energy*, vol. 27, pp. 555-60, 1981.
[98] E. Skoplaki and J. A. Palyvos, "On the temperature dependence of photovoltaic module electrical performance: A review of efficiency/power correlations," *Sol. Energy*, vol. 83, pp. 614-24, 2009.

[99] K. Emery, J. Burdick, Y. Caiyem, D. Dunlavy, H. Field, B. Kroposki, *et al.*, "Temperature dependence of photovoltaic cells, modules and systems," in *25th IEEE Photovoltaic Specialists Conference*, Washington DC, USA, 1996, pp. 1275-8.
[100] D. Moser, M. Pichler, and M. Nikolaeva-Dimitrova, "Filtering Procedures for Reliable Outdoor Temperature Coefficients in Different Photovoltaic Technologies," *J. Sol. Energy Eng.*, vol. 136, pp. 21006-15, 2013.
[101] IEC 60904-3 Photovoltaic devices - Part 3: Measurement principles for terrestrial photovoltaic (PV) solar devices with reference spectral irradiance data, International Electrotechnical Commission, Geneva, Switzerland, 2008.
[102] D. L. King, J. A. Kratochvil, and W. E. Boyson, "Temperature coefficients for PV modules and arrays: measurement methods, difficulties, and results," in *26th IEEE Photovoltaic Specialists Conference*, Anaheim, USA, 1997, pp. 1183-6.
[103] T. Danowicz, T. Rodziewicz, and M. Zabkowska-Waclawek, "Effect of air mass factor on the performance of different PV modules," *Opto-Electron. Rev.*, vol. 12, pp. 69-73, 2004.
[104] A. Nakajima, M. Ichikawa, M. Kondo, K. Yamamoto, H. Yamagishi, and Y. Tawada, "Spectral Effects of a Single-Junction Amorphous Silicon Solar Cell on Outdoor Performance," *Jpn. J. Appl. Phys.*, vol. 43, pp. 2425-31, 2004.
[105] D. King, Kratochvil, J., Boyson, W., *Performance of Amorphous Silicon Photovoltaic Systems, 1985-1989*: Sandia National Laboratories. Photovoltaic Systems Research, 1990.
[106] T. R. Betts, "Investigation of photovoltaic device operation under varying spectral conditions," PhD, Electronic, Electrical and Systems Engineering, Loughborough University, UK, 2005.
[107] T. Ishii, K. Otani, T. Takashima, and Y. Q. Xue, "Solar spectral influence on the performance of photovoltaic (PV) modules under fine weather and cloudy weather conditions," *Prog. Photovoltaics Res. Appl.*, vol. 21, pp. 481-9, 2013.
[108] C. Monokroussos, M. Bliss, Y. N. Qiu, C. J. Hibberd, T. R. Betts, A. N. Tiwari, *et al.*, "Effects of spectrum on the power rating of amorphous silicon photovoltaic devices," *Prog. Photovoltaics Res. Appl.*, vol. 19, pp. 640-8, 2011.
[109] C. Cornaro and A. Andreotti, "Influence of Average Photon Energy index on solar irradiance characteristics and outdoor performance of photovoltaic modules," *Prog. Photovoltaics Res. Appl.*, vol. 21, pp. 996-1003, 2013.
[110] K. Akhmad, A. Kitamura, F. Yamamoto, H. Okamoto, H. Takakura, and Y. Hamakawa, "Outdoor performance of amorphous silicon and polycrystalline silicon PV modules," *Sol. Energ. Mat. Sol. Cells*, vol. 46, pp. 209-18, 1997.
[111] T. Minemoto, S. Nagae, and H. Takakura, "Impact of spectral irradiance distribution and temperature on the outdoor performance of amorphous Si photovoltaic modules," *Sol. Energ. Mat. Sol. Cells*, vol. 91, pp. 919-23, 2007.
[112] T. Minemoto, M. Toda, S. Nagae, M. Gotoh, A. Nakajima, K. Yamamoto, *et al.*, "Effect of spectral irradiance distribution on the outdoor performance of amorphous Si//thin-film crystalline Si stacked photovoltaic modules," *Sol. Energ. Mat. Sol. Cells*, vol. 91, pp. 120-2, 2007.
[113] C. Sirisamphanwong and N. Ketjoy, "Impact of spectral irradiance distribution on the outdoor performance of photovoltaic system under Thai climatic conditions," *Renewable Energy*, vol. 38, pp. 69-74, 2012.
[114] J. Burdick and T. Glatfelter, "Spectral response and I–V measurements of tandem amorphous-silicon alloy solar cells," *Sol. Cells*, vol. 18, pp. 301-14, 1986.
[115] D. L. King, J. A. Kratochvil, and W. E. Boyson, "Measuring solar spectral and angle-of-incidence effects on photovoltaic modules and solar irradiance sensors," in *26th IEEE Photovoltaic Specialists Conference*, 1997, pp. 1113-6.
[116] G. N. Tiwari and S. Dubey, *Fundamentals of Photovoltaic Modules and Their Applications*: Royal Society of Chemistry, 2010.

[117] Y. S. Khoo, J. P. Singh, T. M. Walsh, and A. G. Aberle, "Comparison of angular reflectance losses between PV modules with planar and textured glass under Singapore outdoor conditions," *IEEE J. Photovolt.*, vol. 4, pp. 362-7, 2014.
[118] D. C. Jordan and S. R. Kurtz, "Photovoltaic Degradation Rates—an Analytical Review," *Prog. Photovoltaics Res. Appl.*, vol. 21, pp. 12-29, 2013.
[119] NEA, "Weather Statistics," National Environment Agency (NEA), Singapore, 2010.
[120] Z. Ye, A. Nobre, T. Reindl, J. Luther, and C. Reise, "On PV module temperatures in tropical regions," *Sol. Energy*, vol. 88, pp. 80-7, 2013.
[121] IEC61215 - Crystalline silicon terrestrial photovoltaic (PV) modules -design and type approval, Geneva, Switzerland, 2005.
[122] IEC 61646: Thin-film terrestrial photovoltaic (PV) modules - Design qualification and type approval, International Electrotechnical Commission, Geneva, Switzerland, 2008.
[123] J. H. Wohlgemuth and S. Kurtz, "Reliability testing beyond qualification as a key component in photovoltaic's progress toward grid parity," in *IEEE International Reliability Physics Symposium*, Monterey, California, 2011, pp. 1-8.
[124] H. Ossenbrink and T. Sample, "Results of 12 years of module qualification to the IEC 61215 standard and CEC specification 503," in *3rd World Conference on Photovoltaic Energy Conversion*, 2003, pp. 1882-7.
[125] J. H. Wohlgemuth, D. W. Cunningham, P. Monus, J. Miller, and A. Nguyen, "Long Term Reliability of Photovoltaic Modules," in *4th World Conference on Photovoltaic Energy Conversion*, 2006, pp. 2050-3.
[126] J. H. Wohlgemuth, D. W. Cunningham, A. M. Nguyen, and J. Miller, "Long term reliability of photovoltaic modules," in *20th European Photovoltaic Solar Energy Conference*, Barcelona, Spain, 2005, pp. 1942-6.
[127] C. R. Osterwald, "Standards, Calibration and Testing of PV Modules and Solar Cells," National Renewable Energy Laboratory, USA.
[128] B. Dimmler, "CIGS and CdTe based thin film PV modules,an industrial revolution," in *38th IEEE Photovoltaic Specialists Conference*, Austin, USA, 2012, pp. 1235-7.
[129] K. W. Jansen and A. E. Delahoy, "A laboratory technique for the evaluation of electrochemical transparent conductive oxide delamination from glass substrates," *Thin Solid Films*, vol. 423, pp. 153-60, 2003.
[130] D. E. Carlson, R. Romero, F. Willing, D. Meakin, L. Gonzalez, R. Murphy, *et al.*, "Corrosion effects in thin-film photovoltaic modules," *Prog. Photovoltaics Res. Appl.*, vol. 11, pp. 377-86, 2003.
[131] C. R. Osterwald and T. J. McMahon, "History of accelerated and qualification testing of terrestrial photovoltaic modules: A literature review," *Prog. Photovoltaics Res. Appl.*, vol. 17, pp. 11-33, 2009.
[132] A. Zielnik, "Validating photovoltaic module durability tests," Solar America Board for Codes and Standards, 2013.
[133] P. Sánchez-Friera, M. Piliougine, J. Peláez, J. Carretero, and M. Sidrach de Cardona, "Analysis of degradation mechanisms of crystalline silicon PV modules after 12 years of operation in Southern Europe," *Prog. Photovoltaics Res. Appl.*, vol. 19, pp. 658-66, 2011.
[134] J. H. Wohlgemuth, "Reliability of PV systems," in *SPIE*, San Diego, CA, 2008, pp. 704802-13.
[135] D. H. Otth and R. G. Ross, "Assessing photovoltaic module degradation and lifetime from long term environmental tests," in *29th Institute of Environmental Science Annual Meeting*, LA, USA, 1983, pp. 116-23.

[136] N. C. Park, W. W. Oh, and D. H. Kim, "Effect of Temperature and Humidity on the Degradation Rate of Multicrystalline Silicon Photovoltaic Module," *Int. J. Photoenergy,* vol. 2013, p. 9, 2013.
[137] D. L. Bätzner, G. Agostinelli, M. Campo, A. Romeo, J. Beier, H. Zogg, *et al.*, "Study of spatially resolved impurity diffusion in CdTe solar cells using voltage dependent quantum efficiency," *Thin Solid Films,* vol. 431–432, pp. 421-5, 2003.
[138] N. Strevel, L. Trippel, and M. Gloeckler, "Performance characterization and superior energy yield of First Solar PV power plants in high-temperature conditions," *Photovoltaics International,* pp. 148-54, 2012.
[139] J. Metzdorf, "Calibration of solar cells. 1: The differential spectral responsivity method," *Appl. Opt.,* vol. 26, pp. 1701-8, 1987.
[140] H. Field, "Solar cell spectral response measurement errors related to spectral band width and chopped light waveform," in *26th IEEE Photovoltaic Specialists Conference*, Anaheim, CA, 1997, pp. 350-2.
[141] S. Winter, T. Wittchen, and J. Metzdorf, "Primary reference cell calibration at the PTB based on an improved DSR facility," in *16th European Photovoltaic Solar Energy Conference*, Glasgow, UK, 2000, pp. 1-4.
[142] J. Hohl-Ebinger, G. Siefer, and W. Warta, "Non-linearity of solar cells in spectral response measurements," in *22nd European Photovoltaic Solar Energy Conference* Milan, Italy, 2007, pp. 422-4.
[143] M. Pravettoni, R. Galleano, A. Virtuani, H. Müllejans, and E. D. Dunlop, "Spectral response measurement of double-junction thin-film photovoltaic devices: the impact of shunt resistance and bias voltage," *Meas. Sci. Technol.,* vol. 22, p. 45902, 2011.
[144] IEC 60904-8 Photovoltaic devices - Part 8: Measurement of spectral response of multi-junction photovoltaic (PV) devices, International Electrotechnical Commission, Geneva, Switzerland, 2013.
[145] I. Reda and A. Andreas, "Solar position algorithm for solar radiation application," National Renewable Energy Laboratory (NREL), USA, 2008.
[146] M. Pravettoni, A. Virtuani, H. Mullejans, and R. P. Kenny, "Spectral response measurements of large area thin film multijunction photovoltaic modules at the European solar test installation and spectral mismatch calculation," in *24th European Photovoltaic Solar Energy Conference*, Hamburg, Germany, 2009, pp. 3338-42.
[147] K. Emery, D. Dunlavy, H. Field, and T. Moriarty, "Photovoltaic spectral responsivity measurements," in *2nd World Conference and Exhibition on Photovoltaic Solar Energy Conversion*, Vienna, Austria, 1998, pp. 1-5.
[148] ASTM standard E1021, American Society for Testing Materials, West Conshocken PA, USA.
[149] A. Parisi, L. Curcio, V. Rocca, S. Stivala, A. C. Cino, A. C. Busacca, *et al.*, "Thin film CIGS solar cells, photovoltaic modules, and the problems of modeling," *Int. J. Photoenergy*, vol. 2013, pp. 1-11, 2013.
[150] K. R. Lord, M. R. Walters, and J. R. Woodyard, "Investigation of shunt resistances in single-junction a-Si:H alloy solar cells," *MRS Online Proceedings Library,* vol. 336, pp. 1-8, 1994.
[151] S. Guo, J. P. Singh, I. M. Peters, A. G. Aberle, and T. M. Walsh, "A quantitative analysis of photovoltaic modules using halved cells," *Int. J. Photoenergy,* vol. 2013, pp. 1-8, 2013.
[152] IEC 60904-7 Photovoltaic devices - Part 7: Computation of the spectral mismatch correction for measurements of photovoltaic devices International Electrotechnical Commission, Geneva, Switzerland, 1998.
[153] D. A. Clugston and P. A. Basore, "PC1D version 5: 32-bit solar cell modeling on personal computers," in *26th IEEE Photovoltaic Specialists Conference*, Anaheim, CA, 1997, pp. 207-10.

[154] A. G. Aberle, W. Zhang, and B. Hoex, "Advanced loss analysis method for silicon wafer solar cells," *Energy Procedia,* vol. 8, pp. 244-9, 2011.
[155] A. Khanna, T. Mueller, R. A. Stangl, B. Hoex, P. K. Basu, and A. G. Aberle, "A fill factor loss analysis method for silicon wafer solar cells," *IEEE J. Photovolt.,* vol. 3, pp. 1170-7, 2013.
[156] Y. Tsuno, Y. Hishikawa, and K. Kurokawa, "A method for spectral response measurements of various PV modules " in *23rd European Photovoltaic Solar Energy Conference,* Valencia, Spain, 2008, pp. 2723-7.
[157] M. Pravettoni, A. Komlan, R. Galleano, H. Müllejans, and E. D. Dunlop, "An alternative method for spectral response measurements of large-area thin-film photovoltaic modules," *Prog. Photovoltaics Res. Appl.,* vol. 20, pp. 416-22, 2012.
[158] J. Hohl-Ebinger and W. Warta, "Investigation of large area cell and module spectral response measurement," in *19th European Photovoltaic Solar Energy Conference,* Paris, France, 2004, pp. 2611-4.
[159] H. Field, "Solar cell spectral response measurement errors related to spectral band width and chopped light waveform," in *26th IEEE Photovoltaic Specialists Conference,* Anaheim, CA, 1997, pp. 350-4.
[160] M. Pavettoni, A. Komlan, R. Galleano, H. Mullejans, and E. E. Dunlop, "An alternative method for spectral response measurements of large-area thin-film photovoltaic modules," *Prog. Photovoltaics Res. Appl.,* vol. 20, pp. 416-22, 2012.
[161] A.Virtuani, G. Friesen, D. Chianese, G. C. Dozio, G. Rigamonti, M. Pegurion, *et al.,* "The MPVT (multi-purpose PV module tester) project-a highly innovative and versatile solar simulator," in *25th European Photovoltaic Solar Energy Conference,* Valencia, Spain, 2010, pp. 4361 - 5.
[162] M. Pravettoni, M. Nicola, and G. Friesen, "A filtered pulsed solar simulator for spectral response measurements of multi-junction modules of commercial size," in *27th European Photovoltaic Solar Energy Conference,* Frankfurt, Germany, 2012, pp. 3209-13.
[163] Evaluation of measurement data — Guide to the expression of uncertainty in measurement JCGM, 2008.
[164] M. Harald, Z. Willem, and G. Roberto, "Analysis and mitigation of measurement uncertainties in the traceability chain for the calibration of photovoltaic devices," *Meas. Sci. Technol.,* vol. 20, p. 075101, 2009.
[165] A. Driesse, D. Dirnberger, N. Reich, and C. Reise, "Spectrally Selective Sensors for PV System Performance Monitoring," in *38th IEEE Photovoltaic Specialists Conference,* Austin, USA, 2012.
[166] H. Müllejans, A. Ioannides, R. Kenny, W. Zaaiman, H. A. Ossenbrink, and E. D. Dunlop, "Spectral mismatch in calibration of photovoltaic reference devices by global sunlight method," *Meas. Sci. Technol.,* vol. 16, pp. 1250-4, 2005.
[167] G. Peharz, G. Siefer, and A. W. Bett, "A simple method for quantifying spectral impacts on multi-junction solar cells," *Sol. Energy,* vol. 83, pp. 1588-98, 2009.
[168] "MIDC SPA Calculator," 2012. Available: http://www.nrel.gov/midc/solpos/spa.html
[169] R. Lad, "Outdoor performance rating and spectral effects of photovoltaic modules," PhD, Arizona State University, USA, 2010.
[170] R. Lad, J. Wohlgemuth, and G. TamizhMani, "Outdoor energy ratings and spectral effects of photovoltaic modules," in *35th IEEE Photovoltaic Specialists Conference,* Honolulu, HI, 2010, pp. 2827-32.
[171] M. Nikolaeva-Dimitrova, A. Skoczek, R. P. Kenny, and E. D. Dunlop, "Outdoor Module Performance of Single, Double and Triple-Junction Silicon Based Thin Film Technologies," in *23rd European Photovoltaic Solar Energy Conference,* Valencia, Spain, 2008, pp. 2079-83.

[172] B. Zinßer, G. Makrides, M. Schubert, G. E. Georghiou, and J. H. Werner, "Temperature and irradiance effects on outdoor field performance," in *24th European Photovoltaic Solar Energy Conference*, Hamburg, Germany, 2009, pp. 4083-6.

[173] D. Fischer, F. Bichsel, S. d. Bruijn, P. Goulpie, L. Sansonnens, Y. Ziegler, *et al.*, "Positive effective temperature coefficient of power of +0.75%/°C in flexible a-Si modules in building integrated installations," in *24th European Photovoltaic Solar Energy Conference*, Hamburg, Germany, 2009, pp. 3505-8.

[174] J. Sutterlüti, I. Sinicco, A. Hügli, T. Hälker, and S. Ransome, "Outdoor characterisation and modelling of thin-film modules and technology benchmarking," in *24th European Photovoltaic Solar Energy Conference*, Hamburg, Germany, 2009, pp. 3198-205.

[175] L. Fanni, I. Pola, E. Burà, T. Friesen, and D. Chianese, "Investigation of annealing and degradation effects on a-Si PV modules in real Operating Conditions," in *24th European Photovoltaic Solar Energy Conference* Hamburg, Germany, 2009, pp. 3596-9.

[176] B. Muthirayan, R. Appels, H. Oprins, U. Chatterjee, F. Catthoor, J. Driesen, *et al.*, "Thermal effects due to environmental variables in photovoltaic cells," in *38th IEEE Photovoltaic Specialist Conference*, Austin, USA, 2012, pp. 1001-3.

[177] A. Nobre, R. Malhotra, H. T. Chee, C. Reise, K. Kiefer, R. Ruther, *et al.*, "Degradation analysis of photovoltaic systems in a tropical environment," in *28th European Photovoltaic Solar Energy Conference* Paris, France, 2013, pp. 3673 - 7.

[178] S. R. Williams, T. R. Betts, P. Vorasayan, R. Gottschalg, and D. G. Infield, "Actual PV module performance including spectral losses in the UK," in *31st IEEE Photovoltaic Specialists Conference*, Orlando, Florida, 2005, pp. 1607-10.

[179] T. Strand, L. Mrig, R. Hansen, and K. Emery, "Technical evaluation of a dual-junction same-band-gap amorphous silicon photovoltaic system," *Sol. Energ. Mat. Sol. Cells*, vol. 41-2, pp. 617-28, 1996.

[180] A. Virtuani and L. Fanni, "Seasonal power fluctuations of amorphous silicon thin-film solar modules: distinguishing between different contributions," *Prog. Photovoltaics Res. Appl.*, pp. 2257-66, 2012.

[181] M. Schweiger, I. Ulrich, I. Nixdorf, L. Rimmelspacher, U. Jahn, and W. Herrmann, "Spectral analysis of various thin-film modules using high-precision spectral response data and solar spectral irradiance data," in *27th European Photovoltaic Solar Energy Conference*, Frankfurt, Germany, 2012, pp. 3284-90.

[182] R. Gottschalg, T. R. Betts, D. G. Infield, and M. J. Kearney, "On the importance of considering the incident spectrum when measuring the outdoor performance of amorphous silicon photovoltaic devices," *Measurement Science & Technology*, vol. 15, pp. 460-6, Feb 2004.

[183] J. Y. Ye, T. Reindl, and J. Luther, "Seasonal variation of PV module performance in tropical regions," in *38th IEEE Photovoltaic Specialists Conference*, Austin, Texas, 2012, pp. 2406-10.

[184] M. Pravettoni, A. Virtuani, H. Mullejans, R. P. Kenny, E. D. Dunlop, and K. W. J. Barnham, "Spectral response measurements of large area thin film multijunction photovoltaic modules at the European solar test installation and spectral mismatch calculation," in *24th European Photovoltaic Solar Energy Conference*, Germany, 2009, pp. 3338-42.

[185] R. Shimokawa, F. Nagamine, Y. Miyake, K. Fujisawa, and Y. Hamakawa, "Japanese indoor calibration method for the reference solar cell and comparison with outdoor calibration," *Jpn. J. Appl. Phys.*, vol. 26, 1987.

[186] F. Fabero, N. Vela, and F. Chenlo, "Influence of solar spectral variations of the conversion efficiency of a-Si and m-Si PV devices: a yearly and hourly study," in *13th European Photovoltaic Solar Energy Conference*, Nice, France, 1995, pp. 2281-4.

[187] J. Hohl-Ebinger and W. Warta, "Uncertainty of the spectral mismatch correction factor in STC measurements on photovoltaic devices," *Prog. Photovoltaics Res. Appl.*, vol. 19, pp. 573-9, 2011.
[188] K. Emery and C. Osterwald, "Measurement of Photovoltaic Device Current as a Function of Voltage, Temperature, Intensity and Spectrum," *Sol. Cells*, vol. 21, pp. 313-27, 1987.
[189] J. Y. Ye, T. Reindl, A. G. Aberle, and T. M. Walsh, "Effect of solar spectrum on the performance of various thin-film PV module technologies in tropical Singapore," *IEEE J. Photovolt.*, vol. PP, pp. 1-7, 2014.
[190] Y. Hirata and T. Tani, "Output variation of photovoltaic modules with environmental factors .1. The effect of spectral solar radiation on photovoltaic module output," *Sol. Energy*, vol. 55, pp. 463-8, 1995.
[191] N. Martin and J. M. Ruiz, "A new method for the spectral characterisation of PV modules," *Prog. Photovoltaics Res. Appl.*, vol. 7, pp. 299-310, 1999.
[192] L. R. Carrasco, "Silver Lining of Singapore's Haze," *Science*, vol. 341, pp. 342-3, 2013.
[193] S. V. Salinas, B. N. Chew, J. Miettinen, J. R. Campbell, E. J. Welton, J. S. Reid, *et al.*, "Physical and optical characteristics of the October 2010 haze event over Singapore: A photometric and lidar analysis," *Atmos. Res.*, vol. 122, pp. 555-70, 2013.
[194] J. Y. Ye, K. Ding, T. Reindl, and A. G. Aberle, "Outdoor PV module performance under fluctuating irradiance conditions in tropical climates," *Energy Procedia*, vol. 33, pp. 238-47, 2013.
[195] A. Ianetz, V. Lyubansky, I. Setter, B. Kriheli, E. G. Evseev, and A. I. Kudish, "Inter-comparison of different models for estimating clear sky solar global radiation for the Negev region of Israel," *Energy Convers. Manage.*, vol. 48, pp. 259-68, 2007.
[196] S. Janjai, K. Sricharoen, and S. Pattarapanitchai, "Semi-empirical models for the estimation of clear sky solar global and direct normal irradiances in the tropics," *Appl. Energy*, vol. 88, pp. 4749-55, 2011.
[197] D. Yang, P. Jirutitijaroen, and W. M. Walsh, "Hourly solar irradiance time series forecasting using cloud cover index," *Sol. Energy*, vol. 86, pp. 3531-43, 2012.
[198] A. Nakajima, M. Ichikawa, M. Kondo, K. Yamamoto, H. Yamagishi, and Y. Tawada, "Spectral effects of a single-junction amorphous silicon solar cell on outdoor performance," *Jpn. J. Appl. Phys.*, vol. 43, pp. 24-5, 2004.
[199] L. Amanda and J. Stein, "Improvement and validation of a transient model to predict photovoltaic module temperature," Sandia National Laboratory, USA, 2011.
[200] J. Kurnik, M. Jankovec, K. Brecl, and M. Topic, "Outdoor testing of PV module temperature and performance under different mounting and operational conditions," *Sol. Energ. Mat. Sol. Cells*, vol. 95, pp. 373-6, 2011.
[201] C. M. Whitaker, T. U. Townsend, H. J. Wenger, A. Iliceto, G. Chimento, and F. Paletta, "Effects of irradiance and other factors on PV temperature coefficients," in *22nd IEEE Photovoltaic Specialists Conference*, Las Vegas, USA, 1991, pp. 608-13.
[202] G. Makrides, B. Zinsser, G. E. Georghiou, M. Schubert, and J. H. Werner, "Temperature behaviour of different photovoltaic systems installed in Cyprus and Germany," *Sol. Energ. Mat. Sol. Cells*, vol. 93, pp. 1095-9, 2009.
[203] H. P. Garg and R. K. Agarwal, "Some aspects of a PV/T collector/forced circulation flat plate solar water heater with solar cells," *Energy Convers. Manage.*, vol. 36, pp. 87-99, 1995.
[204] E. Radziemska, "The effect of temperature on the power drop in crystalline silicon solar cells," *Renewable Energy*, vol. 28, pp. 1-12, 2003.

[205] M. A. Green, *Solar cells: operating principles, technology, and system applications*: Prentice-Hall, 1982.
[206] M. A. M. Shaltout, M. M. El-Nicklawy, A. F. Hassan, U. A. Rahoma, and M. Sabry, "The temperature dependence of the spectral and efficiency behavior of Si solar cell under low concentrated solar radiation," *Renewable Energy,* vol. 21, pp. 445 - 58, 2000.
[207] G. H. Yordanov, O.-M. Midtgård, and T. O. Saetre, "Series resistance determination and further characterization of c-Si PV modules," *Renewable Energy,* vol. 46, pp. 72-80, 2012.
[208] C. Hu and R. M. White, *Solar cells: from basics to advanced systems*: McGraw-Hill, 1983.
[209] J. S. Griffith, N. S. Rathod, and J. Paslaski, "Some tests of flat plate photovoltaic module cell temperatures in simulated field conditions," in *15th IEEE Photovoltaic Specialists Conference*, Kissimmee, FL, 1981, pp. 822-30.
[210] E. Skoplaki, A. G. Boudouvis, and J. A. Palyvos, "A simple correlation for the operating temperature of photovoltaic modules of arbitrary mounting," *Sol. Energ. Mat. Sol. Cells,* vol. 92, pp. 1393-402, 2008.
[211] R. Ross, "Interface design considerations for terrestrial solar cell modules," in *12th IEEE Photovoltaic Specialists Conference*, Baton Rouge, LA, USA, 1976, pp. 801-6.
[212] T. Nordmann and L. Clavadetscher, "Understanding temperature effects on PV system performance," in *3rd World Conference on Photovoltaic Energy Conversion*, Osaka, Japan, 2003, pp. 2243-6.
[213] G. Makrides, B. Zinsser, G. E. Georghiou, M. Schubert, and J. H. Werner, "Degradation of different photovoltaic technologies under field conditions," in *35th IEEE Photovoltaic Specialists Conference*, Honolulu, HI, 2010, pp. 2332-7.
[214] K. O. Davis, S. R. Kurtz, D. C. Jordan, J. H. Wohlgemuth, and N. Sorloaica-Hickman, "Multi-pronged analysis of degradation rates of photovoltaic modules and arrays deployed in Florida," *Prog. Photovoltaics Res. Appl.,* vol. 21, pp. 702-12, 2013.
[215] A. Cronin, S. Pulver, D. Cormode, D. Jordan, S. Kurtz, and R. Smith, "Measuring degradation rates of PV systems without irradiance data," *Prog. Photovoltaics Res. Appl.,* vol. 22, pp. 851-62, 2013.
[216] T. Ishii, T. Takashima, and K. Otani, "Long-term performance degradation of various kinds of photovoltaic modules under moderate climatic conditions," *Prog. Photovoltaics Res. Appl.,* vol. 19, pp. 170-9, 2011.
[217] N. Bogdanski, W. Herrmann, F. Reil, M. Kohl, K. A. Weiss, and M. Heck, "PV reliability (cluster II): results of a German four-year joint project - part II, results of three years module weathering in four different climates.," in *25th European Photovoltaic Solar Energy Conference,* Valencia, Spain, 2010, pp. 4339-43.
[218] A. Skoczek, T. Sample, and E. D. Dunlop, "The results of performance measurements of field-aged crystalline silicon photovoltaic modules," *Prog. Photovoltaics Res. Appl.,* vol. 17, pp. 227-40, 2009.
[219] D. Polverini, M. Field, E. Dunlop, and W. Zaaiman, "Polycrystalline silicon PV modules performance and degradation over 20 years," *Prog. Photovoltaics Res. Appl.,* vol. 21, pp. 1004-15, 2013.
[220] D. L. King, M. A. Quintana, J. A. Kratochvil, D. E. Ellibee, and B. R. Hansen, "Photovoltaic module performance and durability following long-term field exposure," *Prog. Photovoltaics Res. Appl.,* vol. 8, pp. 241-56, 2000.
[221] C. R. Osterwald, J. Adelstein, J. A. del Cueto, B. Kroposki, D. Trudell, and T. Moriarty, "Comparison of Degradation Rates of Individual Modules Held at Maximum Power," in *4th World Conference on Photovoltaic Energy Conversion*, 2006, pp. 2085-8.

[222] D. C. Jordan and S. R. Kurtz, "Analytical improvements in PV degradation rate determination," in *35th IEEE Photovoltaic Specialists Conference*, Honolulu, HI, 2010, pp. 2688-93.
[223] R. B. Cleveland, W. S. Cleveland, J. E. McRae, and I. Terpenning, "Stl: A seasonal-trend decomposition procedure based on loess," *Journal of Official Statistics*, vol. 6, p. 70, 1990.
[224] A. Ndiaye, A. Charki, A. Kobi, C. M. F. Kébé, P. A. Ndiaye, and V. Sambou, "Degradations of silicon photovoltaic modules: A literature review," *Sol. Energy*, vol. 96, pp. 140-51, 2013.
[225] R. Gottschalg, C. N. Jardine, R. Ruther, T. R. Betts, G. J. Conibeer, J. Close, *et al.*, "Performance of amorphous silicon double junction photovoltaic systems in different climatic zones," in *29th IEEE Photovoltaic Specialists Conference*, New Orleans, Louisiana, 2002, pp. 1699-702.
[226] M. A. Quintana, D. L. King, T. J. McMahon, and C. R. Osterwald, "Commonly observed degradation in field-aged photovoltaic modules," in *29th IEEE Photovoltaic Specialists Conference*, New Orleans, USA, 2002, pp. 1436-9.
[227] M. D. Kempe, A. A. Dameron, and M. O. Reese, "Evaluation of moisture ingress from the perimeter of photovoltaic modules," *Prog. Photovoltaics Res. Appl.*, pp. 2374-87, 2013.
[228] E. L. Meyer and E. E. v. Dyk, "Monitoring I_{sc}, V_{oc} and performance parameters of photovoltaic modules," in *17th European Photovoltaic Solar Energy Conference*, Munich, Germany, 2001.
[229] E. L. Meyer and E. E. van Dyk, "Assessing the reliability and degradation of photovoltaic module performance parameters," *IEEE Transactions on Reliability*, vol. 53, pp. 83-92, 2004.
[230] S. Dongaonkar and M. A. Alam, "A shade tolerant panel design for thin film photovoltaics," in *38th IEEE Photovoltaic Specialists Conference*, Austin, USA, 2012, pp. 2416-20.
[231] S. Dongaonkar, M. A. Alam, Y. Karthik, S. Mahapatra, W. Dapeng, and M. Frei, "Identification, characterization, and implications of shadow degradation in thin film solar cells," in *IEEE International Reliability Physics Symposium*, Monterey, CA, 2011, pp. 5E.4.1-5E.4.5.
[232] D. J. Coyle, "Life prediction for CIGS solar modules part 1: modeling moisture ingress and degradation," *Prog. Photovoltaics Res. Appl.*, vol. 21, pp. 156-72, 2013.
[233] B. Selin Tosun, R. K. Feist, A. Gunawan, K. Andre Mkhoyan, S. A. Campbell, and E. S. Aydil, "Improving the damp-heat stability of copper indium gallium diselenide solar cells with a semicrystalline tin dioxide overlayer," *Sol. Energ. Mat. Sol. Cells*, vol. 101, pp. 270-6, 2012.
[234] Deutscher Wetterdienst / National Environment Agency